DEVELOPMENT OF ROBUST EXPANDED BED

ADSORPTION PROCESSES FOR cGMP MANUFACTURE

OF BIOPHARMACEUTICAL PRODUCTS

by

Stephanie Ewert

A thesis submitted to The University of Birmingham

for the degree of

DOCTOR OF PHILOSOPHY

School of Chemical Engineering
College of Engineering and Physical Sciences
February 2016

UNIVERSITYOF
BIRMINGHAM

University of Birmingham Research Archive

e-theses repository

Abstract

Expanded Bed Adsorption (EBA) was deemed to be the next big thing in downstream processing receiving much attention after its introduction in the mid 1990s. Sample clarification appeared to be a 'thing of the past' as the increased inter-particle voidage in EBA allowed for direct application of crude feedstocks without blocking the column. Despite acclaimed advantages, such as increased overall yield due to fewer process steps, lower costs and reduced process times, confidence in this technique has waned in recent years, owing to a lack of process robustness and poor understanding of the complexity of the technique as a whole. At the most fundamental level, a persistent lack of detailed knowledge regarding hydrodynamic behaviour within expanded beds impairs optimal operation and prediction of the process.

In this work, the technique of Positron Emission Particle Tracking (PEPT) was employed extensively to study solid phase motion and dispersion in expanded beds of commercial media. Comprehensive interrogation of the internal hydrodynamic properties of expanded beds was initially performed using a 'feedstock-free', 'buffer-only' system for fluidisation. Changes in the position and speed of differently sized positron labelled particle tracers along the length of the bed were identified in response to variations in flow rate, means of fluid distribution and degree of column misalignment. These tracers provided striking evidence of: (i) adsorbent particle classification within the bed; (ii) continuous axial and horizontal motion across surprisingly long distances; and (iii) non-uniform bed expansion with increasing mobile phase velocity. Analysis of PEPT tracking data permitted calculation of solid axial dispersion coefficients for adsorbent particles in EBA for the very first time. The kinetics of bed stabilisation were determined by analysing the time dependent axial positioning of differently sized tracer particles after starting fluidisation, indicating a potential to significantly reduce equilibration times (*cf.* those commonly

reported) and concomitant savings in buffer consumption. Destabilisation of the bed as caused by a marginal vertical misalignment of the column was documented by circular motion patterns of the tracer particles and increased solid axial dispersion coefficients. The results were subsequently compared to previous studies conducted with different commercial adsorbent matrices to obtain a comprehensive interpretation.

Finally, adsorbent particle motion was investigated under 'real process' conditions, i.e. during the application of a porcine serum feedstock. Solid mixing was not significantly increased during feedstock loading. Further, in contrast to previous work using sonicated calf thymus DNA feedstocks, the overall axial position of positron-labelled tracer particles remained relatively constant and stable through the loading phase commensurate with a robust EBA process.

"Nothing in this world that's worth having comes easy."

- Robert Kelso

Acknowledgements

I would like to take this opportunity to thank all those who have contributed to the accomplishment of this dissertation.

First and foremost, I would like to sincerely thank Professor Owen R.T. Thomas for his excellent supervision, his guidance and his trust in my abilities. I would also like to say a huge thank you to Dr Eirini Theodossiou for joining hours-long discussions and for giving me the confidence to believe in myself. Special thanks also to Professor Serafim Bakalis for his ideas and for introducing me to PEPT.

I would also like to send thanks to my industrial supervisors, Dr Emile van de Sandt and Dr Piet den Boer of DSM and DSM Biologics (now Patheon), for their advice and for funding this work in association with my EPSRC CASE studentship. In addition, thank you to the DSP group at Patheon in Groningen, for their warm welcome and help during my time in Groningen - especially Randal Maarleveld, Diana Mulder-Wesseling and Elham Zolghadr.

Furthermore, a huge thank you to Dr Tom Leadbeater and Dr Joseph Gargiuli for all their help and advice regarding the magic that is PEPT. Thank you also to Elaine Mitchell and David French for providing support towards my work in the lab.

Special thanks to all the past and present members of the DSP group in BiochemEng, F7 and associates - Christine Müller, Evan Hsu, Ping Cao, Isaac Vizcaino, Johannes Mohr, Neeraj Jumbu, Alfred Fernandez, Ikhlaas Kasli, Asma Nurul, Hong Li, Stephan Joseph, Ursula Simon and Lukas Wenger. Thanks also to the lunch and staff house crew.

Last, I am forever grateful to my family, my parents and my siblings, for their unconditional love, support and encouragement. Ohne euch wäre ich nichts.

Table of Contents

List of Figures

List of Tables

Abbreviations

AC	Affinity chromatography
AU	Absorbance units
AMTPS	Aqueous micellar two-phase system
ATPE	Aqueous two-phase extraction
ATPS	Aqueous two-phase system
BCA	Bicinchinonic acid
BSA	Bovine serum albumin
CAC	Continuous annular chromatography
CHO	Chinese hamster ovary
CIP	Cleaning-in-place
CTI	Cell transmission index
DLVO	Derjaguin, Landau, Verwey, Overbeek
EBA	Expanded bed adsorption
HETP	Height equivalent to a theoretical plate
HGMF	High-gradient magnetic fishing
HGMS	High-gradient magnetic separation
HIC	Hydrophobic interaction chromatography
HTS	High throughput screening
IEC	Ion exchange chromatography
IgG hc	Immunoglobulin G heavy chain
IgG lc	Immunoglobulin G light chain
IgG	Immunoglobulin G
LED	Light-emitting diode
LoR	Line of response
mAb	Monoclonal antibody
MCSGP	Multicolumn countercurrent solvent gradient purification
MEP	Magnetic extraction phases
PBS	Phosphate buffered saline
PEG	Polyethylenglycol
PEPT	Positron Emission Particle Tracking
PET	Positron emission tomography
PIV	Particle image velocimetry
PSA	Porcine serum albumin

Abbreviations

RFD	Rotating fluid distributor
RTD	Residence time distribution
SBH	Settled bed height
SBV	Settled bed volumes
SDS-PAGE	Sodium dodecyl sulfate polyacrylamide gelelectrophoresis
SEC	Size exclusion chromatography
SMB	Simulated moving bed
TMB	True moving bed
UV	Ultraviolet

Latin Symbols

Bo	Bodenstein number	
$D_{ax,\mathrm{l}}$	Liquid axial dispersion coefficient	m^2/s
$D_{ax,\mathrm{s}}$	Solid axial dispersion coefficient	m^2/s
d_c	Column diameter	mm
d_p	Adsorbent diameter	µm
d_t	Distance travelled by tracer particle	mm
e^+	Positron	
f	Reconstruction fraction	
g	Gravitational force	m/s^2
$h_{T,0}$	Relative tracer position in the settled bed	
$\overline{h}_{T,0}$	Mean relative tracer position in the settled bed	
H	Expanded bed height	m
H_0	Settled bed height	m
$H_{T,0}$	Tracer position in the settled bed	mm
k	Rejection parameter	
n	Richardson-Zaki index	
n	Neutron	
N	Number of events (in PEPT algorithm)	
N	Number of theoretical plates	
P	Pressure	N/m^2
p	Proton	
Pe	Peclet number	
p_i	Position of the tracer particle	
Re_t	Reynolds number at the terminal settling velocity	
Re_p	Particle Reynolds number	
t	time	s
t_m	Mean residence time	s
u_i	Interstitial fluid velocity	cm/h
u_{mf}	Minimum fluidisation velocity	cm/h
u_t	Terminal settling velocity	m/s
$\overline{u}(\Delta t)$	Mean tracer velocity averaged over time Δt	mm/s
v_e	Electron neutrino	

Latin Symbols

v_i	Velocity of the tracer particle	mm/s
w	Spatial resolution of the PEPT camera	mm
y_d	Distance travelled by tracer particle	mm

Greek Symbols

β^+	Positron emission/beta plus decay	
γ-ray	Gamma-ray photon	keV
Δ	Precision of locating a stationary particle	
ΔP	Pressure drop	
ε	Bed voidage	
ε_0	Settled bed voidage	
η	Fluid viscosity	kg/(m s)
ρ_l	Liquid density	g/mL
ρ_p	Particle density	g/mL
$\sigma_\theta{}^2$	Dimensionless variance	
σ	Variance	
ϕ	Stable fraction of the bed	

1. Introduction

1.1. Biopharmaceuticals

Biopharmaceuticals are proteins or nucleic acid based pharmaceutical substances used for therapeutic, prophylactic or in vivo diagnostic purposes which are produced using modern biotechnology techniques, in particular genetic engineering or hybridoma technology (Walsh 2002; Azevedo et al. 2009). In contrast to traditional, chemically synthesized drugs they are much bigger (typically 15-200 kDa cf. around 0.5 kDa (Carta and Jungbauer 2010; Ho and Gibaldi 2013)), and exhibit a much more complex structure, which is generally critical to their biological function. Due to their manufacture from heterogeneous mixtures consisting of products of living organisms, cells, animals or plants, their molecular composition is often difficult to define (Guiochon and Beaver 2011).

Human recombinant insulin was the first biopharmaceutical launched on the market in 1982 and this set the beginning to a new era for the pharmaceutical industry. Since then, a total of 246 biopharmaceutical products have been approved in the United States and European Union (Walsh 2014). According to McKinsey, in 2014 biopharmaceuticals generated global revenues of $163 billion, making up about 20% of the pharma market. With its current annual growth rate of more than 8 percent, it grows around twice as fast as conventional pharma (Otto et al. 2014).

Recombinant proteins and monoclonal antibodies (mAbs) make up the largest shares of biopharmaceuticals on the market (Elvin et al. 2013) with mAbs accounting for 34% of the biopharmaceutical market share in 2006 (Carta and Jungbauer 2010). Future growth is also predicted to continue to be dominated by mAbs and insulins (Walsh 2014).

The highly regulated and controlled manufacturing process of biopharmaceutical products starts with the expression of the target protein in the genetically engineered host cell line. Expression systems range from bacterial strains like *E. coli* to *Saccharomyces cerevisae* as yeast cells to even plants. However, mammalian cells are used to produce the majority of biopharmaceutical proteins due to their ability to carry out complex post-translational modifications such as glycosylation (Carta and Jungbauer 2010). *Chinese Hamster Ovary* (CHO) cells are the most popular mammalian expression system.

The actual biopharmaceutical production can be divided into 'upstream' and 'downstream' (Walsh 2007). In the upstream processing, the respective cell line is grown in bioreactors or fermentation vessels of up to 25.000 L (Carton and Strohl 2013), constituting the product biosynthesis phase. The downstream processing includes the recovery or capture of the product from the broth or the cells, purification and concentration. The process is completed by the final product formulation, involving addition of excipients, sterile filtration and lyophilisation.

In the past years, remarkable progress has been achieved in the upstream processing, with productivity significantly increasing due to advances in molecular biology and host cell engineering, leading to higher cell line productivity, as well as optimised media formulations, feed delivery strategies, process control and bioreactor designs. Recombinant antibody and protein yields have increased notably from a few milligrams to several grams per litre (Gottschalk 2008; Azevedo et al. 2009). This has resulted in a bottleneck in downstream processing and a shift of production costs from upstream to downstream, with the latter accounting for up to 80% of the total manufacturing cost (Guiochon and Beaver 2011). Optimising separation and purification processes has thus become critical to the biopharmaceutical industry in order to improve process efficiency

and economics while simultaneously satisfying the required high quality and regulatory standards.

1.2. Downstream processing

The product recovery and purification during downstream processing is a crucial part of the whole manufacturing process and there are several challenges that have to be met. First and foremost, the purity of the final product is vital, with requirements for therapeutic proteins often exceeding 99% (Hagel et al. 2008). Besides, biopharmaceuticals are mostly high molecular weight proteins with numerous substituents and complex three-dimensional structures. This structure is critical to the biological activity of the molecule and can often only be preserved under certain conditions. Sometimes even only small changes in temperature, pH or ionic strength can lead to an irreversible unfolding of the molecule and its denaturation (Guiochon and Beaver 2011). Furthermore, the product is often present in a complex, heterogeneous fermentation broth whose composition is variable dependent on the upstream process and difficult to characterise (Nfor et al. 2008). Apart from the product, it contains impurities that can be divided into product-related and process-related. Product-related impurities may e.g. be oligomers, aggregates or deamidated product variants and their removal can prove especially challenging due to their structural similarity to the product. The upstream-derived process impurities depend mainly on the selected expression system (see section 1.1) and its culture conditions. In general, biopharmaceuticals derived from mammalian cell culture are produced as extracellular proteins and are secreted into the media, whereas most prokaryotic producer cell types accumulate proteins intracellularly (Walsh 2003). In the latter case, the cell disruption necessary to release the product leads to host cell components accounting for a majority of the impurities. For example endotoxins, which are components of the cell

wall of Gram-negative bacteria, are extremely toxic to humans and their almost complete removal from the final product is required. However, even in secreted products host cell components can be found as impurities due to cell lysis occurring during fermentation. In some cases, the upstream cultivation conditions chosen to yield high titers can particularly lead to lysis of the cells (Carta and Jungbauer 2010).

Overall, the downstream process is highly dependent on the upstream settings. However, there are generic strategies for protein purification which divide the process into different - mostly three or four - stages. These stages are based on the main objectives at each point during the process and make use of various unit operations. One strategy that has been developed has been named *CIPP* - Capture, Intermediate Purification and Polishing (Healthcare 2010), although there are variations to this approach which give the stages slightly different names or sometimes include the final product formulation (Harrison 2003; Nfor et al. 2008).
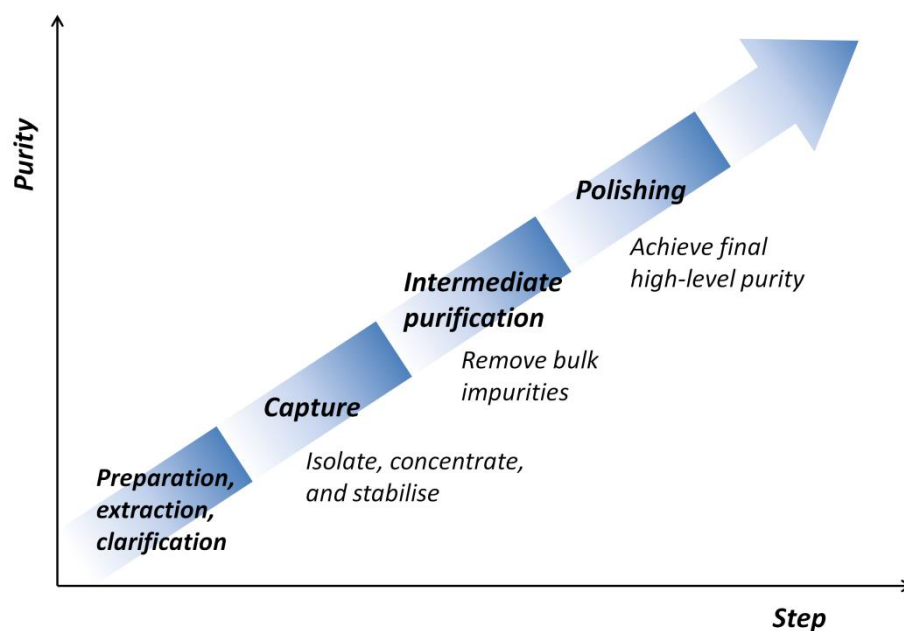
Figure 1.1: The CIPP purification strategy. Adapted from GE Healthcare (2010).

Any strategy starts with the clarification of the fermentation broth, i.e. solid-liquid separation most commonly performed by centrifugation or filtration to remove the cells, cell debris or other particulates. In the case of intracellular products a cell disruption step is interposed to release the target molecule from the cell. In the subsequent capture stage, the key objectives are the isolation, concentration and stabilisation of the target product. Ideally, significant removal of critical contaminants, mainly those exhibiting properties different to those of the product, is achieved at the same time. During the intermediate purification stage, the main objective is the removal of most of the bulk impurities, such as host cell proteins, nucleic acids, endotoxins and viruses. However, if the capture step is already very efficient, the intermediate purification stage can be skipped and potentially more polishing steps can be included. In the polishing stage, the remaining impurities are removed, which are typically similar to the target protein in chemical functionality and physical properties. The ultimate aim is to attain final purity.

To develop a whole biopharmaceutical purification process, the most suitable unit operations have to be selected for each of the above stages and combined successively (Nfor et al. 2008). Over the years, several methods or strategies for such process syntheses have evolved. One of these, and the one that has probably been around the longest, is a knowledge-based approach which relies on rules of thumb, also known as heuristics. Guidelines such as to remove largest quantities and the most plentiful impurities first, to exploit the greatest differences in the properties between the product and impurities, to use different separation bases in successive steps and to sequence steps based on minimising interstage conditioning resulted from experience and are still practical (Wheelwright 1991; Nfor et al. 2008). They are very fast and simple to apply; however, they may also lead to suboptimal process options. An experimental approach

gives a more quantitative analysis of favourable process conditions. This methodology is heavily improved by using high throughput screening (HTS) techniques, which allows for a broader range of experimental conditions to be tested. Platform approaches make use of existing purification processes that serve as template for the separation of closely related products. Model-based and algorithmic methods are based on advances in mathematical programming techniques and computer simulation tools. They depend on the availability of input property data as parameters, but especially combined with high throughput experimentations as hybrid methods they can be very powerful (Nfor et al. 2008; Guiochon and Beaver 2011).

1.2.1.   Liquid chromatography in Downstream Processing

As mentioned before, the selection and successive combination of unit operations constitute the purification process. One of the most widely used and popular unit operations is liquid chromatography. This is a technique that is based on different interactions of the soluble molecules in the liquid phase with the solid phase. The solid or stationary phase is packed in a fixed column and consists most commonly of spherical, porous adsorbent particles. The particles, also called resin, are made of a polymer matrix with a large inner surface containing active groups.

The liquid phase flows through the packed chromatography column and the solutes successively leave the column separated depending on the varyingly strong interactions with the resin surface. The different liquid chromatography techniques are classified according to their separation mechanism. Most forms of chromatography used in protein purification are adsorptive in nature and are carried out in elution mode (Harrison 2003; Walsh 2007). That implies the application of the feed mixture under conditions which promote selective retention of the target protein and subsequent alteration of the mobile

phase to endorse desorption. The most commonly used chromatography techniques, their respective bases for separation and elution conditions are listed in Table 1.1.

Table 1.1: Separation mechanisms of the most relevant chromatographic techniques used in downstream processing.

Name		Separation principle	Elution
IEC	Ion exchange chromatography	Electrostatic interactions	Increasing salt gradient or pH change
AC	Affinity chromatography	Specific adsorption	Competitive displacement or pH change
HIC	Hydrophobic interaction chromatography	Hydrophobic interactions	Decreasing salt gradient
SEC	Size exclusion chromatography	Molecular size and shape	Isocratic

Chromatography is the standard instrument used substantially in all three stages of capture, intermediate purification and polishing. In principle, all of the techniques mentioned above can be used at any stage. However, each technique has its own advantages for it to be employed at a specific point in the process. For example, SEC is mainly used as last step in polishing due to lower throughput and the method-related dilution. On the other hand, IEC is known as the workhorse for capture and intermediate purification and is the most commonly used chromatography method. As mentioned before, a reasonable combination of chromatography steps is often connected to minimise intermediate conditioning. It is therefore sensible, for instance, to employ a HIC after an IEC step as the high salt concentration required for the HIC has already been generated by the IEC elution (Wheelwright 1991).

Generally, the typical chromatographic separation in elution mode is a batch process and can be divided into several consecutive steps. First, the column is equilibrated with running buffer to establish conditions for the subsequent adsorption of the target molecule

to the chromatography matrix. Afterwards, the sample mixture is loaded onto the column and ideally, the target molecule binds reversible to the adsorbent surface. In the following washing step, running buffer is pumped through the column again to remove any unbound or weakly bound components. For the elution, the buffer is changed to set up conditions for desorption according to each separation technique. A cleaning step follows to clear the column of all potentially stronger bound molecules. Another buffer for sanitisation may be used to preserve the chromatography matrix against fouling. Finally, the column is re-equilibrated and returned to the starting conditions.

Current industrial processes for biopharmaceuticals rely considerably on chromatography for capture, purification and polishing (Carta and Jungbauer 2010). This is due to certain advantages of chromatography over other unit operations. First, it attains very high separation efficiencies of up to hundreds or thousands of theoretical plates compared to only a few stages achieved by extraction or membrane filtration. This means that chromatographic processes can accomplish the resolution of mixtures consisting of molecules with very similar properties. Moreover, considering the critical protein stability mentioned above, it presents a gentle method for separation. Connecting several chromatographic techniques creates a high amount of versatility and complementarity. Besides, large volumes of buffer flowing through relatively small volumes of chromatography media in the column results in rapid concentration, which is particularly beneficial for processing dilute solutions as encountered in bioseparations. Furthermore, chromatographic methods are well established in the biopharmaceutical industry and equipment and matrices are readily available (Carta and Jungbauer 2010).

Ongoing efforts to optimise downstream processing regarding economic efficiency, productivity as well as sustainability have lead to different trends in research and development.

One tendency of those endeavours is directly aimed at optimising chromatography in itself. This includes the development of novel matrices and improvement or modification of existing adsorbents. In particular, interest has increased in mixed-mode or multimodal chromatography, which utilises more than one of the above interaction modes (Table 1). This can result in advantages such as higher selectivity and higher loading capacities (Yang and Geng 2011). Furthermore, innovative ideas such as the modification of adsorbents with thermoresponsive polymers applied in a temperature-controlled chromatography set up are being explored (Müller et al. 2013). Another route is to completely change the current support structures altogether and develop new and improved materials as basis for the solid phase. A shift from diffusion limited adsorbents to convective mass transfer media, such as porous membrane adsorbents and monoliths, eliminates two major drawbacks of conventional chromatography matrices: poor pressure tolerance and the need for high residence times (Hardick et al.). However, even though membrane adsorbent structures present the advantage of increased throughput due to higher flow rates, issues with membrane fouling are common. As a consequence, application is mainly limited to the polishing stage. Monolithic columns consist of one piece of a continuous, porous material in which the pores are interconnected into channels (Guiochon 2007). Depending on the size of these channels, high flow rates at a relatively low pressure drop are feasible while at the same time capacities are flow rate independent due to fast convective mass transfer. Monoliths have proven good separation especially for large molecules as the binding sites are easily accessible. On the downside, their low specific surface areas lead to low column capacities compared to traditional packings (Zou et al. 2002).

Another approach aiming at an increased throughput and productivity is the development of continuous chromatographic processes. Two different operation principles have mainly been studied in this area: Firstly, rotating devices like annular and carrousel chromatography, and secondly countercurrent chromatography and related techniques (Jungbauer 2013). However, only annular chromatography is a truly continuous chromatography, whereas all other methods use a cyclic arrangement of several columns in a pseudocontinuous mode.

In continuous annular chromatography (CAC), the adsorbent matrix is packed within the gap of two concentric cylinders and is rotated while the sample is continuously applied. During elution, the mixture is separated and the radial position of each solute is dependent on the affinity to the chromatographic medium; forming its own characteristic spiral band. With regard to countercurrent chromatography, a continuous multicolumn system called simulated moving bed (SMB) has found major attention. It is based on a hypothetical true moving bed (TMB), which assumes that there is a real countercurrent motion between the solid and liquid phase (Seidel-Morgenstern et al. 2008). Traditionally, the bed is divided into four zones with the feed stream entering between the mid sections. Separation of a binary mixture is then performed as the component with the higher affinity to the solid phase is carried in one direction to the extract outlet while the other, less adsorbable component to the other direction and the raffinate outlet. However, the practical application of TMB is difficult and as a consequence, SMB has gained prevalence. In SMB, a countercurrent flow of the solid phase is simulated with a particular arrangement of several columns and periodically switching their valve inlet ports. This technology has been used for a long time in the petrochemical industry (Ruthven and Ching 1989) and then later in the pharmaceutical industry, especially for separation of enantiomers (Juza et al. 2000; Schulte and Strube 2001). A drawback of the typical SMB process is its restriction to binary separations, although various modifications and new

concepts are being developed that could separate up to 4 components (Seidel-Morgenstern et al. 2008; Jungbauer 2013). While SMB is also limited to isocratic processing, an advanced continuous technique has been developed that is capable of performing a linear solvent gradient (Ströhlein et al. 2006). The so called multicolumn countercurrent solvent gradient purification (MCSGP) has recently been shown to achieve multifraction separation with high yields and resolutions (Krättli et al. 2013).

1.2.2.   Integrated downstream processes

Apart from the optimisation of chromatography, another strategy to streamline recovery and purification processes of biopharmaceuticals is the development of integrated techniques. These ideally combine several unit operations, thus reducing process time, running costs and capital expenditure (Schügerl and Hubbuch 2005). Furthermore, considering a virtually inevitable product loss in each step, a reduction in the number of unit operations results in an overall increased product yield (Figure 1.2).
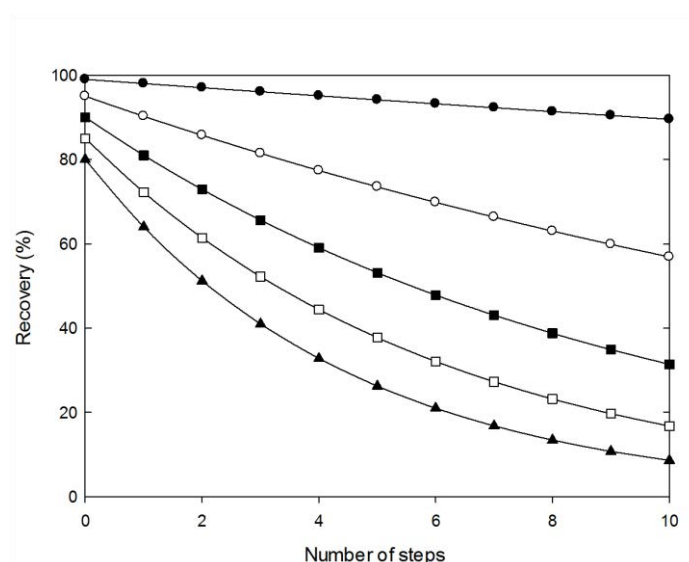
Figure 1.2: Correlation between number of downstream process steps and overall yield. Adapted from Fish and Lilly (1984).

One of these integrated methods is the aqueous two-phase extraction (ATPE). ATPE is a special case of liquid-liquid extraction which involves the selective enrichment of the target protein in one of the two aqueous, immiscible phases. Under certain conditions, usually depending on ionic strength and polymer concentration, the employed biphasic systems (aqueous two-phase systems or ATPS) spontaneously separate into an upper and lower phase (Soares et al. 2015). The phases mainly consist of water, with some of the added polymers featuring a stabilising effect on the protein structure; hence proving ATPS suitable for the partitioning of biomolecules (Azevedo et al. 2009). Moreover, ATPE permits the direct extraction of proteins from crude feedstocks and thus combines recovery, concentration and purification in one step. However, industrial application of ATPE has been hindered mainly due to poor understanding of the partition mechanisms and thus rather empirical method development (Azevedo et al. 2009). Screening of right conditions (e.g. polymer or salt concentration and type) is elaborate, but has been found to be immensely facilitated by the use of high throughput screening platforms (Bensch et al. 2007).

Another approach also eliminating several recovery and sample pretreatment steps involves the application of magnetic adsorbent particles (Franzreb et al. 2006). These can be functionalised, thus specifically binding target proteins from crude feedstocks. The subsequent collection and purification employing high-gradient magnetic separation (HGMS) has been termed high-gradient magnetic fishing (Franzreb et al. 2006). After washing and protein elution, the magnetic particles can be recycled. The characteristically non-porous adsorbents exhibit a high surface are to volume ratio, resulting in high binding capacities and rapid adsorption kinetics (Franzreb et al. 2006).

Recently, there have been efforts to combine the advantages of ATPS and HGMF, applying magnetic adsorbent particles in an aqueous micellar two-phase system

(AMTPS). AMTPS utilise surfactants that induce a phase split usually above or a below a certain temperature. The adsorbent particles partition completely into one of the phases, enhancing partitioning of the target protein. Simultaneously the speed of phase separation is increased by applying a magnet field (Becker et al. 2009; Paulus et al. 2014). These so called 'Magnetic Extraction Phases' (MEP) were also shown to feature in a novel continuous purification process (Fischer et al. 2013).

1.3. Expanded Bed Adsorption (EBA)

As part of the aim to reduce the number of steps in the downstream process, the idea of using a fluidised bed has existed for almost half a century. Bartels (1958) first purified the antibiotic streptomycin from whole broth employing fluidised cation exchangers. Later, Belter et al. (1973) applied anion exchange resin particles in a semi-continuous fluidised system for recovery of novobiocin. In the late 1980s and early 1990s, interest grew to adopt fluidised beds for the purification of a wider range of biomolecules, in particular proteins, directly from whole fermentation broths. While previous processes were based on the traditional chemical view of fluidised beds as well-mixed systems, this was found disadvantageous regarding adsorption performance in comparison to near plug flow conditions in packed beds. Magnetically stabilised beds were proposed as one solution to reduce axial mixing (Burns and Graves 1985), as well as the implementation of baffles to divide the bed into sections (Van Der Wiel 1989). However, scale up of these approaches would be complicated and required expensive equipment (Pharmacia 1997).

Early attempts for protein purification utilised fluidised beds of commercially available packed bed adsorbents (Draeger and Chase 1991; Chase and Draeger 1992). However, these were found unsuitable in systems containing cells and specific requirements were identified. Adsorbents should possess a higher density and a particular size distribution to

achieve a stable bed and expansions at a suitable linear flow velocity. This would result in a 'stratified' or 'classified' liquid fluidised bed, then termed expanded bed.

Consequently, a commercial material was developed consisting of quartz-core-weighted agarose particles. The availability of a purpose-designed adsorbent and suitable equipment made application of expanded bed adsorption (EBA) much easier and led to a rapidly grown interest and attraction (Hjorth 1997). This shows in numerous publications in the mid and late 1990s as well as early industrial applications. In 1996, Genentech (now part of Roche) were looking to replace a tangential-flow filtration step for purification of a tissue plasminogen activator product due to higher cell densities than expected. After considering centrifugation, depth filtration and extraction methods, they ultimately chose EBA to update the process (Scott 2005). As a first company, British Biotech plc submitted an FDA market application for a purification process employing EBA.

However, these first generation EBA processes were soon found to display several technical issues. In particular, the commonly employed fluid distribution system consisting of a mesh and perforated plate led to a build-up of cells and subsequent fouling, making regular back-flushes necessary for cleaning (Frej et al. 1997; Hubbuch et al. 2005). Furthermore, interactions between adsorbent particles and the applied biomass caused deteriorations in the hydrodynamics of the expanded beds, ultimately impairing sorption performance, which could even result in the complete collapse of the bed (Anspach et al. 1999; Feuser et al. 1999; Fernández Lahore et al. 2009). Since then, advances in the field of fluid distribution systems as well as systematic studies of biomass-adsorbent interactions with concurrent development of new adsorbents have strived to overcome these limitations and utilise EBA's full potential.

1.3.1. Concept

Expanded bed adsorption, sometimes also called expanded bed chromatography, is based on liquid chromatography (cf. 1.2.1) with regard to adsorption principles. A feed stream of a mixture containing the target compound as well as impurities is introduced into a column filled with adsorbent particles. Depending on the functionality of the resin, a specific interaction between the target molecules and the matrix promotes adsorption while the contaminants flow through without binding (see Table 1.1 for different interaction bases). After loading the feedstock to the column and subsequent washing of unbound compounds, buffer conditions are changed in order to elute the adsorbed molecule.

In contrast to traditional chromatography however, in which the feed stream is applied from the top, in EBA an upward flow is created by introducing the feed from the bottom. This allows the adsorbent particles to rise from its settled state, increasing the interparticle space so that even cells and cell debris are able to pass through without blocking the bed (Hjorth 1997). Packed bed columns are not suitable to process feed streams with suspended biomass due to particles becoming trapped within the bed, ultimately resulting in fouling or even a complete blockage of the column (Anspach et al. 1999). The possibility to directly apply crude feedstock in EBA eliminates the need for prior clarification steps such as centrifugation or filtration (Chase 1994; Sonnenfeld and Thömmes 2006). The integration of several unit operations, combining solid-liquid separation with initial purification, ideally leads to reduced process time, higher yield and overall lower costs (see also section 1.2.2, Figure 1.3).
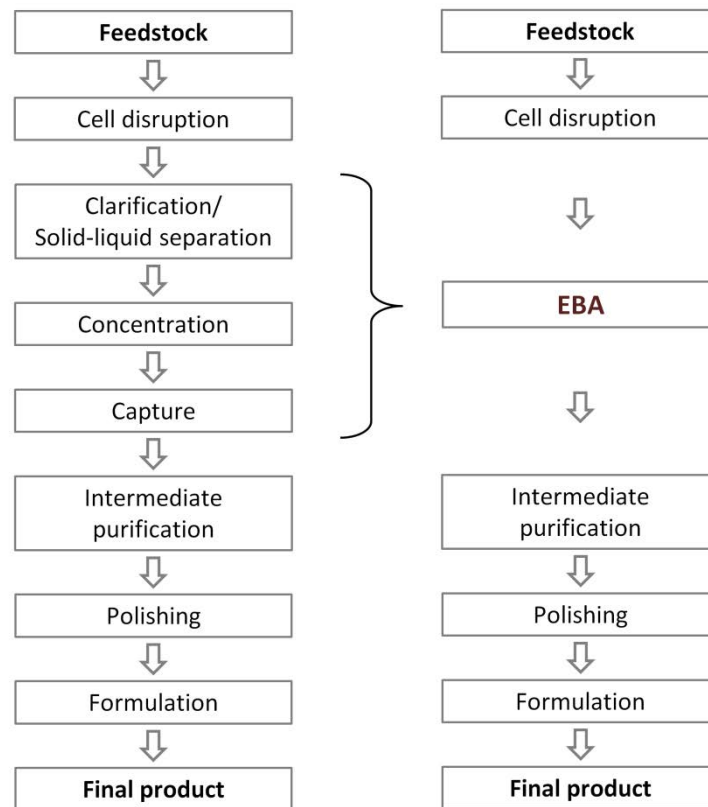
Figure 1.3: Comparison between a conventional downstream process (left) and streamlined purification employing expanded bed adsorption (EBA), thereby combining clarification, concentration and capture in one unit operation.

As mentioned above, in stark contrast to conventional fluidised beds, EBA relies on low backmixing within the column. A well-mixed system, similar to a stirred tank, presents effectively a single equilibrium stage. A single stage however decreases the efficiency of the adsorption process, reduces capacity and resolution (Thömmes et al. 1995; Pharmacia 1997; Thömmes 1997). An essential feature of the EBA technique is the use of specifically designed adsorbents with a defined size and density distribution, resulting in a classified or stratified bed. This means that the larger and denser resin beads are located in the lower part of the bed, while the smaller and lighter particles are found closer to the top (Chase 1994; Hjorth 1997). The resulting gradient of particle sizes and densities considerably reduces mixing of the matrix beads within the bed, ideally leading to a stable, expanded bed (Figure 1.4).
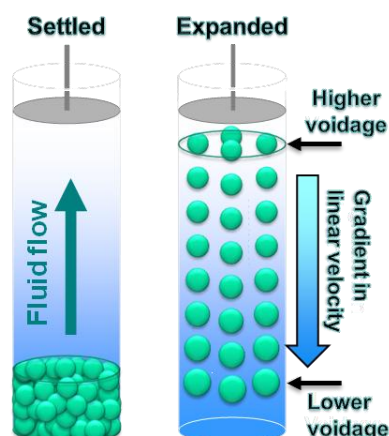
Figure 1.4: Schematic illustration of the expanded bed adsorption process. Size proportions not depicted accurately to clarify gradients in adsorbent particle size, voidage and linear velocity. Copyright by Owen R.T. Thomas.

1.3.2. Operation

First, a specific volume of adsorbent particles is poured into the column to achieve the required settled bed height. This saves the procedure of packing the bed to a sufficient quality, which in conventional chromatography can present a challenging task. As briefly discussed above, similar to traditional chromatography, EBA is predominantly employed in elution mode. During equilibration, a liquid flow velocity is set in order to achieve a certain degree of bed expansion. The resin beads are allowed to find their position within the bed to achieve classification, before the crude feedstock is applied. As the physical properties of the feedstock differ to those of the equilibration buffer, in particular exhibiting a higher viscosity, if the flow rate is kept constant the bed expansion further increases (Anspach et al. 1999). The density of the adsorbent beads has to be high enough to ensure the smallest ones are not being elutriated from the column together with the particulate matter of the feedstock. After loading, a subsequent washing step is required to remove remaining particulates from the column. To guarantee that no feedstock material is left within the bed, it is necessary to apply several column volumes and

perform an intensive wash. The following elution can be carried out in packed or expanded bed mode (Figure 1.5).
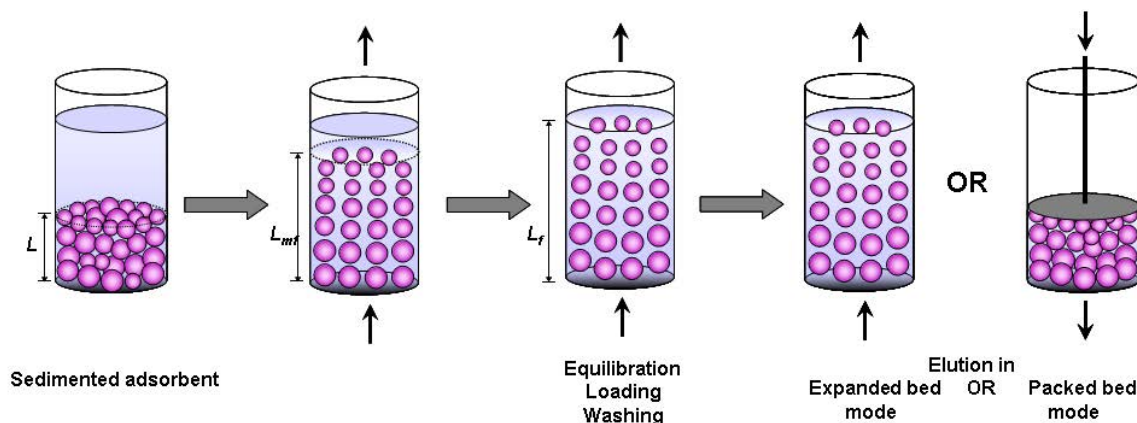
Figure 1.5: Schematic illustration of the expanded bed operation. Copyright by I. Theodossiou.

Elution in packed bed mode reduces the volume of eluent used, thus increasing the product concentration (Chase 1994). Hjorth et al. (1995) found that carrying out elution in expanded mode results in a 40% increased elution volume. Additionally, Chase (1994) highlighted the fact that in packed mode, elution protocols, including flow velocities and gradient procedures, can be chosen independent from bed expansion characteristics. However, Lihme et al. (1999) emphasised that on the other hand, elution in packed bed mode complicates and slows down the process because of the necessary flow reversal, packing and re-expansion of the bed in each cycle. Furthermore, adsorbent particles may aggregate when packed during elution which may subsequently impair re-expansion of the bed. They concluded that the advantages of a simplified and more robust process outweighed the increased elution volume in expanded mode, especially as these could be minimised by using lower flow rates (Hjorth 1999; Lihme et al. 1999).

Due to application of crude feedstock, an intensive cleaning-in-place (CIP) step is required after elution. This ensures the preservation of the adsorbent particles' functionality and the ability to re-use the resin in multiple cycles. Moreover, CIP should prevent the biological hazard of carrying over material between batches by removing all

potentially left impurities (Chase 1994; Hjorth 1997; Anspach et al. 1999). Suitable reagents for CIP procedures usually include 1M NaOH, 70% ethanol, 6M urea or 30% isopropanol (Chase 1994).

1.3.3. Equipment

Most of the equipment needed for the operation of EBA is similar to that used for traditional packed bed chromatography, i.e. pumps, online spectrophotometry, conductivity and pH measurement as well as fraction collection (Chase 1994; Hjorth 1997). Specific requirements have to be met in the design of the columns used for EBA. First, they have to be longer than usual packed bed columns to ensure enough space for expansion. Second, a special fluid distribution system has to be employed in the bottom of the column to evenly introduce the liquid stream over the entire cross-sectional area of the column base (Hubbuch et al. 2001). This should ideally lead to a plug flow-like fluid rise through the bed to minimise back-mixing and maximise the number of theoretical equilibrium stages, resulting in an overall good process performance (Chase 1994).

The first fluid distribution mechanisms used a system of perforated plates and an overlying mesh (Hjorth 1997; Pharmacia 1997; Anspach et al. 1999). The perforated plate creates a pressure drop necessary for the fluid to pass evenly through the base of the column. The mesh or net on top of the perforated plate minimises jet streams and channelling, while at the same time preventing the resin beads from leaving the column (Pharmacia 1997; Hubbuch et al. 2002). The mesh should have a pore size big enough for particulate matter to pass through but small enough to retain the adsorbents in the column. Still, buildup of particulate matter, cells and cell aggregates under the mesh have been reported which resulted in partial blockage of the net, causing turbulence and deteriorated flow distribution (Anspach et al. 1999; Hubbuch et al. 2002). Repeated

backflushes have been suggested to remove particulate buildup (Frej et al. 1997), which however complicate the process and may lead to further aggregation. If CIP procedures are not sufficient and fouling persists, disassembly of the distributor may be necessary (Anspach et al. 1999).

A different fluid distribution system presented by Zafirakos and Lihme (1999) avoids the use of a perforated plate and mesh. This design is based on a laterally connected inlet and a central stirrer blade. A well-mixed zone in the lower part of the bed is created, while stable expansion above could be obtained. Menkhaus and Glatz (2005) compared and evaluated the performance of three different inlet designs - mesh, glass beads and local mixing - for the purification of a human secretory antibody from corn endosperm extracts by EBA. While localised mixing was found to be the least efficient with respect to plate numbers, the mesh type distributor led to clogging of the inlet during crude feed application. Scale-up of the local mixing approach was also questioned as it may be difficult to retain localised mixing to a small zone while maintaining good fluid distribution at larger scale (Hubbuch et al. 2002). For this reason Hubbuch and co-workers (2002) invented a rotating fluid distributor (RFD) and demonstrated that a flow pattern suitable for EBA could be generated in a 150 cm diameter column. Subsequently Arpanaei et al. (2008) compared the rotating fluid distributor to local stirring in large scale columns, where the RFD was found to achieve better hydrodynamic characteristics in both cases studied. Fluid distribution using the local stirrer created dead zones which remained even when increasing rotation rates or flow rates. Furthermore, oscillation rather than rotation of the RFD was investigated but also found to result in increased mixing and poorer performance.

Another aspect of the column design is the outlet. Most systems use a top adapter, which has to be movable in order to operate the column at different bed heights (Hjorth 1997;

Anspach et al. 1999). During operation, the adapter needs to be positioned just above the top of the bed to minimise the dead volume of the liquid (Chase 1994). If elution is to be performed in packed mode, the adapter must be capable of being lowered onto the surface of the settled bed. Altering the position of the upper adapter can be done manually, hydraulically or by using special floating devices (Anspach et al. 1999). Other systems completely omit a top adapter and employ a simple pipe or tube as outlet (Zafirakos and Lihme 1999). Its height is adjustable and it can easily be lowered or raised to minimise the liquid headspace.

A more advanced approach to keep a suitable distance between the top of the bed and the upper adapter has been described by Thelen et al. (1997). They were able to monitor the bed height during application of a cell-containing feedstock by using an ultrasonic sensor. This has only recently been implemented in commercially available columns (Biotechflow Ltd). Ghose et al. (2000) examined bed height monitoring using an LED based sensor configuration. They connected the output to an algorithm for pump control to automatically adjust the flow rate to maintain a constant bed expansion.

During operation, the column should be placed in a perfectly vertical alignment as even small deviations can result in increased dispersion and thus impaired separation efficiency (Anspach et al. 1999; Bruce et al. 1999). Some small scale columns are therefore provided with tri-pod stands allowing easy adjustment in aligning (Pharmacia 1997).

1.3.4. Adsorbents

Apart from column design and appropriate fluid distribution, the design of specific adsorbent particles is a key factor to enhance the efficiency of EBA (Li et al. 2014). The

formation of a stable classified bed generating a low degree of axial mixing is crucial for the chromatographic separation performance. Classification is created by using matrices with a defined size and density distribution. Compared to traditional packed bed resins, EBA adsorbents have to exhibit generally higher densities to avoid elutriation at the top of the bed due to direct application of highly viscous crude feed streams. Denser particles allow higher flow velocities, thereby improving the process' productivity (Mattiasson and Nandakumar 2000). However, flow shouldn't be too fast to impair adsorption kinetics. A compromise has to be found between the adsorbents physical properties such as size, density and pore size, which determine the applicable flow velocities, and adsorption kinetics (Anspach et al. 1999; Lihme et al. 2000).

There are different approaches to manufacturing beads with enhanced density. One of these is based on porous gel materials usually employed for packed bed matrices such as agarose or cellulose. An increase in density is realised by incorporating or encapsulating dispersed solid particles such as quartz, zirconia, titanium or tungsten carbide (Hubbuch et al. 2005; Li et al. 2014). Another approach is to utilise a single high-density, non-porous solid core made of glass or stainless steel and subsequent coating with a porous surface. A different design, sometimes termed 'gel-in-a-shell' (Xia et al. 2007), consists of a soft, high-capacity hydrogel core surrounded by a rigid zirconium oxide shell. In principle, all types of resin designs can be coupled and functionalised with suitable ligands for anion or cation exchange, hydrophobic or mixed-mode interaction as well as affinity adsorption.

Apart from the adsorbent density, the particle size and size distribution is of major importance for an expanded bed operation. Al-Dibouni and Garside (1979) found that at adsorbent size ratios (i.e. the ratio between the maximum and minimum particle diameter) of greater than 2.2, classification rather than mixing dominates the bed behaviour. Lihme et al. (2000) suggest an optimal ratio of about 3 to create a stable classified bed.

Generally, denser particles may be smaller in particle size, thereby reducing mass transfer and increasing dynamic adsorption capacities (Anspach et al. 1999; Xia et al. 2007; Kelly et al. 2013). Karau et al. (1997) investigated the influence of the particle size distribution on the adsorption performance in expanded beds. They studied three different particle size fractions and found reduced dispersion for operation using a wider size distribution, hence confirming Al-Dibouni and Garside. Furthermore, smaller mean particle diameters lead to increased breakthrough capacities due to smaller diffusion path lengths within the adsorbents. However, in columns with a fluid distribution system employing a mesh, smaller particle sizes require a net with smaller pore sizes for retention of the resin beads, making them even more susceptible for blockage (Anspach et al. 1999).

An extensive overview of commercially available as well as 'homemade' adsorbents as used for research purposes and reported in literature, their composition and suppliers (where applicable) is provided by Li et al. (2014).

1.3.5. Hydrodynamic principles

A bed of solid particles transitions into a fluidised state when the weight of the particle is balanced by the fluid-particle interaction force (Di Felice 1995). This is achieved for fluid velocities greater than the minimum fluidisation velocity u_{mf}. At flow rates below u_{mf}, the bed behaves like a packed bed (Anspach et al. 1999). With increasing flow velocities, the column back pressure increases until it is in equilibrium with the particles' gravitational force:

$$\Delta P = (1 - \varepsilon)(\rho_p - \rho_l)gH(\varepsilon) \qquad \text{(Eq. 1.1)}$$

where ΔP is the pressure drop, ε is the bed voidage, ρ_p and ρ_l are the densities of the adsorbent particle and the liquid, g is the gravitational force and H is the height of the

expanded bed. At the point of the minimum fluidisation velocity, all particles are suspended and separated from each other. Further increasing the flow velocity results in an increased bed expansion, while the back pressure remains constant (Figure 1.6).
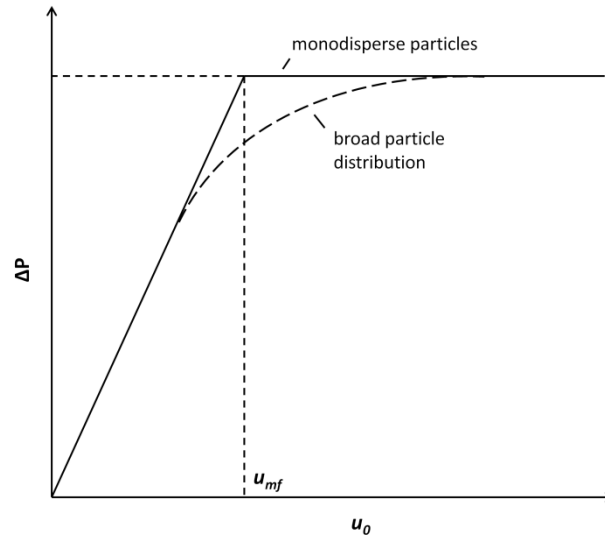
Figure 1.6: Influence of flow velocity on the pressure drop in a sedimented particle bed.

The intersection of the increasing back pressure curve at low flow rates and constant back pressure in the expanded bed determines u_{mf}. However, a sharp transition only occurs for monodisperse particles, whereas in a bed composed of particles with a range of sizes there is a gradual transition from settled to fluidised bed (Anspach et al. 1999; Theodossiou et al. 2002).

The maximum fluid velocity is determined by the particle's terminal settling velocity u_t, above which the adsorbent bead will be washed out of the column (Sonnenfeld and Thömmes 2006). At the terminal settling velocity, the gravitational force, the buoyancy and the flow resistance are in equilibrium. In the creeping flow range where the particle Reynolds number $Re_p < 0.2$, u_t can be described by the well-known Stokes law (Hjorth et al. 1998):

$$u_t = \frac{(\rho_p - \rho_l)d_p^2 g}{18\eta}$$ (Eq. 1.2)

Here, d_p is the adsorbent diameter and η is the fluid viscosity. The particle Reynolds number at the terminal settling velocity Re_t can in turn be calculated from

$$Re_t = \frac{u_t\, d_p \rho_l}{\eta}$$ (Eq. 1.3)

Stokes law (Equation 1.2) shows the important parameters influencing bed fluidisation. The terminal settling velocities of adsorbent particles fluidised in a given feedstream are dictated by their diameters and densities. The larger and denser beads exhibit higher settling velocities and find their location in the lower part of the bed. Their position depends on the local voidage, which in turn determines the local interstitial velocity of the fluid. The bed exhibits an axial gradient of voidage and interstitial fluid velocities and at each point within the bed, the particles' terminal settling velocities are in equilibrium with the interstitial fluid velocity (Hubbuch et al. 2005).

This classification of adsorbent particles has been confirmed by a number of experimental investigations. Willoughby et al. (2000) employed side ports for in-bed sampling at different heights of the expanded bed and found that the particle size was radially constant, while it decreased with increasing axial height. They also showed that the voidage within the bed increased with height and furthermore, it increased at a certain axial position with increased flow velocity. Bruce and Chase (2001) as well as Tong and Sun (2002) observed similar results despite using slightly different sample ports as well as particles with different initial size ranges. It was however emphasised, that the particles were not *tightly* classified within the bed, as particle size distributions at the various heights overlapped, suggesting an overall significant distribution of different-sized beads throughout the column (Bruce and Chase 2001). Both Bruce and Chase (2001) as well as Tong and Sun (2002) found only a small influence of the density to classification, however

this was due to the relatively uniform density distribution of the adsorbents used (Streamline, Pharmacia). In contrast, Tong and Sun also investigated particles with a wide density distribution (6% agarose coated steel beads), which were classified according to their density rather than size.

To describe the degree of bed expansion, a bed expansion factor is often used calculated as the ratio of settled bed height H_0 to the expanded bed height, H. Richardson and Zaki (1954) introduced a correlation for the influence of hindering effects of a cloud of solid particles on their settling velocities. These effects depend on the particle concentration (i.e. voidage) and the correlation is used to predict bed expansion at a given fluid velocity u (Anspach et al. 1999; Theodossiou et al. 2002):

$$\frac{u}{u_t} = \varepsilon^n \qquad\qquad (Eq.\ 1.4)$$

Here n is the Richardson-Zaki index; in the case of EBA operation where $Re_p < 0.2$ and the ratio of particle to column diameter is small ($d_p/d_c < 0.01$), n is constant ($n = 4.65$) (Thömmes et al. 1995; Thömmes 1997; Anspach et al. 1999; Theodossiou et al. 2002). The expansion factor can then be determined with:

$$\frac{H}{H_0} = \frac{(1 - \varepsilon_0)}{(1 - \varepsilon)} \qquad\qquad (Eq.\ 1.5)$$

where ε_0 is the settled bed voidage, which is generally assumed to be 0.4 (Anspach et al. 1999).

However, it has been found in a number of studies that the Richardson-Zaki correlation (Equation 1.4) with the assumptions made for the index n is not suitable for actual EBA operations applying crude feedstock (Karau et al. 1997; Theodossiou et al. 2002; Hubbuch et al. 2005). Different values for both u_t from Equation 1.2 as well as n have

been reported, resulting in the need to experimentally determine both for each individual system (Hubbuch et al. 2005).

As mentioned before, axial mixing of the solid as well as the liquid phase within the bed has to be kept to a minimum to achieve good chromatographic performances (Chase 1994; Hjorth 1997). Axial mixing in EBA is commonly evaluated and characterised by conducting residence time distribution (RTD) studies. There are two models to subsequently analyse RTD data - the tanks-in-series and the dispersion model (Levenspiel 1999; Theodossiou et al. 2002). A pulse or a step input of a tracer is applied to the column and its concentration measured in the exit stream.

In the dispersion model, an axial dispersion coefficient D_{ax} is employed which represents the spreading of the tracer curve and thus characterises the degree of backmixing. In dimensionless form, the term $D_{ax}/(u_i\,H)$ is introduced as vessel dispersion number, where u_i is the interstitial fluid velocity ($u_i = u/\varepsilon$). The vessel dispersion number relates dispersion to convective flow (Theodossiou et al. 2002), so for very small values of $D_{ax}/(u_i\,H)$, dispersion is negligible and plug flow is approximated, while for very large values mixed flow can be assumed.

For low degrees of dispersion ($D_{ax}/(u_i\,H) < 0.01$), the tracer curve changes very little in shape and a symmetrical curve is assumed (Levenspiel 1999). Under these conditions, the dimensionless variance $\sigma_\theta{}^2$ can be calculated as:

$$\sigma_\theta^2 = \frac{\sigma^2}{t_m^2}$$

(Eq. 1.6)

where t_m is the mean residence time and σ the variance. Equation 1.6 can subsequently be used to determine the vessel dispersion number:

$$\sigma_\theta^2 = 2\frac{D_{ax}}{u_i H} \tag{Eq. 1.7}$$

For higher degrees of dispersion and larger deviation from plug flow ($D_{ax}/(u_i H) > 0.01$), however, the tracer response is broad and spread, resulting in a nonsymmetrical curve. In this case, the vessel dispersion number has to be calculated from:

$$\sigma_\theta^2 = 2\left(\frac{D_{ax}}{u_i H}\right) - 2\left(\frac{D_{ax}}{u_i H}\right)^2 \left(1 - \varepsilon^{-\left(\frac{u_i H}{D_{ax}}\right)}\right) \tag{Eq. 1.8}$$

The reciprocal of the vessel dispersion number is often also called Bodenstein number Bo or Peclet number Pe (Yamamoto et al. 1999). However, as Bo is derived from mass transfer and Pe from heat transfer, neither is in fact the correct description (Hubbuch et al. 2005). Still, the value of the dimensionless number is the same irrespective of the term used and both Bo and Pe are widely used in EBA publications.

The tanks-in-series model is based on the assumption of a number N of ideal mixed flow units (or, in the case of EBA, theoretical plates) which are consecutively connected. For high values of N, plug flow is obtained and the tracer response curve becomes symmetrical. Under these circumstances, the tanks-in-series and the dispersion model can be coupled and N determined with:

$$N = \frac{t_m^2}{\sigma^2} \tag{Eq. 1.9}$$

The height equivalent to a theoretical plate HETP can subsequently be calculated:

$$HETP = \frac{H}{N} \tag{Eq. 1.10}$$

It has to be considered however that the experimental procedure to obtain those parameters results in values dependent on the whole system set-up from the tracer input

to the measurement, i.e. including pumps, valves and tubing (Frej et al. 1997). Therefore, overall results may not be directly comparable between different system set-ups. It has however been established as a rule of thumb that for Bo > 40 axial dispersion has little effect on the performance of the EBA operation.

1.3.6. Biomass-adsorbent interactions

Achieving a stable bed with good hydrodynamics in a buffer system is essential for an efficient EBA process, however, the effect of applying crude feedstock containing cells and cell debris on fluidisation and adsorption performance has to be considered (Sonnenfeld and Thömmes 2006). If biomass particulates interact with adsorbent beads, channels and stagnant zones may form during sample application, leading to impaired bed stability and hydrodynamics (Feuser et al. 1999). In extreme cases, when biomass components cause severe agglomeration between adsorbents, this may even result in the complete collapse of the bed (Fernandez-Lahore et al. 1999; Feuser et al. 1999; Theodossiou and Thomas 2002). Besides, the binding capacity and sorption efficiency may be reduced due to deteriorated bed stability as well as penetration of cells or cell debris into the pores and a masking effect of the adsorbent surface (Feuser et al. 1999; Lin et al. 2004). Furthermore, if the biomass is desorbed under elution conditions, the product solution will be contaminated. Otherwise, tightly bound material will require harsh regeneration conditions, which may affect the stationary phase. If even under those conditions the cellular components cannot be removed, irreversible fouling effects may build up over time (Feuser et al. 1999).

For these reasons it is essential for a successful EBA operation that biomass-adsorbent interactions are minimised. A number of methods have been developed over the years which aim to identify, evaluate and control potential interactions as an early part during

the process design (Lin et al. 2001; Lin et al. 2004). In finite bath experiments, a dilute suspension of biomass is incubated with the adsorbent particles in a gently stirred vessel. The cell concentration is measured over time by the decrease of optical density (Fernández-Lahore et al. 2000). Finite bath experiments present a simple and quick tool for initial screening (Lin et al. 2001). In a different technique, a pulse of biomass is applied to a stable expanded bed, while the cell concentrations before and after the bed are measured. A cell transmission index (CTI) can then be calculated as the fraction of biomass leaving the column (Feuser et al. 1999; Hubbuch et al. 2005). A more detailed analysis is provided by residence time distribution studies during application of real feedstock in the EBA process. Non-interacting tracers have to be used which are still detectable against the background of the applied particulate suspension (Fernandez-Lahore et al. 2001). Fluorescent molecules such as tryptophane had been shown to be suitable up to a certain maximum biomass content (Fernandez-Lahore et al. 1999), before potentiometric detectors based on ion-selective electrodes were successfully employed with bromide or lithium ions as tracers (Fernandez-Lahore et al. 2001). The response signal is then analysed using an advanced RTD model, which divides the bed into a stable fraction ϕ with its respective Peclet number (Pe) and a stagnant zone with an impaired fluidisation (1-ϕ).

Since it was found that the severest issues with biomass-adsorbent interactions were encountered using anion exchange adsorbent particles (Feuser et al. 1999; Fernández-Lahore et al. 2000; Lin et al. 2001), it was assumed that the electrostatic interaction between the negatively charged cells and cell debris and the positively charged adsorbents was the most important factor influencing this phenomenon. Zeta-potential measurements indicating the surface charges of the adsorbent as well as the applied biomass could be related to the cell transmission index CTI and were proposed as a fast screening method (Lin et al. 2004). Following from this, the use of the extended DLVO

(Derjaguin, Landau, Verwey, Overbeek) theory was investigated, which apart from electrostatic also accounts for Lifshitz-van der Waals and acid-base interactions for a more comprehensive approach (Vennapusa et al. 2008).

From the results of these tests, a window of operation can be found for optimal feedstock conditions (i.e. pH, conductivity) in order to minimise biomass-adsorbent interactions while simultaneously remaining good target protein binding (Lin et al. 2001). A different attempt examined the effect of a reduction of cell debris size by homogenisation which resulted in a lower degree of biomass adsorption, but also reduced binding capacity (Hubbuch et al. 2006). A complete redesign of expanded bed supports exhibiting 'non-stick' surfaces has been suggested by Theodossiou and Thomas (2002), and different strategies have been explored. One of these involves coating or shielding the adsorbent beads with polyelectrolytes (Dainiak et al. 2002; Dainiak et al. 2002) or with a layer of polymers such as agarose (Viloria-Cols et al. 2004; Jahanshahi et al. 2008) or a synthetic polymer (Vennapusa and Fernandez-Lahore 2010). All of these studies showed a reduction in biomass-adsorbent interactions, however, the technological practicability of casting sufficiently thin and uniform layers without implications on bed expansion properties, hydrodynamics as well as mass transfer has been questioned (Arpanaei et al. 2010). In this work, low temperature glow discharge plasma was successfully used to prepare bi-layered SEC-IEC expanded bed adsorbents with non-adhesive exteriors.

1.4. Positron Emission Particle Tracking (PEPT)

The technique of positron emission tomography (PET) has long been successfully employed in the medical field as a non-invasive imaging method for diagnosis (Maisey 2005). Here, a positron-emitting radioactive tracer is introduced into the body and its location monitored by detection of back-to-back γ-rays formed after annihilation of the

positron with an electron. An image of the tracer distribution is then constructed from a large number of incident γ-rays. PET has similarly been applied in studies of industrial engineering and physical processes (Hawkesworth et al. 1986; Barigou 2004). Due to its ability to investigate fluid flow within dense and opaque systems it shows advantages over optical methods such as particle image velocimetry (PIV) (Barigou 2004). However, PET is not suitable for the study of dynamic systems due to the time required to generate adequate statistics for 3D imaging, and it primarily produces time averages of a steady state system (Leadbeater et al. 2012).

Therefore, a technique called positron emission particle tracking (PEPT) has been invented at the University of Birmingham Positron Imaging Centre which allows the study of rapidly changing flow as often encountered in industrial processes (Parker et al. 1993). PEPT relies on the same principles as PET, but rather than detecting the volume distribution of a tracer fluid, a single radioactive particle is tracked as it moves through the system (Parker et al. 2002; Leadbeater et al. 2012). In contrast to PET, the statistics required for precise location of a point-like source are much less than those for a volume image. Under optimum conditions, PEPT enables the detection of trajectories of a particle moving at speeds up to 10 m/s at rates of circa 1 kHz and with a precision of around 0.5 mm in 3D (Leadbeater et al. 2012). Hence, PEPT demonstrates to be an ideal technique to study granular and liquid process systems, such as fluidised beds, granular gases, stirred tanks, rolling drums, mixing systems and multiphase flow (Parker and McNeil 1996; Parker et al. 2005; Seville et al. 2005; Bakalis et al. 2006; Guida et al. 2009).

1.4.1. Theory and physics behind PEPT

PEPT, similarly to PET, is based on the use of unstable atomic nuclei possessing an excess number of protons. These radioactive isotopes undergo rapid positron emission or β^+ decay. In β^+ decay, one of the excess protons is converted into a neutron (n), a positron (e^+) and an electron neutrino (ν_e):

$$p \rightarrow n + e^+ + \nu_e \qquad \text{(Eq. 1.11)}$$

Isotopes following β^+ decay which are commonly used for PET include ^{11}C, ^{13}N, ^{15}O, ^{18}F, ^{64}Cu, ^{68}Ga and ^{89}Zr. In the case of ^{18}F for example, the isotope decays into ^{18}O after:

$$^{18}_{9}F \rightarrow\ ^{18}_{8}O + e^+ + \nu_e \qquad \text{(Eq. 1.12)}$$

After ejection from the nucleus, the positron loses its kinetic energy in collision with atoms of the surrounding matter (Cherry et al. 2012). Depending on the density of this surrounding matter, but usually within a few millimetres, the positron comes to rest and subsequently combines with an electron in an annihilation reaction. In this, their masses are converted into energy, resulting in two back-to-back (i.e. 180 degrees apart) γ-rays with typical energies of 511 keV each. The events occurring during positron emission decay and the following annihilation are depicted in Figure 1.7.
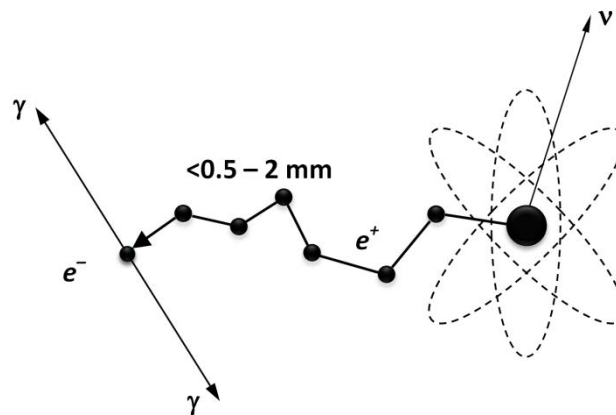
Figure 1.7: Positron emission decay of a radioactive isotope. The positron (e+) is emitted together with a neutrino and moves randomly through the surrounding matter before it annihilates with an electron, resulting in two diametrically opposed 511 keV γ-rays.

The pairs of gamma photons can then be detected by two position-sensitive camera heads, mounted on either side of the field of view (Parker et al. 2008). Simultaneous detection of both γ-rays defines a Line of Response (LoR) along the photon trajectory, on which the annihilation is assumed to have occurred (Leadbeater et al. 2012). A small number of LoRs acquired over a short timescale are then used to determine the location of the point of decay (and thus, the tracer particle) employing an iterative triangulation approach (Leadbeater 2009). These three subsequent steps are illustrated in Figure 1.8.
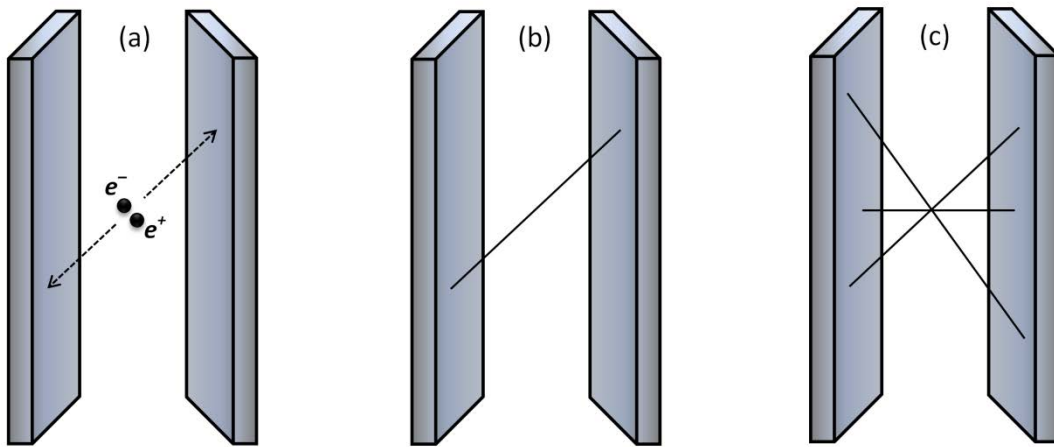
Figure 1.8: Principles of PEPT. (a) Annihilation of a positron and an electron and subsequent coincident detection of the two resulting γ-rays by the camera heads. (b) Reconstruction of a Line of Response (LoR) along the photon trajectory. (c) Location of the point of decay using a number of reconstructed events and triangulation. Adapted from the Positron Imaging Centre, University of Birmingham.

In theory, using a single radioactively labelled particle should lead to all measured LoRs intersecting at the same point, i.e. the point of decay, to within the resolution of the positron camera (Parker et al. 2008). However, in practice some of the events are corrupt and do not reflect the real tracer position. This may be due to scattering of one or both photons or so called random coincidences, when events from separate annihilations occur within very short time and are considered to be coincident. Some radioisotopes exhibit associated γ-rays possessing a different energy than the typical 511 keV. The PEPT algorithm has therefore been developed by Parker et al. (Parker et al. 1993) to eliminate these corrupt events and the consequent background noise.
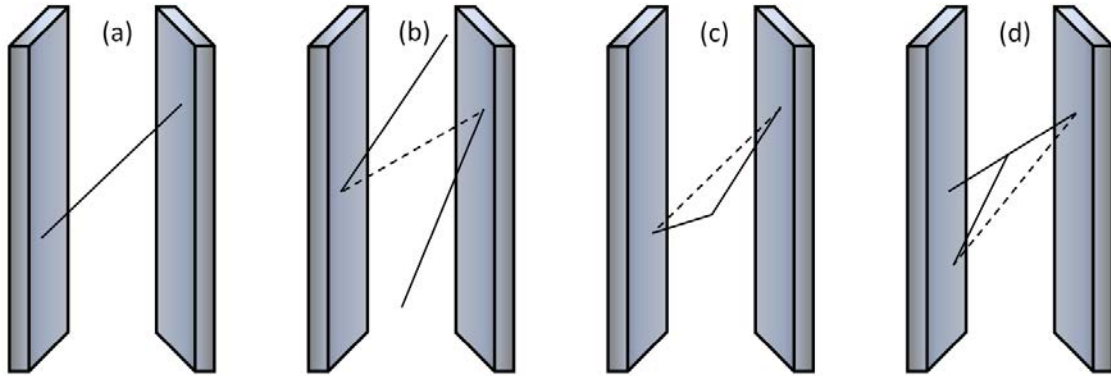
Figure 1.9: Schematic of possible positron emission event types: (a) true, (b) random, (c) scattered, (d) associated. Solid lines depict actual photon trajectories, dashed lines illustrate the reconstructed line of response. Adapted from Leadbeater (2009).

In this algorithm, a small number of events (N) is used and their minimum distance point is calculated as the point closest to where all photon trajectories pass (Leadbeater 2009; Leadbeater et al. 2012). This point is determined by minimising the sum of perpendicular distances between each LoR of the set (N). It is then taken as an initial estimate of the tracer location, as most LoRs will be found close to this position. Events with LoRs that lie furthest away from this point are recognised as corrupt and are discarded. A fixed parameter k is used that determines how many events are rejected by eliminating those with distances larger than the mean deviation of the trajectories from the minimum distance point multiplied by k. Subsequently the minimum distance point is recalculated from the remaining set of events, giving an improved particle location with a smaller mean deviation. This process will be iterated until the set of events is reduced to a specific pre-defined fraction f of the initial set N. The location of the tracer is determined as the minimum distance point for this final fraction of events, with a precision defined by the mean perpendicular distance from each LoR to this point (Leadbeater et al. 2012).

The precision of locating a stationary particle (Δ) can be calculated for an initial set of events N and defined final fraction f as:

$$\Delta = \frac{w}{\sqrt{fN}} \qquad\qquad \text{(Eq. 1.13)}$$

where w is the spatial resolution of the camera found to be circa 5 mm (Parker et al. 2008). The value of f is given by the proportion of corrupt events and depends on the system set-up under study, i.e. the amount of surrounding matter that may lead to scattering of the photons, but also camera geometry and tracer activity, as high activities may result in more random coincidences (Leadbeater 2009). Typical values for f range between 0.05 and 0.4 and an optimum can be found for each system where enough erroneous photon trajectories are discarded while still enough events are kept for reduction of statistical noise (Parker et al. 2008; Leadbeater et al. 2012). As Equation 1.13 indicates, a large number of initial events (N) makes the precision in each location (Δ) in turn very small, thus high data rates give more precise results. However, for a moving tracer particle the timescale over which these events are acquired has to be small enough so that the motion does not impair the location process (Parker et al. 2008). Still, as this is only the case for very fast moving particles and low event rates, large values of N can be used in most scenarios (Leadbeater et al. 2012).

The algorithm described above is based on a single tracer particle within the field of view. As in some cases it may be useful to track more than one particle at the same time, an advanced algorithm has been developed for simultaneous detection of up to three tracer particles (Yang et al. 2006). This is based on the standard PEPT algorithm, in which the discarded events are subsequently re-examined to find second and third particle. The algorithm only works, however, if the activities of the particles significantly differ from each other and if the distances between each other are further than the spatial resolution of the camera. Moreover, it is not capable of tracking at high speeds since it requires a larger number of events than the standard PEPT algorithm. In general, multiple tracking is not

as precise as single tracking and should only be used when necessary (Parker et al. 2008).

1.4.2. Tracer labelling

As briefly described before, the PEPT technique relies on labelling a tracer particle with a positron emitting isotope, subsequently introducing it into the system under study mounted between the positron camera heads and detecting its position over time using the PEPT algorithm. It is essential that suitable particles, either directly from the bulk material or substitutes, can be radioactively labelled and used as tracer. In granular and liquid processes as those studied with PEPT, the particle movement depends on its size, density, shape as well as surface properties. Therefore, in order to realistically reflect the behaviour of the system, representative particles have to be chosen with similar physical and chemical characteristics to those of the particles of interest (Fan et al. 2006; Leadbeater et al. 2012). It is also possible to use PEPT for characterisation of liquid flow. For this, a neutrally buoyant tracer particle is employed to display flow of a specific element of the liquid phase.

Apart from representing the system under study, it is necessary that the tracer particle can be labelled with sufficiently high radioactivity. If the activity is low and not enough events can be detected, the location of the tracer cannot be tracked with adequate precision (see section 1.4.1). Equation 1.13 shows that the number of initial events used for the PEPT algorithm (N) has to be made sufficiently large, in particular for smooth tracking of fast-moving tracers and when many events are corrupt, e.g. due to increased scattering in systems with a lot of surrounding matter. Consequently, tracer particles should exhibit radioactivities in a range from around 300 to 1000 µCi, depending on the experimental conditions (Fan et al. 2006; Leadbeater et al. 2012). Activities in tracers

depend on their size, porosity and composition. In some cases, lower activities are acceptable when particle motion is very slow and high values of N can be used, but usually activities below 100 µCi are considered to be insufficient.

Among the existent positron emitting radioisotopes, those used for labelling have to be chosen according to their half-lives as well as ease of production. Appropriate half-lives should on the one hand be short enough to avoid continued radioactivity, because it may be difficult to remove the tracer from the bulk of particles after an experiment. On the other hand, it should be long enough that detection of the tracer with sufficient activity is possible over the timescale used for the experiment (Fan et al. 2006). The isotopes produced and used at Birmingham's Positron Imaging Centre include ^{66}Ga, ^{22}Na, ^{18}F, ^{61}Cu and ^{64}Cu. Out of these, ^{18}F is the most commonly used, because it only emits 511 keV γ-ray annihilation photons, unlike e.g. ^{22}Na, which has an associated gamma emission at an energy of 1274 keV. Besides, it has a convenient half-life of 110 min, which is suitable for most experimental timescales. Furthermore, the ^{18}F isotope can be readily prepared by the Birmingham MC40 cyclotron. The cyclotron uses a 35 MeV ^{3}He beam to bombard either purified water or solid materials and ^{18}F is generated via two competing nuclear conversion reactions:

$$^{16}O(^{3}He, p)^{18}F \text{ and } ^{16}O(^{3}He, n)^{18}Ne \rightarrow {}^{18}F \qquad \text{(Eq. 1.14)}$$
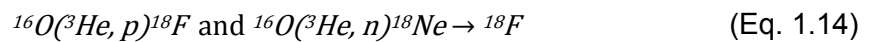
Three different methods to label tracer particles for PEPT have been developed: direct activation, indirect activation via ion-exchange or surface adsorption, and surface modification (Fan et al. 2006; Fan et al. 2006; Parker and Fan 2008; Leadbeater et al. 2012).

In the case of direct activation, a tracer particle is held under the beam from the cyclotron and ^{18}F is generated within the tracer itself by either of the abovementioned conversion reactions 1.14. The final radioactivity achieved in a tracer by direct activation depends on

the particle cross-sectional area, its oxygen content, the intensity of the beam current and the irradiation time. As the bombardment leads to high temperatures, the tracer material must be able to resist these. Therefore, generally only particles with a high melting point, high oxygen content and diameters greater than 1 mm can be directly activated.

Meanwhile, indirect activation can be used to label smaller or heat-sensitive particles. In this case, first a dilute aqueous solution of ^{18}F is prepared via direct bombardment of ultrapure water by the reaction given above (Equation 1.14). Subsequently, the tracer particle is immersed in the radioactive water and ^{18}F ions are transferred from the aqueous phase onto the particle surface via either surface adsorption or ion exchange. The radioactivity achieved with this method is therefore largely dependent on the available surface area of the particle as well as its affinity towards ^{18}F ions. In the case of ion exchange, strong-base anion exchange resins are more suitable than weak ones as the affinity of ^{18}F is stronger towards the former. Radioactivity levels are then affected by the ion-capacity of the resin material. Furthermore, the concentration of ^{18}F in the water and the volume of water used, as well as the exposure time during the procedure influence the final tracer activities. For the use in wet systems, the danger of radioisotopes leaching from the tracer into the surrounding media presents a major problem. ^{18}F ions may dissociate from the particle surface when subjected to aqueous solutions, contaminating the system. Radioactivity spreads within the surrounding media and tracking of the tracer is no longer possible. Leaching can be prevented by coating of the particle surface with paints, lacquers or resins depending on the required surface properties.

The third technique for radioactive labelling, the surface modification, improves the adsorption of ^{18}F ions onto particle surfaces via chemical activation using metallic ions. In this method, the metallic ions (such as Fe^{3+}) are introduced to the solid surfaces as active

sites, to which ^{18}F anions subsequently bind. This greatly improves radioisotope adsorption, leading to increased radioactivity levels. With surface modification, a wider range of solid particles can be used as tracers, thus extending the potential applications of PEPT.

1.4.3.   Data processing and analysis

The positron camera detects pairs of γ-rays and their coordinates are subsequently processed by the PEPT algorithm (see section 1.4.1). The algorithm then generates the particle locations described by its Cartesian coordinates (x, y, z) as a function of time. In the Birmingham camera set up, the y-z-plane is parallel to the two detectors, while the x data describes the horizontal location (Figure 1.10).
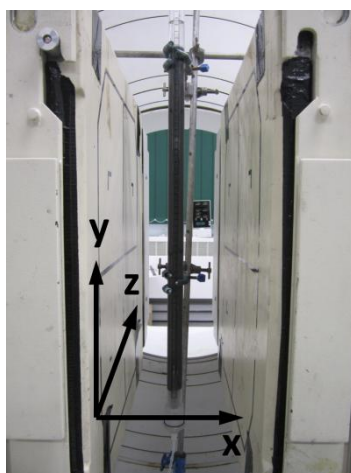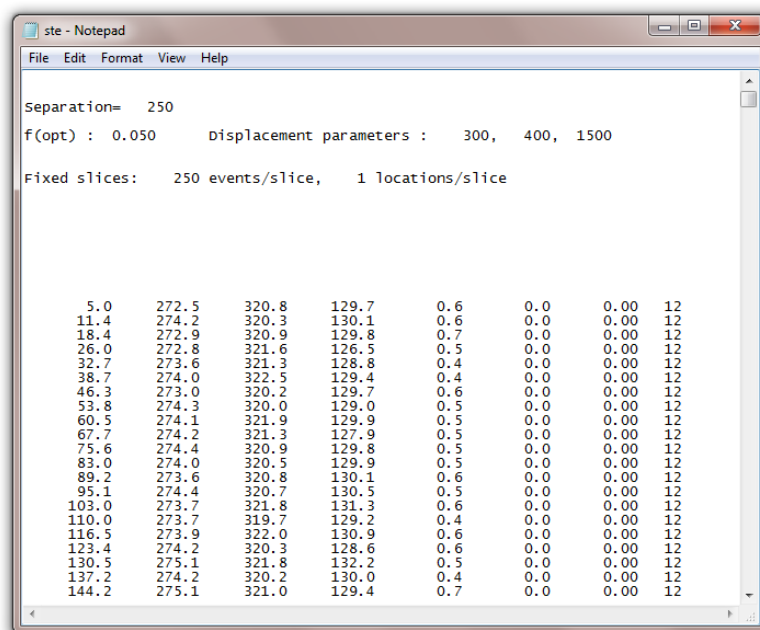
Figure 1.10: Depiction of the Cartesian coordinate system as used by PEPT to describe the tracer particle location in a three dimensional space between the two parallel detector heads.

The Langrangian data set locates the tracer position within the field of view of the camera heads at each point in time. The PEPT algorithm produces these data sets as ASCII files, listing the locations below a header describing experimental and processing details as used in the algorithm. An example of such an ASCII file is illustrated in Figure 1.11.

Figure 1.11: ASCII file produced by the PEPT algorithm, including processing parameters (header), x, y and z coordinates (columns 2, 3 and 4, respectively), error (column 5), shaft angle (column 6), torque (column 7) and number of events used for location (column 8) as a function of time (column 1).

The first column gives the time (in ms) at which each location point was calculated from the beginning of the run. Locations are recorded frequently but the time interval between each location is random due to the randomness of radioactive decay (Leadbeater et al. 2012). Columns 2, 3 and 4 then describe the x, y and z coordinates, respectively, of the location in millimetres from the bottom corner of detector 1. Unlike the usual connotation, the y-axis is always vertical. The fifth column indicates the reliability of the calculated location and thus gives an error probability, which shouldn't exceed values of 10. Columns 6 and 7 give the shaft angle and torque in specific studies of mixing systems. The eighth column shows the actual number of events used to calculate the corresponding location in the final step of the algorithm.

The PEPT data contained in the ASCII file can then be used and manipulated in various ways in order to illustrate the results. Trajectory plots can be produced by plotting one or

each of the three coordinates (x, y, z) as a function of time. This helps to examine the tracer's movement along each axis and to easily identify potential movement patterns. The behaviour of the tracer particle can readily be evaluated as to find regularities or anomalies either over the whole experimental period or within a chosen timeframe. To analyse trajectories in one single direction may be particularly of interest in systems with flows along an axis or where the particle position along a certain axis is significant for the process.

Plotting all coordinates together over a chosen timescale results in three dimensional trajectories, which give more detailed information about the tracer motion within the system. This enables easier interpretation of the acquired data and three dimensional flow patterns can be investigated. Using the graphics functions within a platform such as MATLAB (MathWorks, Natick, Massachusetts, USA), the trajectory plot can be rotated in any direction or zoomed in at any position, allowing to view the tracer path from all perspectives. Besides, the timescale can be added as fourth dimension and the trajectory be colour-coded according to the time at each location, enabling a full reconstruction and comprehension of the actual tracer motion over time.

In addition, the velocity of the tracer particle along the three dimensional trajectory can be determined for each location. These can be calculated either by a two point differentiation or a weighted average approach known as the 'six points' method (Stewart et al. 2001):

$$
\begin{aligned}
v_i = {} & 0.1\left(\frac{\vec{p}_{i+5} - \vec{p}_i}{t_{i+5} - t_i}\right) + 0.15\left(\frac{\vec{p}_{i+4} - \vec{p}_{i-1}}{t_{i+4} - t_{i-1}}\right) + 0.25\left(\frac{\vec{p}_{i+3} - \vec{p}_{i-2}}{t_{i+3} - t_{i-2}}\right) \\
& + 0.25\left(\frac{\vec{p}_{i+2} - \vec{p}_{i-3}}{t_{i+2} - t_{i-3}}\right) + 0.15\left(\frac{\vec{p}_{i+1} - \vec{p}_{i-4}}{t_{i+1} - t_{i-4}}\right) + 0.1\left(\frac{\vec{p}_i - \vec{p}_{i-5}}{t_i - t_{i-5}}\right)
\end{aligned}
$$

(Eq. 1.15)

where v_i is the velocity of the particle at the position p_i and time t_i. This method is commonly used and recommended over the two point method as it smoothes the velocity data and reduces the effects of PEPT measurement errors (Leadbeater et al. 2012). The calculated velocities can then be illustrated as vector plots, which show the time averaged velocity and direction of trajectory of the tracer particle at that location.

Furthermore, the PEPT data is commonly used to determine and plot the tracer occupancy, which defines the fraction of time the tracer spent in a particular volume element. Similarly to the vector plots, for illustration purposes it is often easier and more feasible to integrate the three dimensional data along a symmetry axis of the system and display 2D projections. Occupancy plots are particularly valuable to analyse dead zones or hot spots of high residence times.

Apart from these frequently applied analysis tools there may be further required data manipulation and illustration which depend on the system under study. These have to be developed individually for each system to attain optimal information from PEPT data.

1.5. Aims and outline of the thesis

The overall aim of this work has been to perform detailed investigations of expanded bed adsorption processes in order to obtain a better understanding of the complex hydrodynamics of this unit operation, ultimately improving its process robustness. It has been demonstrated that EBA has the potential to achieve chromatographic performances close to those of packed beds while eliminating the need for prior feedstock clarification. The combination of several unit operations into one and the resulting reduction in processing steps lead to advantages such as increased overall yields and reduced process times. However, for the biopharmaceutical industry, EBA has not managed to

serve as a convincing alternative to the conventional approach employing solid-liquid separation and packed bed chromatography. Early EBA equipment and adsorbents have been susceptible to fouling by the solids present in the crude feedstock, making intensive cleaning necessary. Furthermore, biomass-adsorbent interactions hampered the process, even leading to a complete breakdown of the expanded bed under certain conditions. At the most fundamental level however, there is still a poor understanding of the hydrodynamics within the bed. The complex interdepency of operating parameters causes EBA processing to be difficult to predict and control.

In this work, the advanced imaging technology of Positron Emission Particle Tracking (PEPT) has been employed intensively for in-depth studies of solid phase behaviour within expanded beds. Initially, hydrodynamic investigations are conducted in feedstock-free systems under fluidisation with equilibration buffer (Chapter 2). Using radioactively labelled tracer particles of varying sizes representing the bottom, mid and top parts of the expanded bed in three different columns, the response to variations in flow rate, settled bed height and means of fluid distribution are assessed. Furthermore, kinetics of bed stabilisation and the effect column misalignment are determined. The results are subsequently compared to previous PEPT studies of EBA employing different adsorbent matrices (Chapter 3), allowing for an overall interpretation and evaluation of the existing data. Finally, particle motion behaviour in expanded beds is studied under real process conditions during isolation of IgG from porcine serum (Chapter 4).

1.6. References

Al-Dibouni, M. and J. Garside (1979). "Particle mixing and classification in liquid fluidised beds." Transactions of the Institution of Chemical Engineers **57**: 95-103.

Anspach, F. B., D. Curbelo, et al. (1999). "Expanded-bed chromatography in primary protein purification." Journal of Chromatography A **865**(1-2): 129-144.

Arpanaei, A., A. Heebøll-Nielsen, et al. (2008). "Critical evaluation and comparison of fluid distribution systems for industrial scale expanded bed adsorption chromatography columns." Journal of Chromatography A **1198–1199**: 131-139.

Arpanaei, A., B. Winther-Jensen, et al. (2010). "Surface modification of chromatography adsorbents by low temperature low pressure plasma." Journal of Chromatography A **1217**(44): 6905-6916.

Azevedo, A. M., P. A. J. Rosa, et al. (2009). "Chromatography-free recovery of biopharmaceuticals through aqueous two-phase processing." Trends in Biotechnology **27**(4): 240-247.

Bakalis, S., P. W. Cox, et al. (2006). "Development and use of positron emitting particle tracking (PEPT) for velocity measurements in viscous fluids in pilot scale equipment." Chemical Engineering Science **61**(6): 1864-1877.

Barigou, M. (2004). "Particle Tracking in Opaque Mixing Systems: An Overview of the Capabilities of PET and PEPT." Chemical Engineering Research and Design **82**(9): 1258-1267.

Bartels, C. R. (1958). "A Novel Ion-exchange Method for the Isolation of Streptomycin." Chem. Eng. Prog. **54**: 49-51.

Becker, J. S., O. R. T. Thomas, et al. (2009). "Protein separation with magnetic adsorbents in micellar aqueous two-phase systems." Separation and Purification Technology **65**(1): 46-53.

Belter, P. A., F. L. Cunningham, et al. (1973). "Development of a recovery process for novobiocin." Biotechnology and Bioengineering **15**(3): 533-549.

Bensch, M., B. Selbach, et al. (2007). "High throughput screening techniques in downstream processing: Preparation, characterization and optimization of aqueous two-phase systems." Chemical Engineering Science **62**(7): 2011-2021.

Bruce, L. J. and H. A. Chase (2001). "Hydrodynamics and adsorption behaviour within an expanded bed adsorption column studied using in-bed sampling." Chemical Engineering Science **56**(10): 3149-3162.

Bruce, L. J., S. Ghose, et al. (1999). "The effect of column verticality on separation efficiency in expanded bed adsorption." Bioseparation **8**(1-5): 69-75.

Burns, M. A. and D. J. Graves (1985). "Continuous Affinity Chromatography Using a Magnetically Stabilized Fluidized Bed." Biotechnology Progress **1**(2): 95-103.

Carta, G. and A. Jungbauer (2010). Protein chromatography : process development and scale-up. Weinheim, Wiley-VCH.

Carton, J. M. and W. R. Strohl (2013). Chapter 4 - Protein therapeutics (introduction to biopharmaceuticals). Introduction to Biological and Small Molecule Drug Research and Development. R. Ganellin and S. R. Jefferis. Oxford, Elsevier**:** 127-159.

Chase, H. A. (1994). "Purification of proteins by adsorption chromatography in expanded beds." Trends in Biotechnology **12**(8): 296-303.

Chase, H. A. and N. M. Draeger (1992). "Expanded-Bed Adsorption of Proteins Using Ion-Exchangers." Separation Science and Technology **27**(14): 2021-2039.

Cherry, S. R., J. A. Sorenson, et al. (2012). chapter 3 - Modes of Radioactive Decay. Physics in Nuclear Medicine (Fourth Edition). S. R. C. A. S. E. Phelps. Philadelphia, W.B. Saunders**:** 19-30.

Dainiak, M. B., I. Y. Galaev, et al. (2002). "Direct capture of product from fermentation broth using a cell-repelling ion exchanger." Journal of Chromatography A **942**(1-2): 123-131.

Dainiak, M. B., I. Y. Galaev, et al. (2002). "Polyelectrolyte-Coated Ion Exchangers for Cell-Resistant Expanded Bed Adsorption." Biotechnology Progress **18**(4): 815-820.

Di Felice, R. (1995). "Hydrodynamics of liquid fluidisation." Chemical Engineering Science **50**(8): 1213-1245.

Draeger, N. M. and H. A. Chase (1991). "Liquid Fluidized-Bed Adsorption of Protein in the Presence of Cells." Bioseparation **2**(2): 67-80.

Elvin, J. G., R. G. Couston, et al. (2013). "Therapeutic antibodies: Market considerations, disease targets and bioprocessing." International Journal of Pharmaceutics **440**(1): 83-98.

Fan, X., D. J. Parker, et al. (2006). "Enhancing 18F uptake in a single particle for positron emission particle tracking through modification of solid surface chemistry." Nuclear Instruments and Methods in Physics Research Section A: Accelerators, Spectrometers, Detectors and Associated Equipment **558**(2): 542-546.

Fan, X., D. J. Parker, et al. (2006). "Labelling a single particle for positron emission particle tracking using direct activation and ion-exchange techniques." Nuclear Instruments & Methods in Physics Research Section a-Accelerators Spectrometers Detectors and Associated Equipment **562**(1): 345-350.

Fernández-Lahore, H. M., S. Geilenkirchen, et al. (2000). "The influence of cell adsorbent interactions on protein adsorption in expanded beds." Journal of Chromatography A **873**(2): 195-208.

Fernandez-Lahore, H. M., R. Kleef, et al. (1999). "The influence of complex biological feedstock on the fluidization and bed stability in expanded bed adsorption." Biotechnology and Bioengineering **64**(4): 484-496.

Fernandez-Lahore, H. M., D. Q. Lin, et al. (2001). "The use of ion-selective electrodes for evaluating residence time distributions in expanded bed adsorption systems." Biotechnology Progress **17**(6): 1128-1136.

Fernández Lahore, M., O. Aguilar, et al. (2009). Expanded Bed Chromatography, Surface Energetics of Biomass Deposition. Encyclopedia of Industrial Biotechnology, John Wiley & Sons, Inc.

Feuser, J., M. Halfar, et al. (1999). "Interaction of mammalian cell culture broth with adsorbents in expanded bed adsorption of monoclonal antibodies." Process Biochemistry **34**(2): 159-165.

Fischer, I., C.-C. Hsu, et al. (2013). "Continuous protein purification using functionalized magnetic nanoparticles in aqueous micellar two-phase systems." Journal of Chromatography A **1305**: 7-16.

Fish, N. M. and M. D. Lilly (1984). "The Interactions between Fermentation and Protein Recovery." Bio-Technology **2**(7): 623-627.

Franzreb, M., N. Ebner, et al. (2006). Product recovery by high-gradient magnetic fishing (HGMF). Process-scale bioseparations for the biopharmaceutical industry. A. Shukla, S. Gadam and M. Etzel, Marcel Dekker, New York.

Franzreb, M., M. Siemann-Herzberg, et al. (2006). "Protein purification using magnetic adsorbent particles." Applied Microbiology and Biotechnology **70**(5): 505-516.

Frej, A. K. B., H. J. Johansson, et al. (1997). "Expanded bed adsorption at production scale: Scale-up verification, process example and sanitization of column and adsorbent." Bioprocess Engineering **16**(2): 57-63.

Ghose, S., H. A. Chase, et al. (2000). "Bed height monitoring and control for expanded bed chromatography." Bioprocess Engineering **23**(6): 701-708.

Gottschalk, U. (2008). "Bioseparation in Antibody Manufacturing: The Good, The Bad and The Ugly." Biotechnology Progress **24**(3): 496-503.

Guida, A., X. Fan, et al. (2009). "Positron emission particle tracking in a mechanically agitated solid-liquid suspension of coarse particles." Chemical Engineering Research & Design **87**(4A): 421-429.

Guiochon, G. (2007). "Monolithic columns in high-performance liquid chromatography." Journal of Chromatography A **1168**(1–2): 101-168.

Guiochon, G. and L. A. Beaver (2011). "Separation science is the key to successful biopharmaceuticals." Journal of Chromatography A **1218**(49): 8836-8858.

Hagel, L., G. Jagschies, et al. (2008). 1 - Biopharmaceuticals Today. Handbook of Process Chromatography (Second Edition). L. H. J. Sofer. Amsterdam, Academic Press**:** 1-22.

Hardick, O., S. Dods, et al. "Nanofiber adsorbents for high productivity continuous downstream processing." Journal of Biotechnology.

Harrison, R. G. (2003). Bioseparations science and engineering. New York, Oxford University Press.

Hawkesworth, M. R., M. A. O'Dwyer, et al. (1986). "A positron camera for industrial application." Nuclear Inst. and Methods in Physics Research, A **253**(1): 145-157.

Healthcare, G. (2010). Strategies for Protein Purification - Handbook. Uppsala, Sweden.

Hjorth, R. (1997). "Expanded-bed adsorption in industrial bioprocessing: Recent developments." Trends in Biotechnology **15**(6): 230-235.

Hjorth, R. (1999). Expanded bed adsorption: elution in expanded bed mode. Expanded Bed Chromatography. B. Mattiasson, Springer Netherlands**:** 1-9.

Hjorth, R., S. Kampe, et al. (1995). "Analysis of Some Operating Parameters of Novel Adsorbents for Recovery of Proteins in Expanded Beds." Bioseparation **5**(4): 217-223.

Hjorth, R., P. Leijon, et al. (1998). Expanded Bed Adsorption Chromatography. Bioseparation and Bioprocessing. G. Subramanian, Wiley-VCH Verlag GmbH: 199-226.

Ho, R. J. Y. and M. Gibaldi (2013). Biotechnology and Biopharmaceuticals : Transforming Proteins and Genes into Drugs (2nd Edition). Somerset, NJ, USA, John Wiley & Sons.

Hubbuch, J., J. Thommes, et al. (2005). "Biochemical engineering aspects of expanded bed adsorption." Technology Transfer in Biotechnology: From Lab to Industry to Production 92: 101-123.

Hubbuch, J. J., P. J. Brixius, et al. (2006). "The influence of homogenisation conditions on biomass-adsorbent interactions during ion-exchange expanded bed adsorption." Biotechnology and Bioengineering 94(3): 543-553.

Hubbuch, J. J., A. Heeboll-Nielsen, et al. (2002). "A new fluid distribution system for scale-flexible expanded bed adsorption." Biotechnology and Bioengineering 78(1): 35-43.

Hubbuch, J. J., D. B. Matthiesen, et al. (2001). "High gradient magnetic separation versus expanded bed adsorption: a first principle comparison." Bioseparation 10(1-3): 99-112.

Jahanshahi, M., L. Partida-Martinez, et al. (2008). "Preparation and evaluation of polymer-coated adsorbents for the expanded bed recovery of protein products from particulate feedstocks." Journal of Chromatography A 1203(1): 13-20.

Jungbauer, A. (2013). "Continuous downstream processing of biopharmaceuticals." Trends in Biotechnology 31(8): 479-492.

Juza, M., M. Mazzotti, et al. (2000). "Simulated moving-bed chromatography and its application to chirotechnology." Trends in Biotechnology 18(3): 108-118.

Karau, A., C. Benken, et al. (1997). "The influence of particle size distribution and operating conditions on the adsorption performance in fluidized beds." Biotechnology and Bioengineering 55(1): 54-64.

Kelly, W., P. Garcia, et al. (2013). "Experimental characterization of next-generation expanded-bed adsorbents for capture of a recombinant protein expressed in high-cell-density yeast fermentation." Biotechnology and Applied Biochemistry 60(5): 510-520.

Krättli, M., T. Müller-Späth, et al. (2013). "Multifraction separation in countercurrent chromatography (MCSGP)." Biotechnology and Bioengineering 110(9): 2436-2444.

Leadbeater, T. W. (2009). "The Development of Positron Imaging Systems for Applications in Industrial Process Tomography." PhD Thesis, The University of Birmingham.

Leadbeater, T. W., D. J. Parker, et al. (2012). "Positron imaging systems for studying particulate, granular and multiphase flows." Particuology 10(2): 146-153.

Levenspiel, O. (1999). Chemical reaction engineering. New York, Wiley.

Li, P., P. F. Gomes, et al. (2014). Proteins Separation and Purification by Expanded Bed Adsorption and Simulated Moving Bed Technology. Continuous Processing in Pharmaceutical Manufacturing, Wiley-VCH Verlag GmbH & Co. KGaA: 1-34.

Lihme, A., M. Hansen, et al. (2000). Expanded Bed Adsorption in the Purification of Biomolecules. <u>Downstream Processing of Proteins</u>. M. Desai, Humana Press. **9:** 121-139.

Lihme, A., E. Zafirakos, et al. (1999). "Simplified and more robust EBA processes by elution in expanded bed mode." <u>Bioseparation</u> **8**(1-5): 93-97.

Lin, D.-Q., H. Fernández-Lahore, et al. (2001). "Minimising biomass/adsorbent interactions in expanded bed adsorption processes: a methodological design approach." <u>Bioseparation</u> **10**(1-3): 7-19.

Lin, D.-Q., J. Thömmes, et al. (2004). "The influence of biomass on the hydrodynamic behavior and stability of expanded beds." <u>Biotechnology and Bioengineering</u> **87**(3): 337-346.

Maisey, M. (2005). Positron Emission Tomography in Clinical Medicine. <u>Positron Emission Tomography</u>. D. Bailey, D. Townsend, P. Valk and M. Maisey, Springer London**:** 1-12.

Mattiasson, B. and M. P. Nandakumar (2000). 10 Physicochemical basis of expanded-bed adsorption for protein purification. <u>Separation Science and Technology</u>. A. Satinder, Academic Press. **Volume 2:** 417-430.

Menkhaus, T. J. and C. E. Glatz (2005). "Antibody Capture from Corn Endosperm Extracts by Packed Bed and Expanded Bed Adsorption." <u>Biotechnology Progress</u> **21**(2): 473-485.

Müller, T. K. H., P. Cao, et al. (2013). "Integrated system for temperature-controlled fast protein liquid chromatography comprising improved copolymer modified beaded agarose adsorbents and a travelling cooling zone reactor arrangement." <u>Journal of Chromatography A</u> **1285**: 97-109.

Nfor, B. K., T. Ahamed, et al. (2008). "Design strategies for integrated protein purification processes: challenges, progress and outlook." <u>Journal of Chemical Technology & Biotechnology</u> **83**(2): 124-132.

Otto, R., A. Santagostino, et al. (2014). Rapid growth in biopharma: Challenges and opportunities. <u>From Science to Operations: Questions, Choices and Stragies for Success in Biopharma</u>, McKinsey&Company.

Parker, D. J., C. J. Broadbent, et al. (1993). "Positron Emission Particle Tracking - a Technique for Studying Flow within Engineering Equipment." <u>Nuclear Instruments & Methods in Physics Research Section a-Accelerators Spectrometers Detectors and Associated Equipment</u> **326**(3): 592-607.

Parker, D. J. and X. Fan (2008). "Positron emission particle tracking—Application and labelling techniques." <u>Particuology</u> **6**(1): 16-23.

Parker, D. J., X. F. Fan, et al. (2005). "Positron imaging studies of rotating drums." <u>Canadian Journal of Chemical Engineering</u> **83**(1): 83-87.

Parker, D. J., R. N. Forster, et al. (2002). "Positron emission particle tracking using the new Birmingham positron camera." <u>Nuclear Instruments and Methods in Physics Research Section A: Accelerators, Spectrometers, Detectors and Associated Equipment</u> **477**(1–3): 540-545.

Parker, D. J., T. W. Leadbeater, et al. (2008). "Positron imaging techniques for process engineering: recent developments at Birmingham." <u>Measurement Science & Technology</u> **19**(9).

Parker, D. J. and P. A. McNeil (1996). "Positron emission tomography for process applications." Measurement Science & Technology **7**(3): 287-296.

Paulus, A., I. Fischer, et al. (2014). "Use of Continuous Magnetic Extraction for removal of feedstock contaminants in flow-through mode." Separation and Purification Technology **127**: 174-180.

Pharmacia (1997). Expanded Bed Adsorption: Principles and Methods. Uppsala, Sweden.

Richardson, J. F. and W. N. Zaki (1954). "Sedimentation and fluidization: Part I." Transactions of the Institution of Chemical Engineers **32**: 35-52.

Ruthven, D. M. and C. B. Ching (1989). "Counter-current and simulated counter-current adsorption separation processes." Chemical Engineering Science **44**(5): 1011-1038.

Schügerl, K. and J. Hubbuch (2005). "Integrated bioprocesses." Current Opinion in Microbiology **8**(3): 294-300.

Schulte, M. and J. Strube (2001). "Preparative enantioseparation by simulated moving bed chromatography." Journal of Chromatography A **906**(1–2): 399-416.

Scott, C. (2005). Chromatographic Chemistries for Biotechnology Development. Enabling Cell Therapy Manufacturing, BioProcess International.

Seidel-Morgenstern, A., L. C. Keßler, et al. (2008). "New Developments in Simulated Moving Bed Chromatography." Chemical Engineering & Technology **31**(6): 826-837.

Seville, J. P. K., A. Ingram, et al. (2005). "Probing processes using positrons." Chemical Engineering Research & Design **83**(A7): 788-793.

Soares, R. R. G., A. M. Azevedo, et al. (2015). "Partitioning in aqueous two-phase systems: Analysis of strengths, weaknesses, opportunities and threats." Biotechnology Journal **10**(8): 1158-1169.

Sonnenfeld, A. and J. Thömmes (2006). Expanded Bed Adsorption for Capture from Crude Solution. Process Scale Bioseparations for the Biopharmaceutical Industry, CRC Press**:** 59-82.

Stewart, R. L., J. Bridgwater, et al. (2001). "Granular flow over a flat-bladed stirrer." Chemical Engineering Science **56**(14): 4257-4271.

Ströhlein, G., L. Aumann, et al. (2006). "A continuous, counter-current multi-column chromatographic process incorporating modifier gradients for ternary separations." Journal of Chromatography A **1126**(1–2): 338-346.

Thelen, T. V., A. P. Mairal, et al. (1997). "Application of Ultrasonic Backscattering for Level Measurement and Process Monitoring of Expanded-Bed Adsorption Columns." Biotechnology Progress **13**(5): 681-687.

Theodossiou, I., H. D. Elsner, et al. (2002). "Fluidisation and dispersion behaviour of small high density pellicular expanded bed adsorbents." Journal of Chromatography A **964**(1-2): 77-89.

Theodossiou, I. and O. R. T. Thomas (2002). "DNA-induced inter-particle cross-linking during expanded bed adsorption chromatography - Impact on future support design." Journal of Chromatography A **971**(1-2): 73-86.

Thömmes, J. (1997). Fluidized bed adsorption as a primary recovery step in protein purification. New Enzymes for Organic Synthesis, Springer Berlin Heidelberg. **58:** 185-230.

Thömmes, J., M. Halfar, et al. (1995). "Purification of monoclonal antibodies from whole hybridoma fermentation broth by fluidized bed adsorption." Biotechnology and Bioengineering **45**(3): 205-211.

Thömmes, J., M. Weiher, et al. (1995). "Hydrodynamics and performance in fluidized bed adsorption." Biotechnology and Bioengineering **48**(4): 367-374.

Tong, X.-D. and Y. Sun (2002). "Particle size and density distributions of two dense matrices in an expanded bed system." Journal of Chromatography A **977**(2): 173-183.

Van Der Wiel, J. P. (1989). "Continuous recovery of bioproducts by adsorption." PhD Thesis, TU Delft.

Vennapusa, R., S. M. Hunegnaw, et al. (2008). "Assessing adsorbent–biomass interactions during expanded bed adsorption onto ion exchangers utilizing surface energetics." Journal of Chromatography A **1181**(1–2): 9-20.

Vennapusa, R. R. and M. Fernandez-Lahore (2010). "Effect of chemical additives on biomass deposition onto beaded adsorbents." Journal of Bioscience and Bioengineering **110**(5): 564-571.

Viloria-Cols, M. E., R. Hatti-Kaul, et al. (2004). "Agarose-coated anion exchanger prevents cell-adsorbent interactions." Journal of Chromatography A **1043**(2): 195-200.

Walsh, G. (2002). "Biopharmaceuticals and biotechnology medicines: an issue of nomenclature." European Journal of Pharmaceutical Sciences **15**(2): 135-138.

Walsh, G. (2003). Biopharmaceuticals : biochemistry and biotechnology. Hoboken, NJ, John Wiley.

Walsh, G. (2007). "Engineering biopharmaceuticals." Biopharm International **20**(11): 64-68.

Walsh, G. (2007). Pharmaceutical biotechnology : concepts and applications. Chichester, England ; Hoboken, NJ, John Wiley & Sons.

Walsh, G. (2014). "Biopharmaceutical benchmarks 2014." Nat Biotech **32**(10): 992-1000.

Wheelwright, S. M. (1991). Protein purification : design and scale up of downstream processing / Scott M. Wheelwright. Munich, Hanser.

Willoughby, N. A., R. Hjorth, et al. (2000). "Experimental measurement of particle size distribution and voidage in an expanded bed adsorption system." Biotechnology and Bioengineering **69**(6): 648-653.

Xia, H. F., D. Q. Lin, et al. (2007). "Evaluation of new high-density ion exchange adsorbents for expanded bed adsorption chromatography." Journal of Chromatography A **1145**(1-2): 58-66.

Yamamoto, S., N. Akazaki, et al. (1999). Factors affecting dispersion in expanded bed chromatography. Expanded Bed Chromatography. B. Mattiasson, Springer Netherlands**:** 33-41.

Yang, Y. and X. Geng (2011). "Mixed-mode chromatography and its applications to biopolymers." Journal of Chromatography A **1218**(49): 8813-8825.

Yang, Z., D. J. Parker, et al. (2006). "Multiple-particle tracking—an improvement for positron particle tracking." Nuclear Instruments and Methods in Physics Research Section A: Accelerators, Spectrometers, Detectors and Associated Equipment **564**(1): 332-338.

Zafirakos, E. and A. Lihme (1999). EBA columns with a distribution system based on local stirring. Expanded Bed Chromatography. B. Mattiasson, Springer Netherlands**:** 85-91.

Zou, H., X. Huang, et al. (2002). "Monolithic stationary phases for liquid chromatography and capillary electrochromatography." Journal of Chromatography A **954**(1–2): 5-32.

2. Investigating particle movement in expanded beds using positron emission particle tracking

2.1. Abstract

Expanded Bed Adsorption (EBA) is a form of liquid fluidized bed adsorption chromatography employing dense chromatographic media of defined size distribution. EBA's main advantage stems from its ability to perform chromatographic separations with crude feedstocks, thereby combining three separate tasks – clarification, concentration and initial capture/purification – in one single unit operation. While a lot of work has been done on examining the liquid axial dispersion in expanded beds, understanding of support particle movement (solid phase dispersion) is still limited. To address this, the powerful, non-invasive tomography technique 'Positron Emission Particle Tracking' (PEPT) was employed to directly visualise the motion of individual support particles within the interiors of expanded beds.

In this study, surrogate support particle tracers were fabricated by adsorbing the radionuclide ^{18}F generated by irradiating deionised water with a ^{3}He beam from the Birmingham MC40 Cyclotron on to differently sized alumina particles (density = 3.0 - 3.3 g/mL). Subsequent coating with lacquer was performed to prevent ^{18}F leaching into the surrounding fluid phase. Single ^{18}F labelled tracer particles of varying size and density were inserted within expanded beds of Patheon's Rhobust® MabDirect Protein A matrix (20 - 200 microns; density = 2.5 - 3.5 g/mL) contained in various EBA contactors differing in diameter and fluid distribution system. The columns were individually positioned between the detectors of Birmingham's ADAC Forte Positron camera and the XYZ positions of the individual particle tracers within the beds were tracked as a function of

fluidisation velocity for extended times by following ^{18}F beta plus decay in pseudo-real time. The results identify PEPT as a powerful and sensitive tool for interrogating fluidised bed systems. In addition to providing evidence of classification and non-uniform bed expansion in all fluidised beds under study, PEPT was used to determine kinetics of bed stabilisation and identify changes in tracer position and speed along the length of the bed in response to variations in flow rate, degree of column misalignment, and means of fluid distribution.

2.2. Introduction

Expanded bed adsorption (EBA) is an integrated downstream processing technique that has the potential of simplifying protein purification by combining solid-liquid separation and capture of the target molecule in a single unit operation (Chase 1994; Hjorth 1997; Thömmes 1997; Anspach et al. 1999). An upward flow through a column filled with adsorbent resin increases the interparticle space so that even cells and cell debris can pass the bed without blocking. This allows the application of EBA to directly separate and purify biological products from unclarified, crude feedstocks. The reduction of process steps aims at increased overall yield, reduced operational time and lower costs (Hubbuch et al. 2005). An essential feature of the EBA technique is the use of specifically designed adsorbents with a defined size and density distribution, resulting in classification or stratification of the bed. The resin particles position within the bed according to their terminal settling velocities, at which point the gravitational force, the buoyancy and the flow resistance are balanced. The resulting gradient of bead sizes and densities greatly reduce the axial dispersion within the column, which is crucial to achieve an efficient process with high chromatographic separation performance and resolution.

Classification of adsorbent particles during EBA processing has been confirmed by a number of experimental investigations, mainly using in-bed sampling at different heights along the column. Willoughby et al. (2000) employed side ports at 5-cm vertical intervals in a modified 5 cm diameter column, which allowed samples being taken from various points along the bed length during runs. They measured the axial size distribution and mean voidage of Streamline Phenyl adsorbents (100 - 550 µm) and found that the particle size was radially constant, while it decreased with increasing axial height. Furthermore, they observed an increasing voidage along the bed with height, while voidage also increased at a particular axial position (at a certain sample port) with increased flow velocity. Similar trends were shown by Bruce and Chase (2001) as well as Tong and Sun (2002), despite studying different resin beads with different size ranges (Streamline SP with 100 - 400 µm and Streamline with 80 - 500 µm, respectively). However, the particles were not tightly classified within the bed as particle size distributions at the various heights along the column overlapped, suggesting an overall significant distribution of different-sized beads throughout the bed. Using adsorbents with a relatively uniform density (Streamline SP and Streamline, respectively), only a small influence on classification due to the density was found in both works (Bruce and Chase 2001; Tong and Sun 2002). In contrast, Tong and Sun also investigated particles with a wide density distribution (6% agarose coated steel beads, 60 - 250 µm), which were classified according to their density rather than size. More recently, Lin et al. (2013) measured mean bead size, density and local bed voidage along a 2 cm diameter nozzle column using adsorbent particles with a wide size and density distribution (3% crosslinked agarose containing tungsten carbide, 47 - 236 µm, 2.8 - 3.2 g/mL; Patheon, Netherlands). They found a decreasing mean bead size and wet density of the beads with increasing bed height, while the local bed voidage increased. Kaczmarski and Bellot (2004) as well as Yun et al. (2004) introduced models for prediction of particle size and local voidage

along the bed, which they subsequently improved to take into account a broader density range (Yun et al. 2004).

In addition to the axial distributions of adsorbent particles and bed voidages, the local liquid axial dispersion has similarly been studied by in-bed sampling (Bruce and Chase 2001; Yun et al. 2005; Lin et al. 2015). Instead of an overall evaluation of axial dispersion for the whole expanded bed, local variations along the bed height were proposed to give a more accurate description of the liquid mixing and therefore separation efficiency of the bed. Residence time distributions (RTD) were measured using the tracer pulse response method at each sample point along the column. While Bruce and Chase (2001) as well as Yun et al. (2005) found decreasing values for local axial dispersion coefficients with increasing bed height, Lin et al. (2015) observed a minimum at 0.6 - 0.8 relative bed height and then increasing dispersion again at the top bed zone.

However, in-bed sampling methods only give limited information about the specific point in time at which the sample is taken. Furthermore, while a considerable amount of work has been done in the investigation of liquid axial mixing, the dispersion of the solid phase, i.e. the adsorbent particles, seems mostly disregarded. A few workers (Wright and Glasser 2001; Kaczmarski and Bellot 2004; Li et al. 2005) have included solid dispersion in their models. They employed a correlation proposed by Van Der Meer et al. (1984) to calculate the solid dispersion coefficient, D_s, using experimental values for the superficial velocity u:

$$D_s = 0.04u^{1.8}$$

(Eq. 2.1)

Wright and Glasser (2001) suggested that this correlation was the most suitable of those available, since it was developed using dispersion measurements between two fractions of differing particle size. However, this inherently implies the assumption that solid dispersion is not a function of the position along the column. For protein adsorption during

the EBA process, Thömmes (1997) reported that values of solid dispersion are expected to make up less than 10% of the liquid axial dispersion. Still, to the best knowledge of the author no experimental studies are available to date to evaluate solid dispersion.

This work presents a novel tool for investigation of adsorbent particle behaviour within expanded beds. Using the technique of Positron Emission Particle Tracking (PEPT, see also Section 1.4), a single radioactively labelled tracer particle is introduced into the system and its position tracked over time. Following earlier work by Liu (2009) and Souquet (2007; 2011), who employed PEPT in beds of Streamline (GE Healthcare, Uppsala, Sweden) and QHyperZ (Pall, Port Washington, NY, USA), adsorbent particle movement in beds of a resin with a broader density distribution were examined in this study (Rhobust®; Patheon, Groningen, Netherlands). The influences of the superficial fluid velocity, the column diameter, the settled bed height, the fluid distribution system as well as the column vertical alignment on the motion and solid dispersion of particles at different axial positions within the bed are investigated.

2.3. Materials and methods

2.3.1. Materials

The expanded bed adsorbent used in this study, Rhobust® MabDirect Protein A (20 - 200 µm, 2.8 - 3.2 g/mL) was a gift from Patheon, Groningen, Netherlands and is comprised of cross-linked agarose and incorporated tungsten carbide. γ-Alumina particles for use as PEPT tracers were purchased from Alfa Aesar (Ward Hill, MA, USA) and coated with a lacquer from James Briggs Ltd (Royton, Greater Manchester, UK). Di-sodium hydrogen phosphate heptahydrate was sourced from Merck KGaA (Darmstadt, Germany; CAS # 7782-85-6); potassium phosphate monobasic (CAS # 7778-77-0),

sodium chloride (CAS # 7647-14-5) and potassium chloride (CAS # 7447-40-7), for phosphate buffered saline (PBS; 136 mM NaCl, 2.7 mM Potassium chloride, 8.9 mM phosphate; pH 7.0) were purchased from Sigma-Aldrich Company Limited (St. Louis, MO, USA).

2.3.2. PEPT tracer fabrication

γ-Alumina particles with a density of 3.0 - 3.3 g/mL, and thus similar to that of the adsorbent matrix employed in this study, were used as foreign tracers. Sizes covering the particle size distribution range of the adsorbent (20 - 200 µm) were picked to interrogate the behaviour of the bottom, mid and top part of the bed. For each representative part, a few tracer particles of roughly the same size were chosen and labelled together with ^{18}F using the indirect activation method as described by Leadbeater et al. (2012). Briefly, the particles were exposed to an aqueous solution of ^{18}F, which was previously prepared by direct bombardment of purified water using a ^{3}He beam from the Birmingham MC40 Cyclotron (Fan et al. 2006). One millilitre of this solution was then added to the selected particles. ^{18}F ions were transferred from the aqueous phase onto the particle surface via surface adsorption and the excess water was dried off with the help of an infrared lamp. The tracer particles were subsequently coated with lacquer to prevent the leaching of radioisotopes into the surrounding fluid phase. This was done by dipping the selected particle into a drop of lacquer and subsequent rolling to spread it evenly and as thinly as possible across the whole surface before leaving to dry for a few minutes.

The activities of the tracers using this method are mostly dependent on the initial concentration of ^{18}F ions in the aqueous solution used and the exposed surface area of the particle, leading to generally higher activities in bigger particles and lower activities in smaller particles. Furthermore, with decreasing particle size, the influence of the lacquer

coating on the tracer particle's density increases. Therefore, it is more challenging to produce sufficiently activated, good tracers from smaller particles than from relatively bigger ones.

2.3.3. Experimental set up

The respective EBA column containing Rhobust® MabDirect Protein A resin used was mounted between the two parallel PEPT detector camera heads, which were adjusted to the closest face-to-face separation possible (250 mm) to achieve optimal data acquisition. The column's vertical position was ensured using a digital level (Torpedo DWL-200, Digi-Pas, Avon, CT, USA) to give accuracies of alignment as close as 0.1°. The column was then connected to an ÄKTAprime plus system (GE Healthcare, Uppsala, Sweden) and an interposed outlet peristaltic pump (Watson Marlow, Falmouth, UK), so that fluidisation could be attained via recirculation of PBS (Figure 2.1).
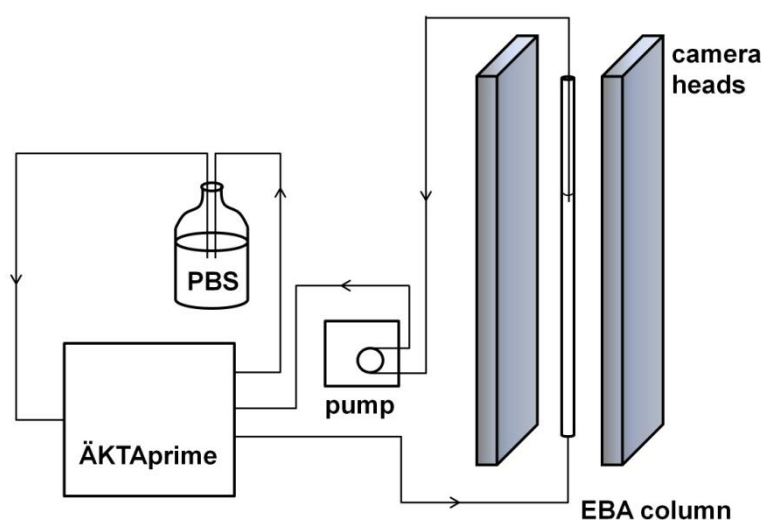
Figure 2.1: Schematic representation of the set up used for PEPT experiments.

2.3.4. Bed expansion tests

Previous to the PEPT experiments, expansion characteristics of the Rhobust® matrix in each column were examined by measuring the expanded bed height at various flow rates using phosphate buffered saline (PBS). The expansion factor is determined as the ratio of expanded bed height H to the settled bed height H_0. From the resulting expansion profiles, the required flow velocities for the desired expansions were calculated.

2.3.5. Experimental procedure

The various columns and conditions investigated in this study are listed in Table 2.1.

Table 2.1: Columns and settings used for the PEPT experiments.

Column Ø (cm)	Fluid distribution system	Vertical alignment	H_0 (cm)	H/H_0	Manufacturer
1	4 port nozzle and cone inlet	90.0°	15.5	1.6 - 1.8 - 2.0 - 2.2 - 2.4 - 2.6 - 2.8	Patheon
2	4 port nozzle and cone inlet	90.0°	25.5	1.6 - 1.8 - 2.0 - 2.2 - 2.4	Patheon
		89.5°	25.5	1.6 - 1.8 - 2.0 - 2.2 - 2.4	
		89.0°	25.5	1.6 - 2.0 - 2.4	
2.5	Perforated plate & overlying net	90.0°	27.5	1.6 - 1.8 - 2.0 - 2.2 - 2.4 - 2.6 - 2.8	GE Healthcare

Initially, a 2 cm diameter column with a 4 port nozzle and cone inlet and 70 cm length provided by Patheon (Groningen, Netherlands) was assessed with PEPT using Rhobust® MabDirect Protein A resin of 25.5 cm settled bed height (SBH or H_0).

As stated above, alumina tracer particles radioactively labelled with ^{18}F were used as surrogates for the Rhobust® adsorbent beads and added to the resin from the top of the column. To facilitate each individual tracer particle's way to its distinct position within the bed, the experiment was started at 2.2 fold expansion. Afterwards, flow rates were

changed to achieve expansions from 1.6 to 2.4 fold. Data acquisition with the PEPT software was started when the expected expanded bed height was visually observed (after approximately 10 min) and the tracer locations were recorded for 45 minutes at each flow rate or bed expansion.

A smaller nozzle inlet column with a diameter of 1 cm (Patheon, Groningen, Netherlands) with Rhobust® adsorbents of 15.5 cm settled bed height was studied in a similar way. However, in this set of experiments, the flow was stopped at the end of each run at a particular fluid velocity (corresponding to a particular bed expansion) and the adsorbents were let to settle for 15 minutes. During those 15 minutes, data acquisition was stopped and then re-started with each start of flow to collect location data during initial rise of the particles. In addition to the previously studied bed expansions, 2.6 and 2.8 fold expansions were also examined.

A 2.5 cm diameter Streamline Column (GE Healthcare, Uppsala, Sweden) was subsequently investigated with Rhobust® adsorbents of 27.5 cm settled bed height. In contrast to the Patheon columns, the inlet fluid distribution of this system comprises of a perforated distribution plate and an overlying net. Experiments were carried out as described above for the 1 cm Patheon nozzle column.

To investigate the influence of column alignment, the 2 cm Patheon nozzle inlet column was deliberately misaligned by 0.5° to the vertical (ensured using a digital level again) and experiments were carried out for a top and mid representative tracer particle in a settled bed of 26.5 cm Rhobust® resin, as described above. For the 'mid' particle it was possible to run further three expansions (1.6, 2.0 and 2.4 fold) with a misalignment of 1.0° to the vertical.

2.3.6. Residence time distribution (RTD) studies

Residence time distributions were measured for each flow velocity during the PEPT experiments by a negative step input conductivity signal as described by Barnfield Frej et al. (1997) using PBS. From this, the number of theoretical plates (N) was calculated:

$$N = \frac{t_m{}^2}{\sigma^2} \tag{Eq. 2.2}$$

where t_m is the mean residence time and σ is the variance, which is a measure of the spread of the tracer as it leaves the column.

The liquid axial dispersion coefficient $D_{ax,}$, which describes the degree of axial mixing of the mobile phase within the column, can then be calculated using Equation 2.3 assuming only small deviations from plug flow:

$$D_{ax,l} = \frac{u_i \, H}{2 \, N} \tag{Eq. 2.3}$$

where $u_i = \frac{u}{\varepsilon}$ is the interstitial fluid velocity, u is the superficial fluid velocity, ε is the bed voidage and H is the height of the expanded bed. The bed voidage was calculated from Equation 2.4 below:

$$\frac{H}{H_0} = \frac{(1 - \varepsilon_0)}{(1 - \varepsilon)} \tag{Eq. 2.4}$$

where H_0 is the height of the settled bed, and ε_0 is the settled bed voidage, which is assumed to be 0.4 (Anspach et al. 1999).

RTDs were determined in duplicates 45 minutes after start up of flow.

2.3.7. Data analysis

Using PEPT, the position of the labelled tracer particle was determined by means of triangulation from a number of detected pairs of γ-rays. In practice, some of the detected events are corrupt due to scattered or random coincidences. Therefore an iterative algorithm was developed by Parker et al. (1993) to eliminate and reject these corrupt events. The algorithm calculated the point which minimises the sum of perpendicular distances between the reconstructed paths of all events within the initial sample. The reconstructions lying furthest away from this point were assumed to be corrupt and removed from the set of events. A new minimum distance point was calculated from the remaining events and the algorithm was iterated until only a predefined fraction of the initial event sample remained.

The resulting data consisting of the tracer coordinates (x, y, z) over time was then used to plot axial as well as three-dimensional trajectories. Furthermore, occupancies were determined and plotted as the fraction of time spent by the tracer particle in a specific volume element. Tracer velocities were calculated using a six point weighted average method (Stewart et al. 2001):

$$
\begin{aligned}
u_i = {} & 0.1\left(\frac{\vec{p}_{i+5} - \vec{p}_i}{t_{i+5} - t_i}\right) + 0.15\left(\frac{\vec{p}_{i+4} - \vec{p}_{i-1}}{t_{i+4} - t_{i-1}}\right) + 0.25\left(\frac{\vec{p}_{i+3} - \vec{p}_{i-2}}{t_{i+3} - t_{i-2}}\right) \\
& + 0.25\left(\frac{\vec{p}_{i+2} - \vec{p}_{i-3}}{t_{i+2} - t_{i-3}}\right) + 0.15\left(\frac{\vec{p}_{i+1} - \vec{p}_{i-4}}{t_{i+1} - t_{i-4}}\right) + 0.1\left(\frac{\vec{p}_i - \vec{p}_{i-5}}{t_i - t_{i-5}}\right)
\end{aligned}
$$

(Eq. 2.5)

where u_i is the velocity of the particle at the position p_i and time t_i. Calculated velocities are illustrated as velocity vectors describing the average velocity of the tracer passing through a particular volume element. The total scalar velocity is determined from the velocities in each single Cartesian direction as:

$$u = \sqrt{u_x^2 + u_y^2 + u_z^2} \qquad \text{(Eq. 2.6)}$$

The solid axial dispersion was determined using a method developed and described by Parker et al. (1997), who employed PEPT to study solid dispersion in rotating drums. In a similar way, Kiared et al. (1997) analysed solid dispersion in liquid fluidised beds. This involves the distribution of distances $y_d(t)$ that the tracer moves axially during time intervals t. The width of these distributions corresponds to the variance, which is equal to $\langle y_d^2(t) \rangle$, the mean-square of the axial displacement, and can be calculated from:

$$\langle y_d^2(t) \rangle = 2D_{ax,s}t \qquad \text{(Eq. 2.7)}$$

where $D_{ax,s}$ is the solid axial dispersion coefficient. Parker et al. (1997) suggested to split the data into sequences of time intervals in order to obtain statistically independent data. While they used time intervals of 10 s over a run of 3000 s providing 300 independent samples, in this study only the last 900 seconds of data were used. Therefore, a time interval of 3 s was employed to achieve a similar amount of samples and the solid axial dispersion coefficient was calculated by Equation 2.7 and t = 3s.

2.4. Results and discussion

2.4.1. Bed expansion characteristics

Bed expansions of the Rhobust® MabDirect Protein A matrix in each column under the conditions as found during the PEPT experiments are shown in Figure 2.2. Due to the sensitivity of the electronics required for the PEPT technology, the laboratory is kept at a temperature of around 19°C. As the temperature influences the liquid viscosity, it equally affects the degree of bed expansion (Pharmacia 1997; Anspach et al. 1999). The

difference in temperature has therefore to be considered when comparing bed expansion

to those measured at normal room temperatures.
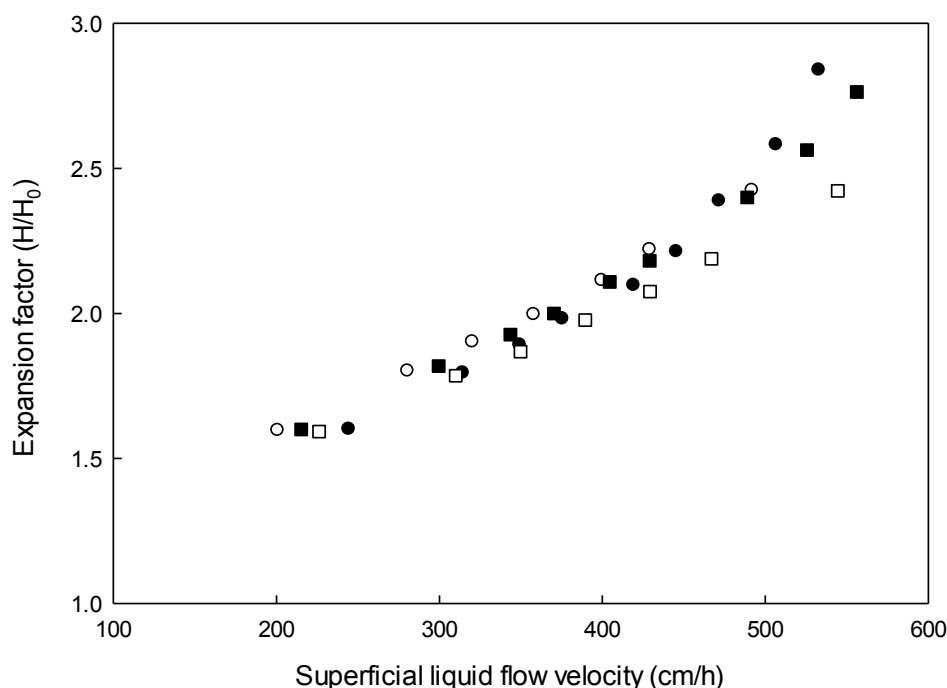
Figure 2.2: Bed expansion with increasing superficial fluid velocity for Rhobust® MabDirect Protein A resin fluidised with PBS at a room temperature of ~19°C in a 1 cm diameter nozzle inlet column (●), 2 cm diameter nozzle inlet column (○), 2.5 cm diameter Streamline column (■), and a 0.5° vertically misaligned 2 cm diameter nozzle inlet column (□).

Generally, flow velocities from around 200 - 560 cm/h were employed to achieve bed

expansions of 1.6- to just above 2.8-fold. A good accordance with the expected linear

behaviour is found in all cases up to superficial fluid velocities of 450 cm/h. However,

slightly higher expansions were observed at elevated fluid flow in particular above around

450 cm/h for the 1 cm diameter nozzle inlet column (filled circles) and less steep for the

2.5 cm diameter Streamline column above 500 cm/h (filled squares). This may be due to

wall effects, which would be more predominant in a smaller column. Still, the different

columns and fluid distributors have little effect on the bed expansion, apart from the

vertical misalignment. As shown previously by Bruce et al. (1999), the inclination leads to

lower expanded bed heights at constant fluid flow velocities compared to perfectly vertical columns, or vice versa, higher flow rates are needed to achieve the same bed expansion.

2.4.2. PEPT tracer characterisation

As described above, a few alumina particles were labelled together and one of each batch was chosen and added to the resin from the open top of the column. After initial fluidisation, the tracer particle was expected to find its axial position roughly as anticipated, either in the bottom, mid or top part of the column. However, the labelling method and particularly the coating technique resulted in difficulties with respect to controlling the size and densities of the tracer particles. Therefore, it was found to be more suitable describing the particles by their relative position in the settled bed, which is defined as:

$$h_{T,0} = \frac{H_{T,0}}{H_0}$$
(Eq. 2.8)

where $H_{T,0}$ is the position of the tracer particle in the settled bed and H_0 the height of the settled bed.

In the experiments where flow was stopped in between each flow rate, it was observed that the tracer particles were found back to roughly the same position after each flow rate applied. This is shown for all three tracer particles plotted together in Figure 2.3 exemplarily for the 2.5 cm Streamline column.
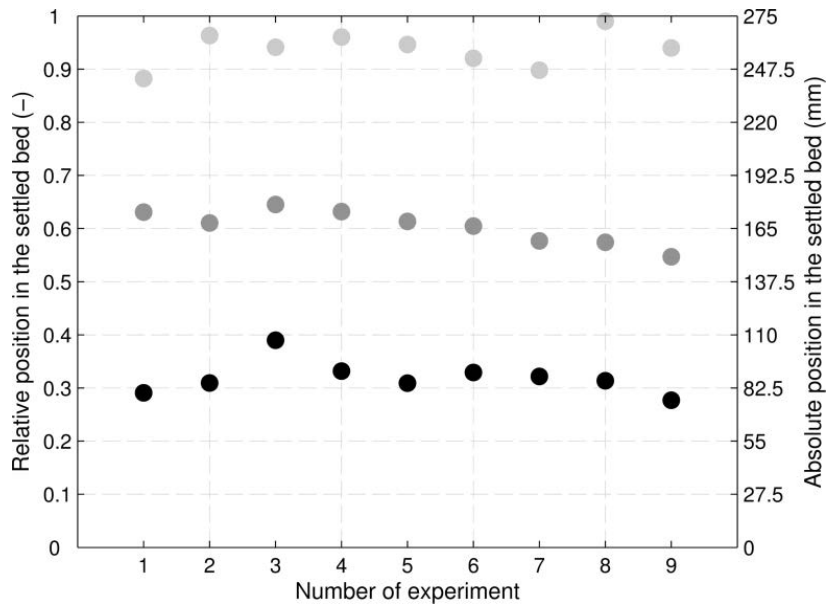
Figure 2.3: ^{18}F-labelled alumina tracer particles' relative and absolute positions in the settled bed after each flow rate applied with sizes of 360 µm (black), 260 µm (dark grey) and 130 µm (light grey) within an expanded bed of Rhobust® MabDirect Protein A adsorbents in a 2.5 cm diameter Streamline column (initial settled bed height H_0 = 27.5 cm).

The tracer particle's relative position in the settled bed after each run was also used as quality control of the tracer manufacturing. Particles returning to their specific position confirmed that no deterioration, e.g. abrasion of the coating, occurred during the run.

From all runs performed with a particular tracer particle, a mean relative tracer position in the settled bed could then be determined from Equation 2.9 as:

$$\overline{h}_{T,0} = \frac{\sum h_{T,0}}{\#runs}$$

(Eq. 2.9)

When plotting $\overline{h}_{T,0}$ against the size of the original alumina particle, a linear approximation can still be found (Figure 2.4, R^2 = 0.8608).
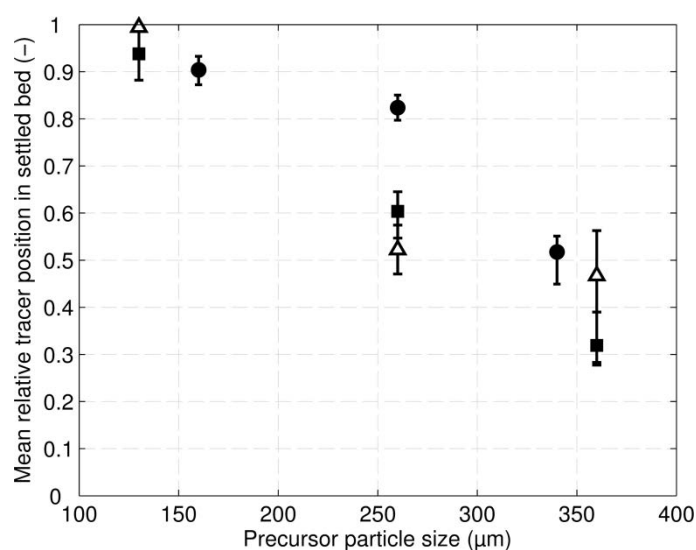
Figure 2.4: Correlation between the mean (symbol), maximum and minimum (error bars) ^{18}F labelled tracer particle positions in settled beds of Rhobust$^{®}$ MabDirect Protein A with precursor alumina particle size in a 1 cm diameter nozzle inlet column with H_0 = 15.5 cm (●), 2.5 cm diameter Streamline column with H_0 = 27.5 cm (■), and a 0.5° vertically misaligned 2 cm diameter nozzle inlet column with H_0 = 25.5 cm (△).

The error bars in Figure 2.4 indicate maximum and minimum relative positions within one set of experiments (e.g. nine runs/flow rates as shown in Figure 2.3). Their lengths again show the consistency of the tracer particles' positioning in the settled bed. The mean relative tracer positions in the settled bed will be used throughout this work to define the tracer particles employed.

2.4.3. Tracer motion in expanded beds of Rhobust® particles

2.4.3.1. Effect of superficial fluid velocity

Figure 2.5 shows the three-dimensional trajectories of three tracer particles representing the bottom, the mid and the top of the expanded bed with increasing superficial liquid flow velocities of the fluidisation buffer (PBS) in a 2 cm nozzle inlet column with initial settled bed height of 25.5 cm. Only location data of the last 15 minutes are displayed, following 30 minutes of equilibration.
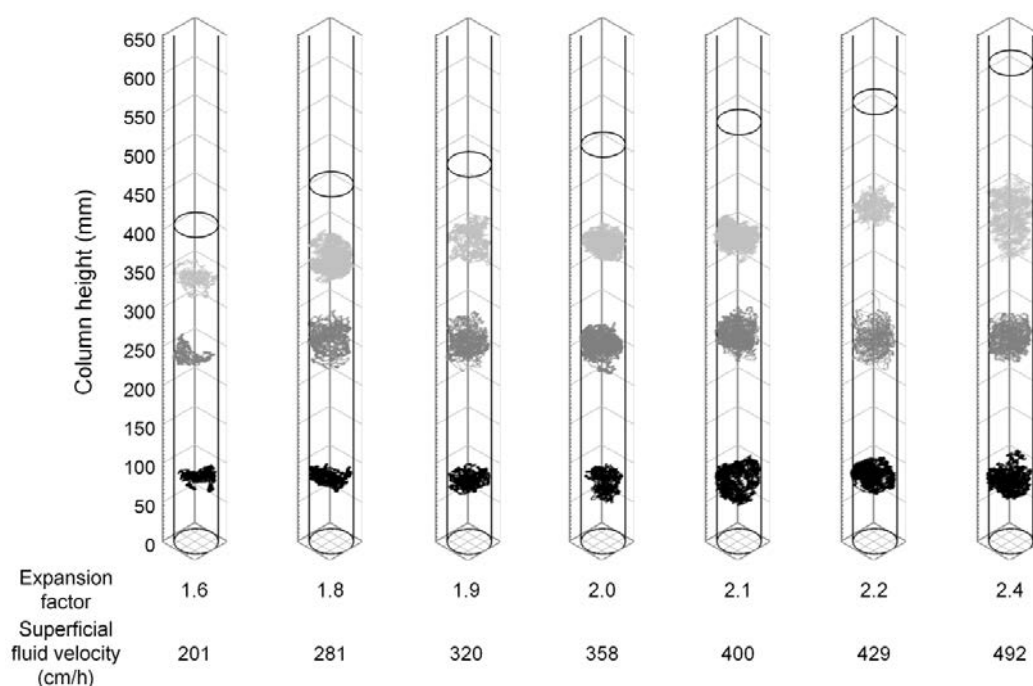
Figure 2.5: Superimposed three-dimensional trajectories of ^{18}F-labelled alumina tracer particles within an expanded bed of Rhobust® MabDirect Protein A adsorbents with initial settled bed height H_0 = 25.5 cm in a 2 cm diameter nozzle inlet column at increasing superficial fluid velocities and expansion factors. Column boundaries and expanded bed height are displayed as black lines, the detected locations of a 'bottom', 'mid' and 'top' tracer as black, dark grey and light grey lines, respectively.

In these experiments, the tracer particles' relative position in the settled bed $h_{T,0}$ could not be determined as flow was not stopped between change of liquid velocity (see Section 2.3.4).

First, the three-dimensional renditions confirm the general behaviour of stratification or classification of the adsorbent particles within the expanded bed, as the largest particle is located near the bottom whereas smaller and lighter particles move further up in the bed. Moreover, the tracer particles appear to exhibit a random motion both in axial as well as horizontal direction. To illustrate the randomness and that no particular movement pattern could be found, a close up of the mid tracer particle's trajectory at 2.0-fold expansion is representatively shown in Figure 2.6.
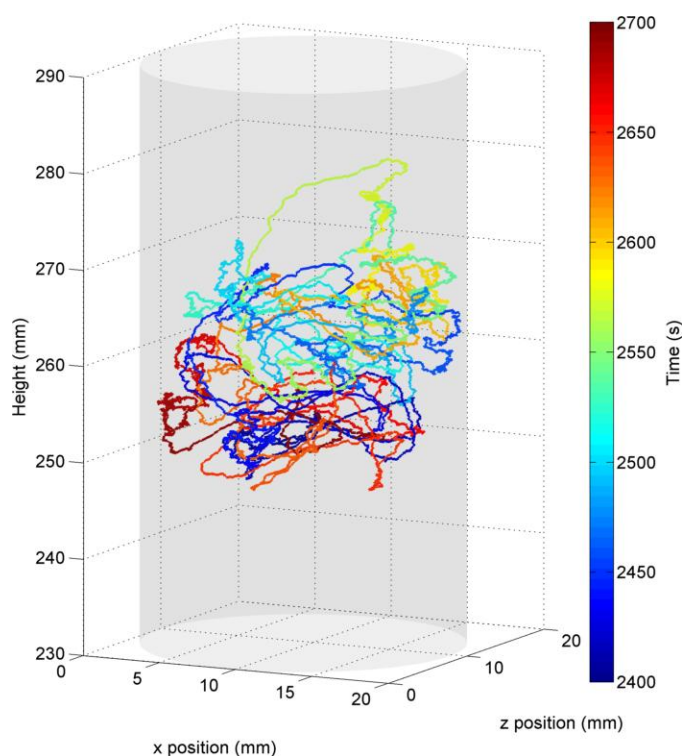
Figure 2.6: Three-dimensional trajectory of an ^{18}F-labelled alumina tracer particle over time within an expanded bed of Rhobust[®] MabDirect Protein A adsorbents in a 2 cm diameter nozzle inlet column (initial settled bed height H_0 = 25.5 cm; 358 cm/h superficial fluid velocity corresponding to a 2.0-fold bed expansion). Column boundaries are displayed in transparent grey.

Here, only the last 300 seconds of data are shown in order to facilitate identification of the tracer path. During this time, the tracer particle moves randomly through the whole volume of the cylindrical part of the column within the axial motion range. No particular hot spots, where the tracer particle would only move in a specific area at a certain time, are visible.

Considering only data from the last 5 (Figure 2.6) and 15 minutes (Figure 2.5), respectively, of each run is shown, the particles seem to travel rather large distances. These distances, representing the length of the trajectories shown above, can be determined from the mean tracer velocities calculated for the data points acquired during this time (Figure 2.7).

Figure 2.7: Mean velocities of ^{18}F-labelled alumina tracer particles representing the bottom (black), mid (dark grey) and top (light grey) parts of the column versus bed expansion during the last 15 minutes of data acquisition in an expanded bed of Rhobust® MabDirect Protein A adsorbents in a 2 cm diameter nozzle inlet column (initial settled bed height H_0 = 25.5 cm).

Overall, no clear trend can be observed when comparing the mean tracer velocities at different bed expansions or superficial fluid velocities, although there may be a slight increase in speed at higher degrees of bed expansion for all three tracer particles. The distance travelled by the particle in the relative timeframe (d_t) can be calculated as

$$d_t = \overline{u}(\Delta t)\,\Delta t \qquad \text{(Eq. 2.10)}$$

where $\overline{u}(\Delta t)$ is the mean tracer velocity averaged over the time Δt, in this case 15 minutes. Therefore, the mid tracer particle for instance, moving at an average pace of 4.76 mm/s, travelled across a total distance of 4.28 m within 900 seconds, which is more than 200 times the column's cross section. This contrasts with the suggestion that during fluidisation, adsorbent particles only exhibit small, circular movements (Pharmacia 1997; Drossard 2005).

Interestingly, while the tracer particle representing the top covers the largest axial motion range (Figure 2.5), it moves at relatively low speed. The axial motion range is further

illustrated in Figure 2.8, where it is represented by the lengths of the error bars indicating

maximum and minimum axial position within the last 15 minutes of fluidisation.

Figure 2.8: Superimposed mean (square), maximum and minimum (error bars) axial positions of ^{18}F-labelled alumina tracer particles representing the bottom (black), mid (dark grey) and top (light grey) parts of the column versus superficial liquid flow velocity in expanded beds of Rhobust® MabDirect Protein A adsorbents in a 2 cm diameter nozzle inlet column during the last 15 minutes of fluidisation. Expanded bed heights are marked with black dashes.

When concentrating on the axial motion range, Figure 2.8 also shows the disagreement of

these results with the visual observation of some authors who described more particle

movement in the lower regions of the column (Hjorth et al. 1995; Thömmes et al. 1995;

Karau et al. 1997). While the bottom tracer may not be representative of the bed

behaviour in the region directly above the fluid distributor, still, it exhibits the smallest

ranges in axial positions relatively low in the expanded compared to the other regions

higher up. Here, as mentioned above, the 'top' tracer axially moves the furthest at highest

flow rates. The smaller tracer velocities may, however, be misleading when only visually

inspecting the column and leading to the description of notably less particle movement

higher in the column by previous authors.

Apart from the axial motion range, Figure 2.8 also depicts the mean axial tracer position $\overline{H}_T(\Delta t)$ over the time Δt, in this case 15 minutes. The results highlight another interesting observation: Strikingly, there seems to be a pattern regarding the axial positioning of the tracer particles with increasing superficial flow velocity. The tracer representing bottom and mid of the bed appear to hardly rise up in the bed. Only the smallest, lightest particles move higher up in the bed with higher flow rates, meaning that the expansion is mainly generated by those particles in the top of the bed.

While the axial motion ranges give an overall view of the part of the column the tracer particle travels through, the solid axial dispersion presents a more detailed picture of the axial motion over time. The solid axial dispersion coefficient $D_{ax,s}$ was calculated from Equation 2.7 (*cf.* Section 2.3.7) to quantify axial mixing of the adsorbent particles in the bottom, mid and top part of the expanded bed (Figure 2.9).

Figure 2.9: Solid axial dispersion coefficients of ^{18}F-labelled alumina tracer particles representing the bottom (black), mid (dark grey) and top (light grey) parts of the column versus bed expansion in an expanded bed of Rhobust® MabDirect Protein A adsorbents in a 2 cm diameter nozzle inlet column, during the last 15 min of data acquisition (initial settled bed height $H_0 = 25.5$ cm).

First, it has to be noted that the overall values of the solid axial dispersion coefficient calculated in this study were found to be much larger than those determined from the

correlation proposed by Van der Meer et al. (1984). Using Equation 2.1 (*cf.* Section 2.2), the range of applied superficial flow rates of *ca.* 200 - 500 cm/h would result in values for $D_{ax,s}$ between 1.4 - 7.0 x 10^{-8} m^2/s; *i.e.* two orders of magnitude lower than those found here by analysis of the PEPT data. Yet again, similar to the overall distances travelled by the tracer particles, this highlights that solid motion and mixing in expanded beds may have been underestimated to date.

The use of Equation 2.1 for calculation of solid axial dispersion coefficients in expanded beds is generally questionable, since Van der Meer et al. (1984) used binary particle systems of two fractions with different particle sizes, rather than a gradient as used in EBA. Also, the correlation was stated to be valid for fluid velocities of 0.002 < u < 0.02 m/s, corresponding to 720 – 7200 cm/h and therefore much higher than flow rates usually applied in EBA. Furthermore, particle diameters were between 519 and 713 µm and thus much bigger than usual EBA particles, in particular the Rhobust beads used in this study.

Still, comparing these overall values to solid axial dispersion coefficients in common, non-classified solid-liquid fluidised beds, as expected much lower solid dispersion was found here for expanded beds. Although difficult to put side by side as particle sizes and liquid velocities are usually larger in common fluidised beds, solid axial dispersion coefficients were determined in the range of 1 - 10 x 10^{-4} m^2/s, *i.e.* approximately two orders of magnitude higher than those calculated here (Kennedy and Bretton 1966; Dorgelo et al. 1985; Yutani and Fan 1985; Kang et al. 1990).

However, Figure 2.9 illustrates that indeed, as Van der Meer et al. (1984) suggested, solid axial dispersion depends on the superficial fluid velocity (or bed expansion) and increases with increasing flow rate. Furthermore, it shows that solid dispersion is a function of the position along the column height, which was not accounted for in previous models using

Van der Meer's correlation (Wright and Glasser 2001; Kaczmarski and Bellot 2004; Li et al. 2005). Here, highest solid axial dispersion can be found in the middle of the bed, while lower values are observed for the top and bottom positions, respectively. This seems to contradict findings by Lin et al. (2015), who determined the local effective liquid axial dispersion by measuring RTDs along the column in a similar set-up as employed in this study. They observed a minimum of $D_{ax,l}$ at relative bed heights between 0.6 - 0.8, which is represented by the 'mid' tracer particle with a $h_{T,0}$ of around 0.60 (from correlation). The interrelationship between the liquid axial dispersion and the solid axial dispersion seems therefore still unclear.

2.4.3.2. *Influence of settled bed height, column diameter and fluid distribution system*

The effects of settled bed height, column diameter as well as the fluid distribution system on the tracer motion in expanded beds of Rhobust® MabDirect Protein A matrix were investigated by performing PEPT studies in a smaller, 1 cm diameter nozzle inlet column with a lower settled bed height of 15.5 cm as well as a 2.5 cm Streamline column with a perforated plate and mesh as fluid distributor. As described in paragraph 2.3.4, in these two sets of experiments, the flow was stopped at the end of each run at a particular fluid velocity (corresponding to a particular bed expansion) and the adsorbents were let to settle for 15 minutes. This allowed the tracers to be characterised by their relative positions in the settled bed ($h_{T,0}$) as explained in paragraph 2.4.2. Furthermore, additional bed expansions at degrees of 2.6 and 2.8 fold were also examined. Results are shown in the following and compared to the previously investigated 2 cm diameter nozzle inlet column.

Figure 2.10 and Figure 2.11 show the three-dimensional trajectories of three tracer particles representing the bottom, the mid and the top of the expanded bed with increasing superficial liquid flow velocities in both of the different column types under study. Again, only location data of the last 15 minutes are displayed, following 30 minutes of equilibration.
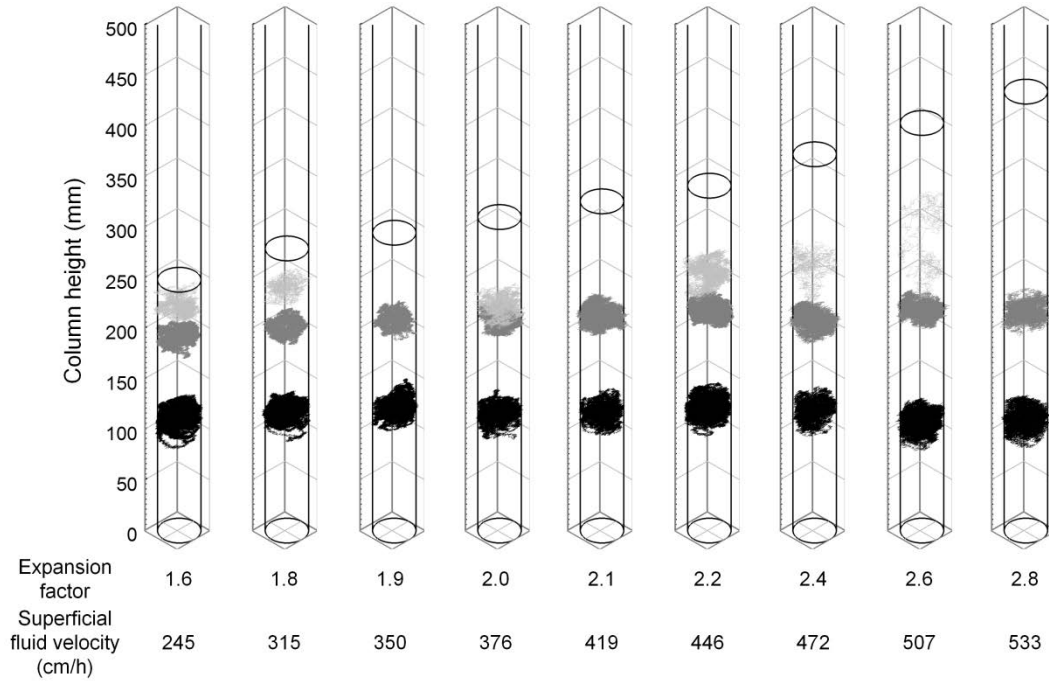
Figure 2.10: Superimposed three-dimensional trajectories of ^{18}F-labelled alumina tracer particles specified as $h_{T,0}$ = 0.52 (black), 0.82 (dark grey) and 0.90 (light grey) within an expanded bed of Rhobust® MabDirect Protein A adsorbents with initial settled bed height H_0 = 15.5 cm in a 1 cm diameter nozzle inlet column at increasing superficial fluid velocities and expansion factors. Column boundaries and expanded bed height are displayed as black lines.
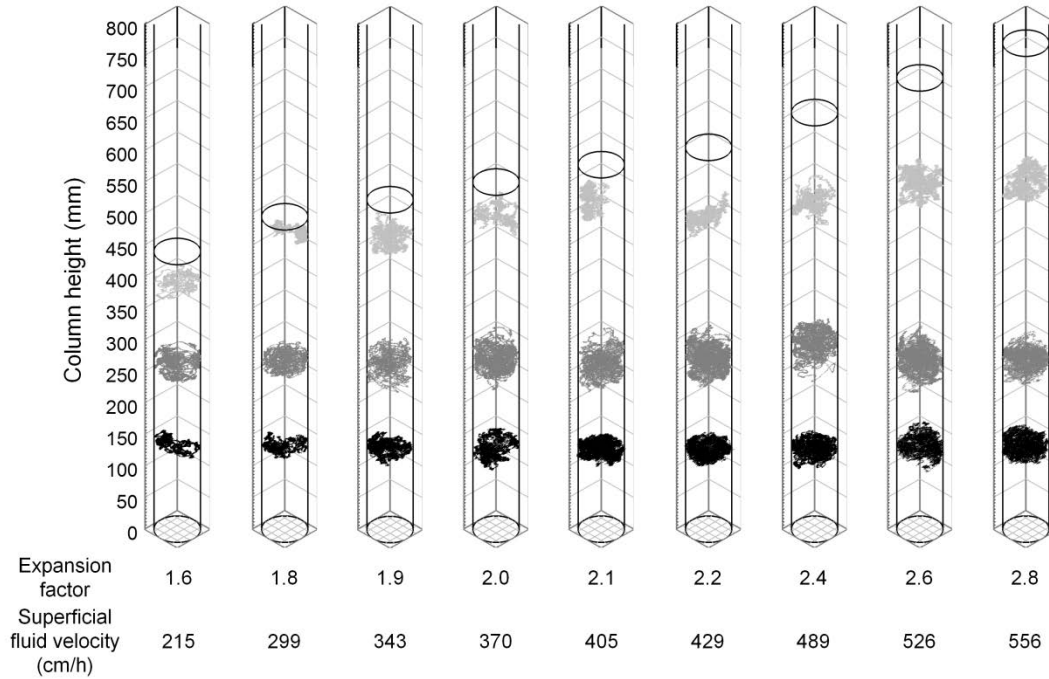
Figure 2.11: Superimposed three-dimensional trajectories of ^{18}F-labelled alumina tracer particles specified as $h_{T,0}$ = 0.32 (black), 0.60 (dark grey) and 0.94 (light grey) within an expanded bed of Rhobust® MabDirect Protein A adsorbents with initial settled bed height H_0 = 27.5 cm in a 2.5 cm diameter Streamline column at increasing superficial fluid velocities and expansion factors. Column boundaries and expanded bed height are displayed as black lines.

In Figure 2.10, data could not be obtained for all flow rates for the tracer particle representing the top due to low activity, which particularly presents an issue for smaller particles.

Overall, the results shown in Figure 2.10 and Figure 2.11 confirm the previous observation of general stratification or classification of the adsorbent particles within the expanded bed. Yet again, random motion of the tracer particle both in axial as well as horizontal direction can be found over considerable path lengths. The mean tracer particle velocities in all three columns studied, corresponding to 15 minutes of data as shown in the superimposed three-dimensional trajectories above, are depicted in Figure 2.12.
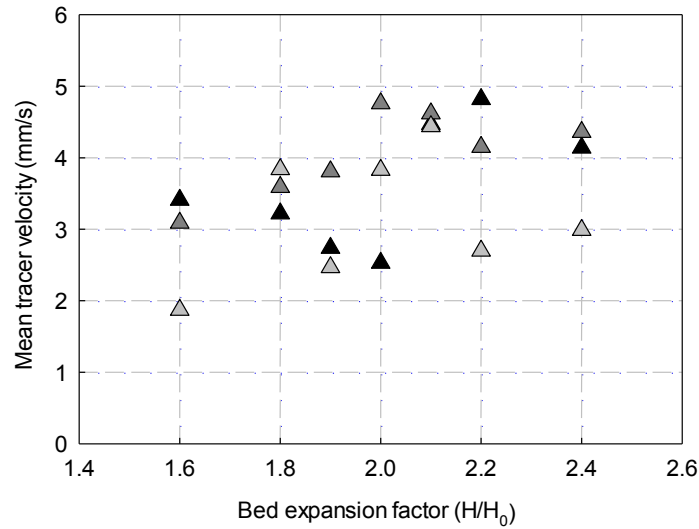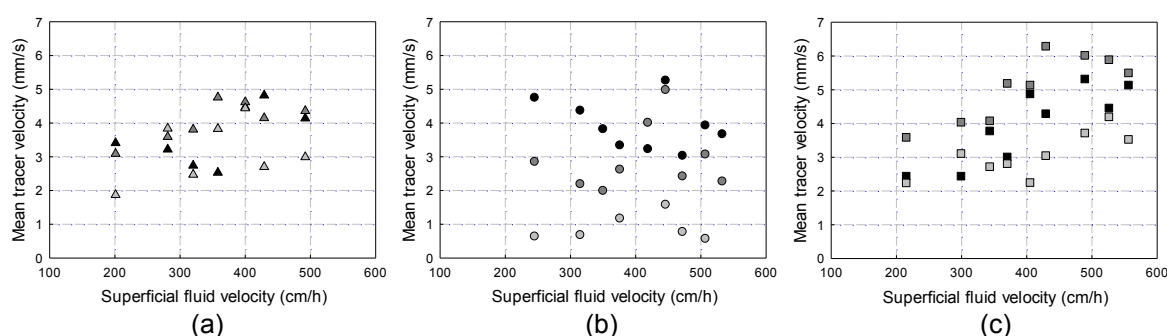

Figure 2.12: Mean velocities of ^{18}F-labelled alumina tracer particles representing the bottom (black), mid (dark grey) and top (light grey) parts of the bed versus superficial fluid velocity in expanded beds of Rhobust® MabDirect Protein A adsorbents during the last 15 minutes of data acquisition; (a) in a 2 cm diameter nozzle inlet column with H_0 = 25.5 cm, (b) in a 1 cm diameter nozzle inlet column with H_0 = 15.5 cm and (c) in a 2.5 cm diameter Streamline column with H_0 = 27.5 cm.

Comparing the tracer velocities found in the 1 cm diameter nozzle inlet column and the 2.5 cm diameter Streamline column in Figure 2.12 b and c with the previously shown velocities in the 2 cm nozzle inlet column in Figure 2.12 a, the overall values appear to be in the same range of up to 7 mm/s. A similar trend of increasing tracer velocities with increasing superficial fluid velocity as observed in the 2 cm nozzle inlet column was confirmed in the Streamline column. In contrast, for the 1 cm nozzle inlet column, no distinct behaviour of the tracer particles regarding their mean velocity dependent on the superficial fluid velocity could be identified. However, Figure 2.12 b shows a different

trend as the bottom representative tracer particle exhibits highest mean velocities while the top tracer moves the slowest. Mean tracer velocities appear to decrease with increasing bed height for all liquid flow rates applied. While this is not as obvious in the other two columns, still, the lightest, 'top' representative tracers (indicated in light grey in all of the above graphs) demonstrate lowest mean velocities for most superficial fluid velocities applied. Considering the increasing voidage with increasing bed height reported by several authors (Willoughby et al. 2000; Bruce and Chase 2001; Tong and Sun 2002; Lin et al. 2013), this may be explained by a lesser extent of interparticle collisions. It is difficult to identify the exact reason why this trend is more pronounced in the 1 cm nozzle inlet column, as it may be due to the lower settled bed height as well as the smaller column diameter.

Regarding the axial positioning of the tracer particles, interestingly, a similar pattern as described in Section 2.4.3.1 for the 2 cm nozzle inlet column was also observed in the other two columns (Figure 2.13).

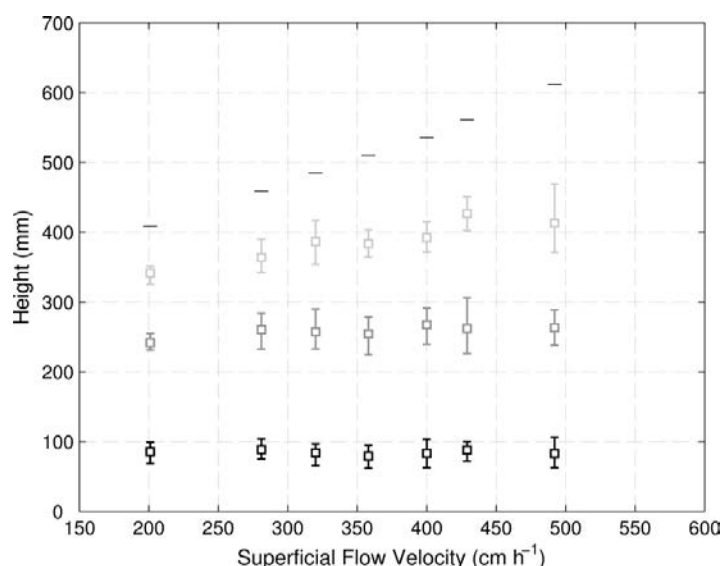(a)   (b)   (c)
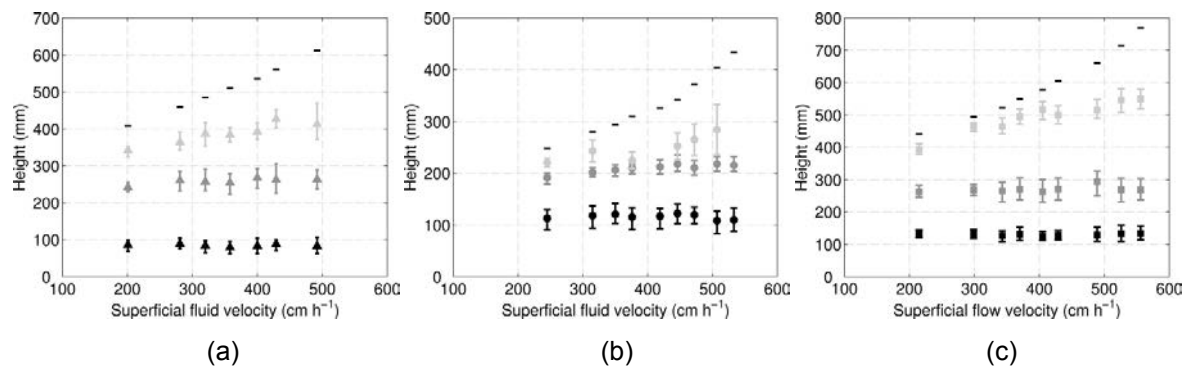
Figure 2.13: Superimposed mean (symbol), maximum and minimum (error bars) axial positions of ^{18}F-labelled alumina tracer particles representing the bottom (black), mid (dark grey) and top (light grey) parts of the column versus superficial fluid velocity in expanded beds of Rhobust® MabDirect Protein A in (a) a 2 cm diameter nozzle inlet column with H_0 = 25.5 cm, (b) a 1 cm diameter nozzle inlet column with H_0 = 15.5 cm and (c) a 2.5 cm diameter Streamline column with H_0 = 27.5 cm. Expanded bed heights are marked with black dashes.

Figure 2.13 b and c illustrate that despite slightly different positioning of the tracers within the bed, still, the tracer particles both in the 1 cm nozzle inlet column as well as the 2.5 cm Streamline column overall behave very similar with regard to increasing superficial

fluid velocity compared to those in the 2 cm nozzle inlet column (Figure 2.13 a). While the tracers representing the bottom and mid (indicated in black and dark grey) stay at their respective positions within the expanded bed at all flow rates applied, it is only the top tracers that move up and create the increased expansion at higher fluid velocities. This non-uniformity of bed expansion is therefore shown to be independent of the column type and thus independent of the fluid distribution system, as well as independent of the settled bed height.

Apart from the axial positions, motion ranges are indicated by the length of the error bars in Figure 2.13. Similar to the previously described behaviour in the Streamline column, the axial range of motion appears to increase only for the top tracer at increased superficial fluid velocities. Full absolute and relative axial motion range values are shown in Appendix 6.1.

The non-uniformity of bed expansion can be further demonstrated when analysing the ratio of the mean relative tracer position in the expanded bed to the mean relative tracer position in the settled bed, calculated by $\frac{\overline{h}_T}{\overline{h}_{T,0}}$, where $\overline{h}_T = \frac{\overline{H}_T(\Delta t)}{H}$ (Figure 2.14).
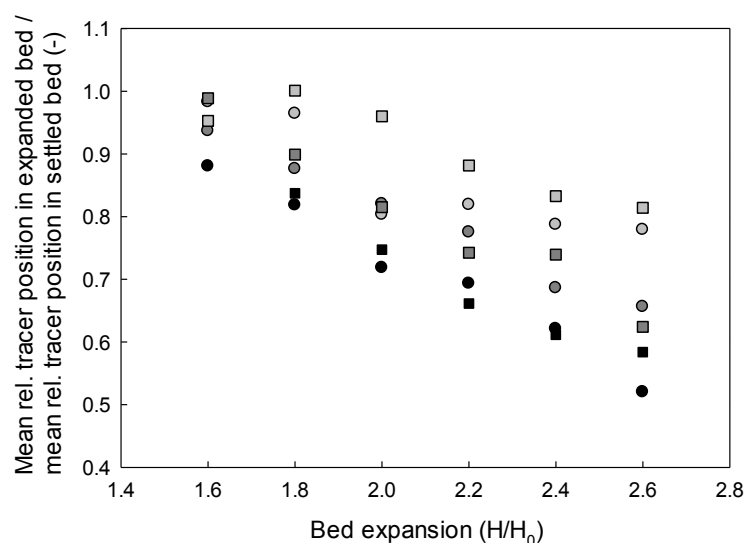
Figure 2.14: Ratios of ^{18}F-labelled alumina tracer particles' mean relative positions in the expanded bed to their mean relative positions in the settled bed versus bed expansion for tracers representing the bottom (black), mid (dark grey) and top (light grey) parts in expanded beds of Rhobust® MabDirect Protein A in a 1 cm nozzle inlet column (circles) and 2.5 cm Streamline column (squares).

If expansion was uniform, the ratio illustrated in Figure 2.14 would be 1 or close to, meaning the particles' relative position in the expanded bed matches those in the settled bed. This appears to be the case for lowest degrees of expansions only. However, with increasing expansions, just the tracers further up in the bed (shown in light grey) stay at a level of around 80% of their original relative position in the settled bed or higher, whereas mid (dark grey) and bottom (black) representing tracer particles drop down to 50 - 65%.

This phenomenon seems difficult to explain. If particles in the bottom and mid of the bed stay at their particular axial position in the column even at increasing superficial fluid velocity, it would imply that the interparticle void is not increasing as there is no space created by particles moving further up in the column. However, if the interparticle void is constant, the interstitial liquid velocity must increase with increasing volume flow. On the other hand, the axial position of the particle is dependent on the equilibrium between the particle's terminal settling velocity and the interstitial fluid velocity in the bed. The non-uniform expansion behaviour may thus have to result from interparticle collisions specifically developing at higher liquid flow velocities.

The axial mixing of the adsorbent particles in the different columns can be analysed when comparing the solid axial dispersion coefficients of the tracer particles under all conditions tested (Figure 2.15).
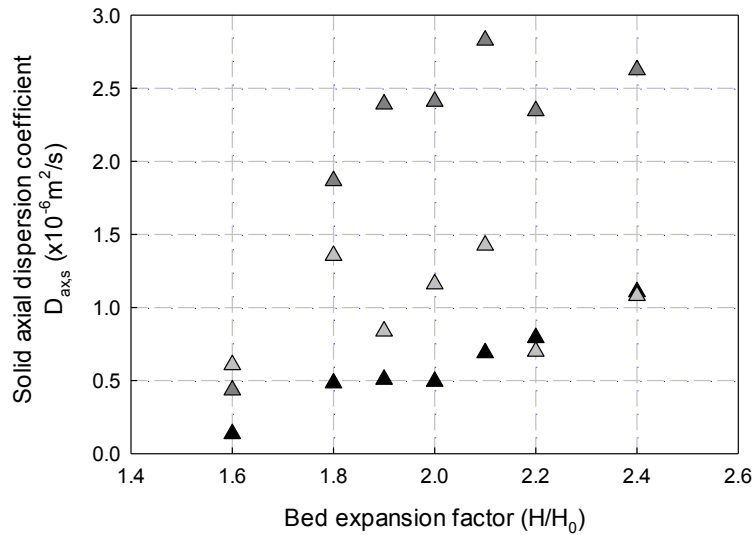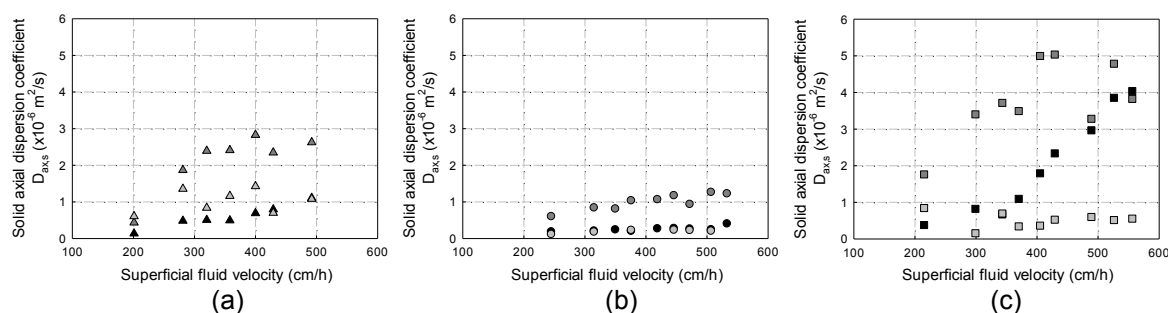

Figure 2.15: Solid axial dispersion coefficients of ^{18}F-labelled alumina tracer particles representing the bottom (black), mid (dark grey) and top (light grey) parts of the column versus superficial fluid velocity in an expanded bed of Rhobust[®] MabDirect Protein A adsorbents during the last 15 minutes of data acquisition; (a) in a 2 cm diameter nozzle inlet column with H_0 = 25.5 cm, (b) in a 1 cm diameter nozzle inlet column with H_0 = 15.5 cm and (c) in a 2.5 cm diameter Streamline column with H_0 = 27.5 cm.

In general, the values for the solid axial dispersion coefficients found in the 1 cm diameter nozzle inlet column and the 2.5 cm diameter Streamline column in Figure 2.15 b and c confirm the trend previously shown in the 2 cm nozzle inlet column in Figure 2.15 a with respect to increasing dispersion at increasing superficial fluid velocities. This is more pronounced in the Streamline column, where the highest overall values are observed. In comparison, the lowest dispersion is found in the 1 cm nozzle inlet column. It could therefore be assumed that solid axial dispersion depends on the column radius and ultimately on the volume distribution of the adsorbents within the column. However, considering the lower initial settled bed height in the 1 cm nozzle column as well as the different fluid distribution system in the Streamline column, the findings may not be attributable to one single parameter, but are rather a result of all of the parameters mentioned above.

2.4.3.3.   *Tracer axial positioning and stabilisation time*

When plotting the axial tracer particles' position over the entire time period of data acquisitioning (i.e. *ca.* 45 minutes), the random nature of motion mentioned above becomes distinct in the arbitrary up and down of the graphs (Figure 2.16).
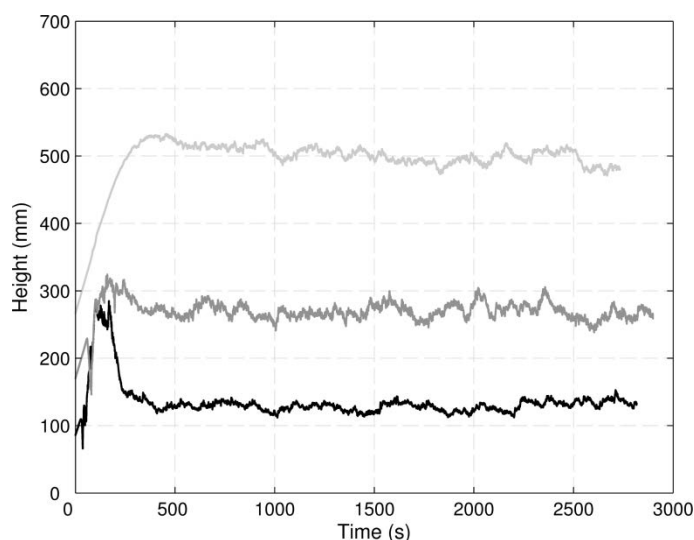
Figure 2.16: Superimposed axial positions of ^{18}F-labelled alumina tracer particles specified as $h_{T,0}$ = 0.32 (black), 0.60 (dark grey) and 0.94 (light grey) against time within an expanded bed of Rhobust$^{®}$ MabDirect Protein A adsorbents in a 2.5 cm diameter Streamline column (initial settled bed height H_0 = 27.5 cm; superficial liquid flow velocity of 370 cm/h corresponding to a 2.0-fold expansion).

Shown exemplarily above are axial trajectories of all three used tracer particles in the 2.5 cm diameter Streamline column for a 2.0-fold expansion (full axial trajectories for all columns and flow rates can be found in Appendix 6.2). After an initial rise and fall, which creates a form of overshooting after start up of flow, the tracer particles find a mean axial position. Around this mean position, they then randomly move up and down, which defines their axial range of motion.

Certain conclusions can be drawn from this with respect to defining an equilibration time required for the expanded bed to stabilise. The current suggested practice allows for 30 minutes of equilibration time in order to achieve a 'stable' expanded bed (Pharmacia 1997). However, when comparing axial trajectories for each of the tracer particles plotted

together for all liquid velocities applied, Figure 2.17 a - c show that it takes less than this

time (1800 seconds) for all tracers in to find their final mean position within the bed.

(a)   (b)   (c)
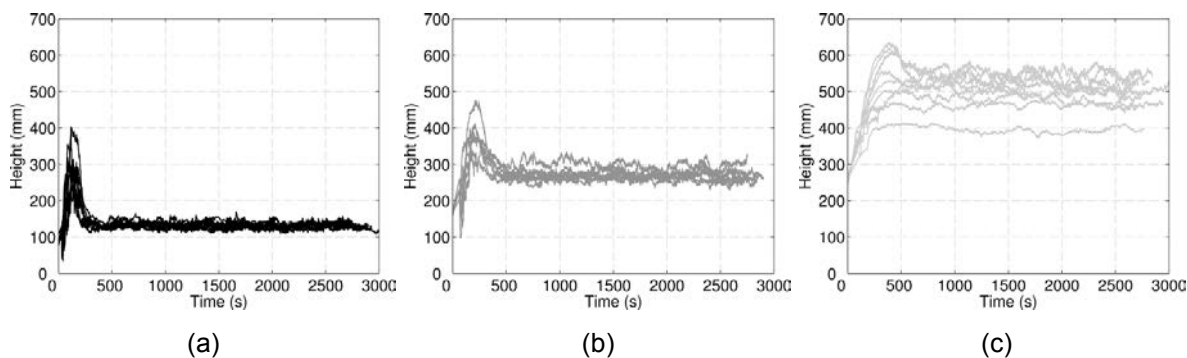
Figure 2.17: Axial positions of ^{18}F-labelled alumina tracer particles specified as (a) $h_{T,0}$ = 0.32, (b) 0.60 and (c) 0.94 against time within an expanded bed of Rhobust® MabDirect Protein A adsorbents in a 2.5 cm diameter Streamline column superimposed each for all flow rates applied (initial settled bed height H_0 = 27.5 cm).

The initial rising behaviour at the start of the fluid flow, during which the bottom and mid

tracer particles in particular appear to overshoot their later found mean position, might be

explained by a plug-like rise of the resin at the beginning of pumping liquid. From visual

inspection during the flow start up, it could be suggested that because of the previously

settled bed, adsorbent particles initially tend to slightly 'stick' together and rise up as 'plug'

before loosening from the bottom and dropping down again. This would also explain why

the mid tracers sink down later than the bottom ones and why the top particles hardly

show this overshooting behaviour at all.

While the time for each tracer particle to reach its main axial position seems independent

of the flow rate, the overshooting distance, defined by the maximum axial position the

tracer particle reaches during this initial rise compared to the mean axial position found

later, increases with increasing flow rate. This most likely results from the resin 'plug'

rising faster and higher within the column at higher liquid velocities.

Overall, in this particular case for the 2.5 cm diameter Streamline column, the

overshooting of tracers appears to end and relatively stable mean positions are found

after roughly 200 - 300 s for the particle representing the bottom (*cf.* Figure 2.17 a), around just under 500 s for the mid (Figure 2.17 b) and around or just over 500 s for the top part of the bed (Figure 2.17 c). Judging a bed 'stable', meaning that every particle in the bed has found its mean axial position, would infer a maximum equilibration time of less than 10 minutes. Comparing this to the suggested 30 minutes leads to a massive potential for reduction of process time as well as buffer consumption.

Furthermore, stabilisation times were even shorter for the 1 cm diameter nozzle inlet column, which were found to be 200 - 300 s for all three tracer particles. This difference in stabilisation time and behaviour compared to the Streamline column might be related to the lower settled bed height and lower overall adsorbent volume in the smaller column.

2.4.4. Influence of column vertical alignment

Using the technique of PEPT also enables gaining insight about bed instabilities e.g. caused by a vertical misalignment of the column. Axial trajectories of the three column alignments under study (0.0°, 0.5° and 1.0° misaligned to the vertical) were plotted and compared for 1.6-, 2.0- and 2.4-fold expansion in Figure 2.18 (full axial trajectories for all expansions can be found in Appendix 6.1).
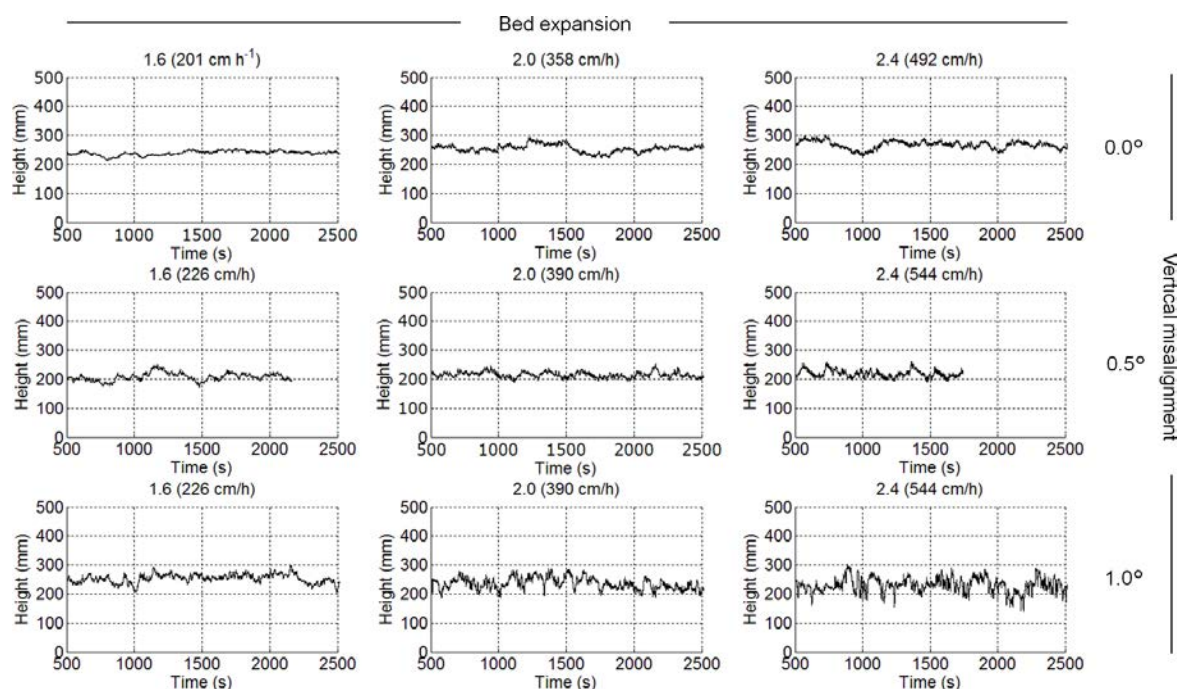
Figure 2.18: Axial position vs. time plots for ^{18}F-labelled alumina tracer particles specified as $h_{T,0} \approx 0.60$ (top, from correlation), 0.52 (mid) and 0.47 (bottom) planted in expanded beds of Rhobust® MabDirect Protein A adsorbents in a 2 cm diameter nozzle inlet column operated at different expansions (1.6, 2.0 and 2.4) and column misalignments to the vertical (0°, 0.5° and 1.0°).

As shown above, the motion range of the tracer particle distinctively increases with increasing vertical misalignment, in particular for higher flow rates or bed expansions, respectively. Moreover, the frequency of the axial motion increases, resulting in a more pronounced 'up and down' movement of the tracer particle at higher degrees of misalignment. Overall, the vertical misalignment leads to a destabilisation of the bed due to increased movement of the resin particles.

This is further illustrated when focussing exemplarily on the 2.0-fold expansion and analysing the tracer particle's axial and horizontal velocities as shown by velocity vectors in Figure 2.19.
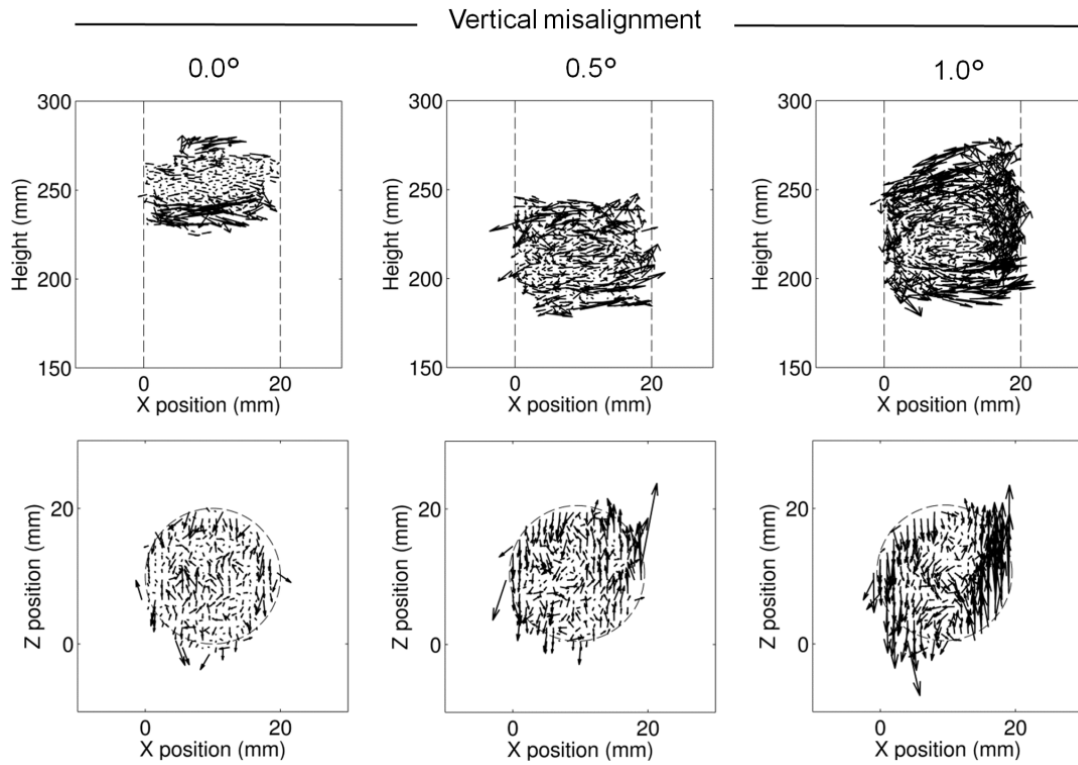
Figure 2.19: Axial (top) and horizontal (bottom) velocity vectors for ^{18}F-labelled alumina tracer particles specified as $h_{T,0} \approx 0.60$ (left, from correlation), 0.52 (mid) and 0.47 (right) planted in expanded beds of Rhobust® MabDirect Protein A adsorbents in a 2 cm diameter nozzle inlet column operated at 2.0-fold expansion for different column misalignments to the vertical (0°, 0.5° and 1.0°).

The axial vectors again depict the increased motion range as mentioned above. Furthermore, while vectors and thus the tracer particle's directions of movement are rather random for the perfectly vertically aligned and probably still for the 0.5° misaligned column, they show the development of a distinct circular motion pattern in axial direction in the 1° misaligned column. Although not indicated in Figure 2.19 due to the marginal extent considering dimensions, the column was tilted in negative x-direction. Therefore, particles are found to travel up the high side (the right side in Figure 2.19) and then down the opposite, low side of the column. This provides conclusive evidence for Bruce et al. (1999), who suggested a similar circular particle movement from visual observation.

Moreover though, horizontal velocity vectors depict an additional motion pattern in the cross section of the column. While vectors in the perfectly vertical column indicate random

directions, a pattern appears to be developing for the 0.5° and most distinctively for the 1.0° misaligned column. The tracer particle moves to one direction on the high side and back on the opposite, the low side of the column. Beyond the axial, this also results in a horizontal circulation, ultimately leading to a quasi elliptic movement.

To further illustrate this movement pattern, a close up of the mid tracer particle's trajectory in the 1° vertically misaligned column at 2-fold expansion is shown in Figure 2.20, only for the last 300 seconds of data acquisitioned.
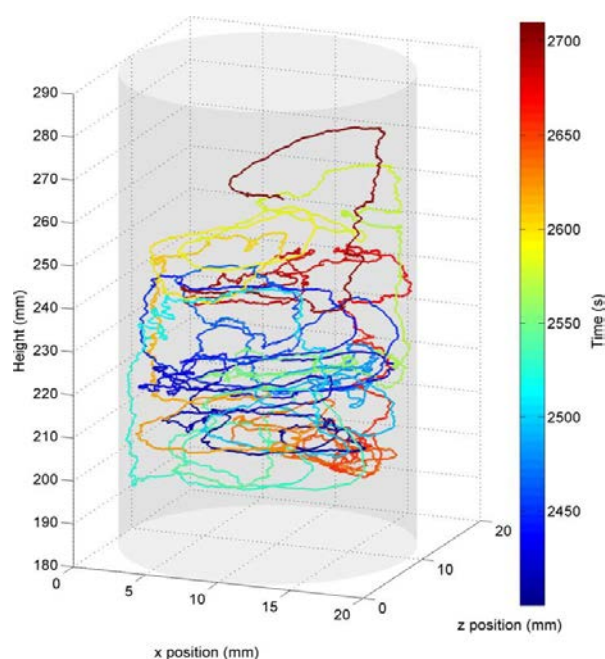
Figure 2.20: Three-dimensional trajectory of an ^{18}F-labelled alumina tracer particle ($h_{T,0}$ = 0.47) over time within an expanded bed of Rhobust® MabDirect Protein A adsorbents in a 2 cm diameter nozzle inlet column 1.0° misaligned to the vertical (initial settled bed height H_0 = 27.5 cm; superficial fluid velocity of 390 cm/h corresponding to a 2.0-fold bed expansion). Column boundaries are displayed in transparent grey.

Although again not depicted here due to the marginal extent of the column tilt considering dimensions, the misalignment lead to the column leaning in negative 'x position' direction. It is evident from Figure 2.20 that there are clear trajectories showing the upward motion of the tracer particle on the high (right) side, while it is obviously travelling downwards on the low (left) side of the column. Furthermore, the swaying circular movement in

horizontal direction becomes apparent, giving an idea about the quasi-elliptical motion suggested above.

The destabilisation of the bed due to increased particle and related liquid dispersion is also demonstrated by the according RTD results (Table 2.2). Calculated values of the solid axial dispersion coefficients as well as overall mean tracer velocities from the last 15 minutes of data are listed in comparison.

Table 2.2: Effect of column misalignment on plate numbers and axial dispersion coefficients.

Column misalignment	Bed expansion H/H_0	Mean plate number N	Mean liquid axial dispersion coefficient $D_{ax,l}$ ($\times 10^{-6}$ m^2 s^{-1})	Solid axial dispersion coefficient $D_{ax,s}$ ($\times 10^{-6}$ m^2 s^{-1})	Mean tracer velocity (mm/s)
0.0°	1.6	65	3.22	0.43	3.09
	2.0	68	5.78	2.41	4.76
	2.4	88	5.48	2.63	4.36
0.5°	1.6	41	5.21	2.02	4.85
	2.0	44	9.08	3.12	4.48
	2.4	51	12.44	4.68	7.33
1.0°	1.6	14	15.12	2.88	3.75
	2.0	13	30.95	4.81	5.77
	2.4	13	47.39	5.75	7.82

Table 2.2 shows the generally increasing plate numbers and decreasing values for the liquid axial dispersion coefficients with increasing bed expansion for all three column alignments. A similar behaviour has been found and explained previously by Theodossiou et al. (2002). More importantly, plate numbers significantly decrease and liquid axial dispersion coefficient values drastically increase with increasing column misalignment to the vertical. Values of the solid axial dispersion coefficient show a similar trend as they

increase with increased misalignment, although this is not as pronounced as for the liquid dispersion. Moreover, the mean tracer velocities illustrate the particles' motions at higher speeds, particularly at higher bed expansion in the misaligned columns. The information given in Table 2.2 hence confirms the overall increased solid as well as liquid mixing and the resulting bed destabilisation within misaligned columns.

2.5. Conclusion

Using the technique of positron emission particle tracking, tracer particles representing the bottom, mid and top parts of expanded beds of Rhobust® were investigated in three different columns. Influences of the superficial fluid velocity, settled bed height, column diameter, fluid distribution system and column vertical alignment on the particle motion were examined. Classification of the bed was confirmed as the largest tracer particles positioned themselves in the lower part of the bed, while smaller and lighter particles were located further up in the bed. Axial positions of bottom and mid representative tracer particles were found to be independent of the superficial fluid velocity in all of the three different columns and conditions studied. A non-uniform bed expansion was observed, in which only the top part of the bed accounted for the increased expansion at increasing flow rates, and interparticle collisions were proposed as a reason for this phenomenon.

Overall mean tracer velocities and solid axial dispersion were compared in the three contactors studied. Generally, for both the tracer velocities as well as the solid axial dispersion coefficients in all cases, values were found to be much larger than suggested in previous works, indicating that solid mixing may have been underestimated to date. In each system, the tracer particles representing the top part of the bed showed lowest velocities, while solid dispersion was most pronounced in the mid.

Bed stabilisation kinetics were determined by analysing the tracer particles' axial positioning over time after starting fluidisation. The time to reach a stable expanded bed was shown to be a maximum of 10 minutes in a 2.5 cm Streamline column and even shorter in a 1 cm diameter nozzle inlet column. Adjusting equilibration times based on this would lead to a reduction in process time as well as buffer consumption.

Vertical misalignment of the column resulted in an axial and horizontal circular movement pattern of the tracer particle, visualised by three-dimensional trajectories over time. The destabilisation of the bed was further documented by increasing liquid and solid axial dispersion with increasing misalignment to the vertical.

2.6. References

Anspach, F. B., D. Curbelo, et al. (1999). "Expanded-bed chromatography in primary protein purification." Journal of Chromatography A 865(1-2): 129-144.

Bruce, L. J. and H. A. Chase (2001). "Hydrodynamics and adsorption behaviour within an expanded bed adsorption column studied using in-bed sampling." Chemical Engineering Science 56(10): 3149-3162.

Bruce, L. J., S. Ghose, et al. (1999). "The effect of column verticality on separation efficiency in expanded bed adsorption." Bioseparation 8(1-5): 69-75.

Chase, H. A. (1994). "Purification of proteins by adsorption chromatography in expanded beds." Trends in Biotechnology 12(8): 296-303.

Dorgelo, E. A. H., A. P. van der Meer, et al. (1985). "Measurement of the axial dispersion of particles in a liquid fluidized bed applying a random walk method." Chemical Engineering Science 40(11): 2105-2111.

Drossard, J. (2005). Downstream Processing of Plant-Derived Recombinant Therapeutic Proteins. Molecular Farming, Wiley-VCH Verlag GmbH & Co. KGaA: 217-231.

Fan, X., D. J. Parker, et al. (2006). "Labelling a single particle for positron emission particle tracking using direct activation and ion-exchange techniques." Nuclear Instruments & Methods in Physics Research Section a-Accelerators Spectrometers Detectors and Associated Equipment 562(1): 345-350.

Frej, A. K. B., H. J. Johansson, et al. (1997). "Expanded bed adsorption at production scale: Scale-up verification, process example and sanitization of column and adsorbent." Bioprocess Engineering 16(2): 57-63.

Hjorth, R. (1997). "Expanded-bed adsorption in industrial bioprocessing: Recent developments." Trends in Biotechnology 15(6): 230-235.

Hjorth, R., S. Kampe, et al. (1995). "Analysis of Some Operating Parameters of Novel Adsorbents for Recovery of Proteins in Expanded Beds." Bioseparation 5(4): 217-223.

Hubbuch, J., J. Thommes, et al. (2005). "Biochemical engineering aspects of expanded bed adsorption." Technology Transfer in Biotechnology: From Lab to Industry to Production 92: 101-123.

Kaczmarski, K. and J.-C. Bellot (2004). "Theoretical Investigation of Axial and Local Particle Size Distribution on Expanded Bed Adsorption Process." Biotechnology Progress 20(3): 786-792.

Kang, Y., J. Nah, et al. (1990). "Dispersion and fluctuation of fluidized particles in a liquid-solid fluidized bed." Chemical engineering communications 97(1): 197-208.

Karau, A., C. Benken, et al. (1997). "The influence of particle size distribution and operating conditions on the adsorption performance in fluidized beds." Biotechnology and Bioengineering 55(1): 54-64.

Kennedy, S. C. and R. H. Bretton (1966). "Axial dispersion of spheres fluidized with liquids." Aiche Journal 12(1): 24-30.

Kiared, K., F. Larachi, et al. (1997). "Flow Structure of the Solids in a Three-Dimensional Liquid Fluidized Bed." Industrial & Engineering Chemistry Research 36(11): 4695-4704.

Leadbeater, T. W., D. J. Parker, et al. (2012). "Positron imaging systems for studying particulate, granular and multiphase flows." Particuology 10(2): 146-153.

Li, P., G. Xiu, et al. (2005). "Experimental and modeling study of protein adsorption in expanded bed." Aiche Journal 51(11): 2965-2977.

Lin, D.-Q., W. Shi, et al. (2015). "Evaluation and characterization of axial distribution in expanded bed: II. Liquid mixing and local effective axial dispersion." Journal of Chromatography A 1393: 65-72.

Lin, D.-Q., H.-F. Tong, et al. (2013). "Evaluation and characterization of axial distribution in expanded bed. I. Bead size, bead density and local bed voidage." Journal of Chromatography A 1304: 78-84.

Liu, H. (2009). "Application of new materials and tools in bioseparations." PhD Thesis, University of Birmingham.

Parker, D. J., C. J. Broadbent, et al. (1993). "Positron Emission Particle Tracking - a Technique for Studying Flow within Engineering Equipment." Nuclear Instruments & Methods in Physics Research Section a-Accelerators Spectrometers Detectors and Associated Equipment 326(3): 592-607.

Parker, D. J., A. E. Dijkstra, et al. (1997). "Positron emission particle tracking studies of spherical particle motion in rotating drums." Chemical Engineering Science 52(13): 2011-2022.

Pharmacia (1997). Expanded Bed Adsorption: Principles and Methods. Uppsala, Sweden.

Souquet, J. (2011). "Advances in Expanded Bed Adsorption Chromatography." PhD Thesis, University of Birmingham.

Souquet, J., H. Liu, et al. (2007). "Exposing expanded beds to PEPT." Journal of Biotechnology 131(2, Supplement): S191.

Stewart, R. L., J. Bridgwater, et al. (2001). "Granular flow over a flat-bladed stirrer." Chemical Engineering Science 56(14): 4257-4271.

Theodossiou, I., H. D. Elsner, et al. (2002). "Fluidisation and dispersion behaviour of small high density pellicular expanded bed adsorbents." Journal of Chromatography A 964(1-2): 77-89.

Thömmes, J. (1997). Fluidized bed adsorption as a primary recovery step in protein purification. New Enzymes for Organic Synthesis, Springer Berlin Heidelberg. 58: 185-230.

Thömmes, J., M. Weiher, et al. (1995). "Hydrodynamics and performance in fluidized bed adsorption." Biotechnology and Bioengineering 48(4): 367-374.

Tong, X.-D. and Y. Sun (2002). "Particle size and density distributions of two dense matrices in an expanded bed system." Journal of Chromatography A 977(2): 173-183.

Van der Meer, A., C. Blanchard, et al. (1984). "Mixing of particles in liquid fluidised beds." Chemical engineering research & design 62(4): 214-222.

Willoughby, N., G. Habib, et al. (2000). "The use of rapid on-line monitoring of products and contaminants from within an expanded bed to control separations exhibiting fast breakthrough characteristics and to maximize productivity." Biotechnology and Bioengineering 70(3): 254-261.

Willoughby, N. A., R. Hjorth, et al. (2000). "Experimental measurement of particle size distribution and voidage in an expanded bed adsorption system." Biotechnology and Bioengineering 69(6): 648-653.

Wright, P. R. and B. J. Glasser (2001). "Modeling mass transfer and hydrodynamics in fluidized-bed adsorption of proteins." Aiche Journal 47(2): 474-488.

Yun, J., D.-Q. Lin, et al. (2004). "Measurement and modeling of axial distribution of adsorbent particles in expanded bed: taking into account the particle density difference." Chemical Engineering Science 59(24): 5873-5881.

Yun, J., S.-J. Yao, et al. (2005). "Variation of the local effective axial dispersion coefficient with bed height in expanded beds." Chemical Engineering Journal 109(1–3): 123-131.

Yun, J., S.-J. Yao, et al. (2004). "Modeling axial distributions of adsorbent particle size and local voidage in expanded bed." Chemical Engineering Science 59(2): 449-457.

Yutani, N. and L. T. Fan (1985). "Mixing of randomly moving particles in liquid—solid fluidized beds." Powder Technology 42(2): 145-152.

3. Solid axial dispersion and particle motion in expanded beds of varying matrices

3.1. Abstract

Positron emission particle tracking investigations of solid phase movement in beds of various EBA matrices were compared and analysed. Results obtained in previous studies using 'foreign' Chelex-100 resin beads in beds of Streamline (100 - 300 µm, 1.2 g/mL) and UFC (100 - 300 µm, 1.5 g/mL; Liu 2009) and 'native' Q HyperZ adsorbents (40 - 105 µm, 3.2 g/mL; Souquet 2011) were re-evaluated with respect to new insights gained in this work employing Rhobust® matrix (20 - 200 µm, 2.5 - 3.5 g/mL). In addition, further PEPT analysis examining a ^{18}F-labelled 'native' Q HyperZ during fluidisation with PBS was conducted.

Despite using different tracer particles and labelling techniques, columns and mobile phases, a non-uniform bed expansion with increasing fluid velocity was found in all beds of Streamline, Q HyperZ and Rhobust®. However, while lower parts in Streamline and Q HyperZ beds in fact contracted with increases in flow rate, they remained axially constant in Rhobust®. Still, in all cases bed expansion appeared to be created only by the smallest and lightest adsorbent beads in the top part of the bed. Furthermore, previous findings from Chapter 2 allowed a circular motion pattern observed by Liu (2009) to be attributed to a possible vertical misalignment of the column. Comparison of relative axial motion ranges of the respective tracer particles in each bed suggested increased stability and less solid axial dispersion in beds of Rhobust®. Kinetics of bed stabilisation for Q HyperZ adsorbents appeared to be comparable to those previously described for Rhobust® and indicate the universal potential for a reduction in equilibration times.

3.2. Introduction

Expanded bed adsorption (EBA) systems rely on the use of specialised adsorbent particles and their design is an essential feature of the process (Chase 1994; Hjorth 1997). Matrices with a defined distribution of particle size and potentially density create a particle classification along the axis of flow. In a classified bed, axial mixing and dispersion is minimised, thereby enhancing multistage chromatographic performance (Kelly et al. 2013). In addition, EBA adsorbents have to exhibit a generally higher density compared to traditional packed bed resins. This prevents elutriation of the beads at the top of the bed during application of highly viscous crude feed streams. Denser particles furthermore allow for higher flow velocities and therefore improved process productivity (Mattiasson and Nandakumar 2000). However, an increased fluid velocity may impair adsorption kinetics. A compromise has to be found between the adsorbents physical properties such as size, density and pore size, which determine the applicable flow velocities, and adsorption kinetics (Anspach et al. 1999; Lihme et al. 2000).

Considerable effort has been made in research over the years to optimise EBA adsorbents regarding their hydrodynamic as well as adsorptive properties. Various materials and preparation methods were explored as small high-density adsorbents were suggested to reduce diffusion limitations while allowing the use of high flow rates (Thömmes 1997). Different approaches for an increase in density were investigated such as incorporating or encapsulating dispersed solid particles including quartz, zirconia, titanium, stainless steel powder, glass or tungsten carbide (Griffith et al. 1997; Pai et al. 2000; Lei et al. 2005; Lin et al. 2006; Xia et al. 2007; Asghari and Jahanshahi 2012; Asgari et al. 2014). Another approach was to utilise a single high-density, non-porous solid core made of glass or stainless steel and subsequent coating with a porous surface or layers of pellicular media (Pålsson et al. 2000; Theodossiou et al. 2000; Theodossiou

et al. 2002; Zhou et al. 2004). Furthermore, methods to increase bed capacities by optimising adsorbent and ligand design were investigated (Wright et al. 1999; Hubbuch et al. 2005) while other studies focussed on minimising biomass-adsorbent interactions (Dainiak et al. 2002; Viloria-Cols et al. 2004; Jahanshahi et al. 2008; Arpanaei et al. 2010; Vennapusa and Fernandez-Lahore 2010) (see also Sections 1.3.4 and 1.3.6).

However, to date there remain few commercially available adsorbents which can be narrowed to three major matrix series (Li et al. 2014). First introduced to the market was the Streamline series (GE Healthcare Life Scienes, Little Chalfont, UK) which consists of cross-linked agarose containing dispersed quartz sand (100 - 300 µm, 1.2 g/mL; Pharmacia 1997). The HyperZ series from Pall Corporation (Portsmouth, UK) is based on a soft, high-capacity hydrogel core surrounded by a rigid zirconium oxide shell (40 - 105 µm, 3.2 g/mL; Xia et al. 2007). Last, Patheon's Rhobust® series is comprised of 3 % cross-linked agarose with encapsulated tungsten carbide (20 - 200 µm, 2.5 - 3.5 g/mL; Patheon, Groningen, Netherlands).

Positron emission particle tracking (PEPT) has successfully been employed to study the solid dispersion in each of those three commercially available matrices. Liu (2009) examined particle motion in beds of Streamline as well as UFC (UpFront Chromatography, now part of Patheon) using Chelex-100 resin beads radioactively labelled with ^{61}Cu or ^{66}Ga as 'foreign' tracers. Souquet (2011) employed PEPT for the investigation of solid phase behaviour in beds of Q HyperZ. Due to the different composition of the adsorbents and the use of a different labelling technique, it was feasible to directly label Q HyperZ particles with ^{66}Ga and track its position as 'native' tracer. In Chapter 2 of the present work, particle movement tracking was focussed on Rhobust® adsorbents. Similar to Liu's (2009) work, 'foreign' tracers were used with similar physical properties regarding size and density to those of the resin beads. However, a

different material (alumina instead of Chelex-100), a different labelling technique and a different radioisotope (^{18}F instead of ^{61}Cu/^{66}Ga) were employed.

In this study, the results regarding solid phase dispersion using various EBA matrices as examined with PEPT were evaluated and compared. Furthermore, an additional PEPT investigation in a bed of Q HyperZ adsorbents was conducted. Using a similar technique as employed for the examination of Rhobust® beads, a 'native' Q HyperZ particle was labelled with ^{18}F. Consequently, in addition to comparing different adsorbents, various labelling techniques, radioisotopes and tracer materials could be assessed.

3.3. Materials and methods

3.3.1. Materials

The expanded bed adsorbent used in this study, Q HyperZ, was a gift from Pall Europe Limited (Portsmouth, United Kingdom) consists of a soft, high-capacity hydrogel core surrounded by a rigid zirconium oxide shell. Araldite from Halfords Group plc (Redditch, UK) was used for coating. Di-sodium hydrogen phosphate heptahydrate was sourced from Merck KGaA (Darmstadt, Germany; CAS # 7782-85-6); potassium phosphate monobasic (CAS # 7778-77-0), sodium chloride (CAS # 7647-14-5) and potassium chloride (CAS # 7447-40-7), for phosphate buffered saline (PBS; 136 mM NaCl, 2.7 mM Potassium chloride, 8.9 mM phosphate; pH 7.0) were purchased from Sigma-Aldrich Company Limited (St. Louis, MO, USA).

3.3.2. PEPT tracer fabrication

In this study, Q HyperZ particles were used as 'native' tracers. A few tracer particles of roughly the same size (90 μm) were chosen and jointly labelled with ^{18}F using the indirect activation method as described by Leadbeater et al. (2012). Briefly, the particles were exposed to an aqueous solution of ^{18}F, which was previously prepared by direct bombardment of purified water using a ^{3}He beam from the Birmingham MC40 Cyclotron (Fan et al. 2006). 2.5 mL of this solution was then added to the selected particles. The volume chosen here was higher compared to previous works using alumina particles due to difficulties in labelling Q HyperZ particles with sufficient activity. ^{18}F ions were transferred from the aqueous phase and attached to the particle surface by adsorption. The excess water was then dried off with the help of an infrared lamp. The tracer particles were subsequently coated with araldite to prevent the leaching of radioisotopes into the surrounding fluid phase. This was done by dipping the selected particle into a drop of araldite and subsequent rolling to spread it evenly and as thinly as possible across the whole surface before drying.

Due to overall poor radioactivity achieved in the Q HyperZ particles and as smaller particles result in even lower activities, it was not possible to label smaller Q HyperZ particles with sufficient radioactivity for PEPT experiments.

3.3.3. Experimental set up

A 2.5 cm diameter glass column with a perforated plate and overlying mesh inlet system (Streamline 25; GE Healthcare, Little Chalfont, UK) was used in this study. It was mounted between the two parallel PEPT detector camera heads, which were adjusted to the closest face-to-face separation possible (250 mm) to achieve optimal data acquisition. The column's vertical position was ensured using a digital level (Torpedo DWL-200, Digi-

Pas, Avon, CT, USA) to give accuracies of alignment as close as 0.1°. The column was then connected to an ÄKTAprime plus system (GE Healthcare, Little Chalfont, UK) and an interposed outlet pump (Watson Marlow, Falmouth, UK), so that fluidisation could be attained via recirculation of phosphate buffered saline (see also section 2.3.3., Figure 2.1).

3.3.4. Bed expansion tests

The expansion characteristics of the Q HyperZ matrix were examined by measuring the expanded bed height at various flow rates using phosphate buffered saline (PBS). First, after adding the slurry to the column, the bed was fluidised for approximately 0.5 h allowing for a classified arrangement of the adsorbents in order to achieve an accurate value for the settled bed height H_0. The expansion factor at each superficial fluid velocity was then determined as the ratio of expanded bed height to the settled bed height (H/H_0). From the resulting expansion profiles the required flow velocities for the desired expansions were calculated and used for the PEPT experiments.

3.3.5. Experimental procedure

A single Q HyperZ particle radioactively labelled with [18]F (90 µm) was selected and added to the resin (H_0 = 15.4 cm) from the top of the column. The bed was fluidised at 2.2-fold expansion for 20 min to allow the tracer to find its position within the classified arrangement of adsorbents. Subsequently, the bed was let to settle before starting the PEPT runs.

For these, flow rates were used to achieve expansions from 1.6 to 2.8-fold. Data acquisition was started at the beginning of fluidisation to collect location data during initial

rise of the particles. Due to low radioactivity, the bed was only fluidised for approximately 30 min at each fluid velocity. Subsequently, data acquisition was ended when the flow was stopped and the adsorbents were let to settle for 15 minutes. Afterwards, the next run was started at a different fluid velocity.

3.3.6. Data analysis

Using PEPT, the position of the labelled tracer particle is determined by means of triangulation from a number of detected pairs of γ-rays. In practice, some of the detected events are corrupt due to scattered or random coincidences. Therefore an iterative algorithm was developed by Parker et al. (1993) to eliminate and reject these corrupt events. It calculates the point which minimises the sum of perpendicular distances between the reconstructed paths of all events within the initial sample. The reconstructions lying furthest away from this point are assumed to be corrupt and removed from the set of events. A new minimum distance point is calculated from the remaining events and the algorithm is iterated until only a predefined fraction of the initial event sample remains.

The resulting data consisting of the tracer coordinates (x, y, z) over time was then used to plot axial as well as three-dimensional trajectories. Tracer velocities were calculated using a six point weighted average method (Stewart et al. 2001):

$$u_i = 0.1 \left(\frac{\vec{p}_{i+5} - \vec{p}_i}{t_{i+5} - t_i} \right) + 0.15 \left(\frac{\vec{p}_{i+4} - \vec{p}_{i-1}}{t_{i+4} - t_{i-1}} \right) + 0.25 \left(\frac{\vec{p}_{i+3} - \vec{p}_{i-2}}{t_{i+3} - t_{i-2}} \right)$$
$$+ 0.25 \left(\frac{\vec{p}_{i+2} - \vec{p}_{i-3}}{t_{i+2} - t_{i-3}} \right) + 0.15 \left(\frac{\vec{p}_{i+1} - \vec{p}_{i-4}}{t_{i+1} - t_{i-4}} \right) + 0.1 \left(\frac{\vec{p}_i - \vec{p}_{i-5}}{t_i - t_{i-5}} \right)$$

(Eq. 3.1)

where u_i is the velocity of the particle at the position p_i and time t_i. The mean axial velocity is calculated from the average of the velocities along the y axis, while the mean horizontal velocity is determined from the velocities in x and y direction as:

$$u_h = \sqrt{u_x^2 + u_z^2} \qquad \text{(Eq. 3.2)}$$

3.4. Results and discussion

3.4.1. Bed expansion characteristics

Bed expansions of the various matrices in the columns as examined for the respective PEPT experiments are shown in Figure 3.1. While Liu (2009) employed a XK26 column (GE Healthcare, Little Chalfont, UK) with a perforated mesh and overlying Ballotini beads as fluid distributor for his studies regarding Streamline (100 - 300 µm, 1.2 g/mL) and UFC (100 - 300 µm, 1.5 g/mL), Souquet examined Q HyperZ adsorbent particles (40 - 105 µm, 3.2 g/mL) in a Streamline 25 column. Both used tap water for fluidisation. In contrast, in the present work, equilibration buffer (PBS) was used throughout. In addition to the previously described experiments with Rhobust®, in which three different columns were tested (1 and 2 cm diameter nozzle inlet columns and Streamline 25), hydrodynamics of Q HyperZ beads were analysed in a Streamline 25 column. A full list of the various materials, conditions and settings used in the different experiments can be found in Table 6.1: Conditions and settings for the different PEPT studies of EBA compared in Chapter 3.Table 6.1 in Appendix 6.4.
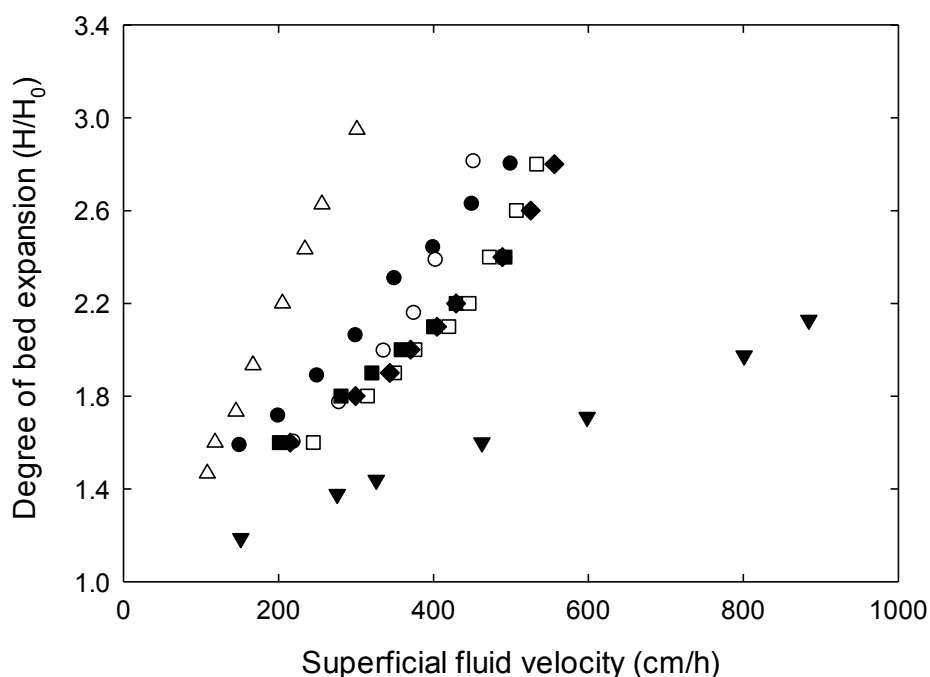
Figure 3.1: Bed expansion with increasing superficial fluid velocity for Rhobust®, Streamline, UFC and Q HyperZ matrices in various EBA columns. (●) Q HyperZ, Streamline 25 column, tap water (Souquet 2011); (○) Q HyperZ, Streamline 25 column, PBS; (■) Rhobust® MabDirect Protein A, 2 cm ø nozzle column, PBS; (□) Rhobust® MabDirect Protein A, 1 cm ø nozzle column, PBS; (◆) Rhobust® MabDirect Protein A, Streamline 25 column, PBS; (△) Streamline, XK26 column, tap water (Liu 2009); (▼) UFC, XK26 column, tap water (Liu 2009).

Figure 3.1 demonstrates the influence of the adsorbent properties on the bed expansion behaviour. Streamline adsorbents are affected the most by the increasing superficial fluid velocity as they exhibit the lowest density. Beds of similarly sized (100 - 300 μm), but denser UFC particles are least affected and show a shallow slope. The expansion curves of Rhobust® and Q HyperZ adsorbents are situated in between those two extremes, as they are generally smaller, but also denser than the Streamline and UFC particles. Possessing similar densities (2.5 - 3.5 g/mL cf. 3.2 g/mL), the slightly bigger Rhobust® beads (20 - 200 μm cf. 40 - 105 μm) require higher fluid velocities for the same degree of bed expansion compared to Q HyperZ.

However, the behaviour of Q HyperZ in the present study differs to some extent to that shown by Souquet (2011), especially at lower flow rates. This may be due to a combination of effects by the different mobile phases used (PBS *cf.* tap water) as well as

potential temperature differences. As described in Chapter 2, the temperature in the present work was set at 19° C throughout due to the PEPT electronics. However, temperatures were not mentioned in Liu's (2009) and Souquet's (2011) work, which suggests that bed expansion tests were performed at normal room temperature of approximately 23° C. In their technical note to EBA processes, GE Healthcare (1997) demonstrated that at constant fluid velocity, the degree of bed expansion in a buffer system decreases by approximately 0.1 with an increase in temperature of 2° C.

3.4.2. Comparing tracer particle motion in beds of various EBA matrices

3.4.2.1.   Bed expansion with increasing superficial fluid velocity

Liu (2009) first demonstrated the use of positron emission particle tracking for the investigation of adsorbent particle behaviour in beds of Streamline as well as UFC in a XK26 column using Chelex-100 resin beads radioactively labelled with ^{61}Cu or ^{66}Ga as 'foreign' tracers. Souquet (2011) followed up on Liu's work employing PEPT for the investigation of hydrodynamics of Q HyperZ beds in a Streamline 25 column. Due to the different composition of the adsorbents and the use of a different labelling technique, it was feasible to directly label Q HyperZ particles with ^{66}Ga and track its position as 'native' tracer.

In this study, an additional PEPT investigation in beds of Q HyperZ adsorbents in a Streamline 25 column was conducted. Using a similar indirect activation method as employed for the examination of Rhobust$^{®}$ beads, a 'native' Q HyperZ particle was labelled with ^{18}F. Furthermore, in contrast to Souquet's (2011) work, the bed was fluidised with PBS instead of tap water.

The three-dimensional trajectories resulting from the abovementioned investigations within the respective adsorbent beds at increasing superficial fluid velocities are shown in Figures 3.3 to 3.6.
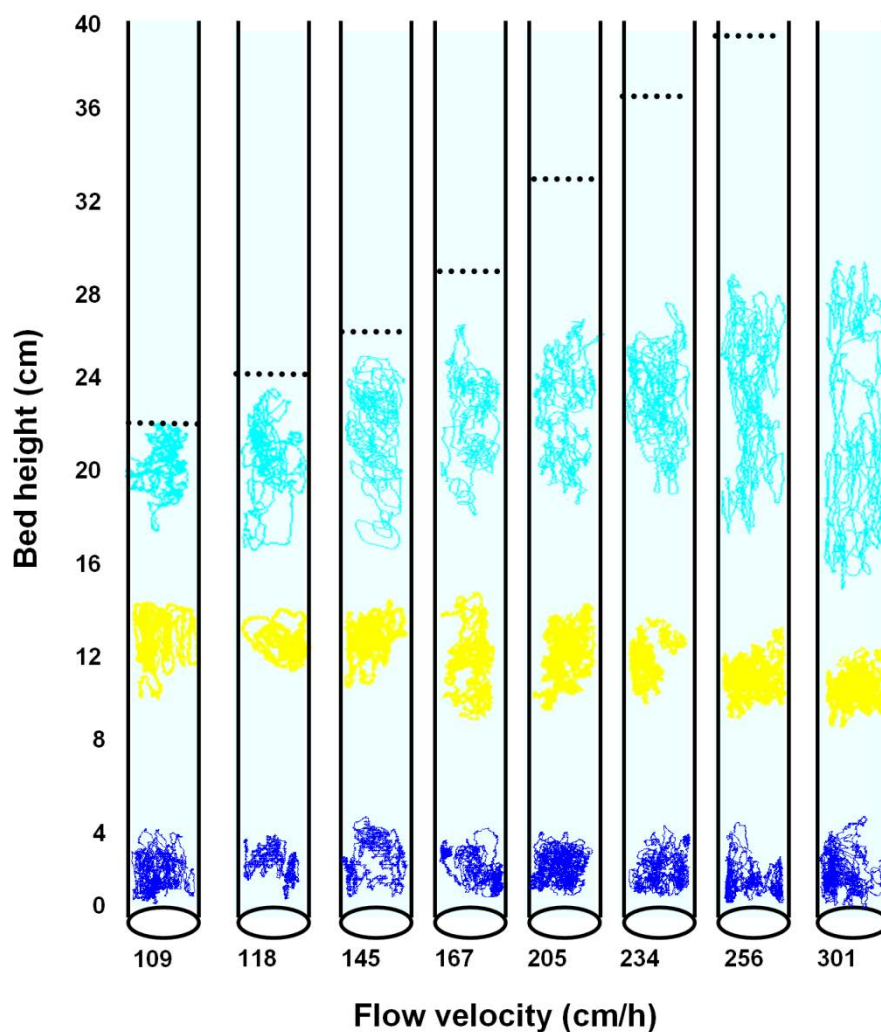
Figure 3.2: Superimposed three-dimensional trajectories of radioactively labelled Chelex-100 tracer particles within an expanded bed of Streamline adsorbents with initial settled bed height H_0 = 15.0 cm in a XK26 column dependent on the superficial liquid flow velocity. Locations of a 220 µm [61]Cu-labelled tracer are displayed in blue, those of a 150 µm and 110 µm [66]Ga-labelled tracer in yellow and turquoise, respectively. Black lines represent column boundaries and expanded bed heights (dotted). Taken from Liu (2009). Copyright by Haiyang Liu.
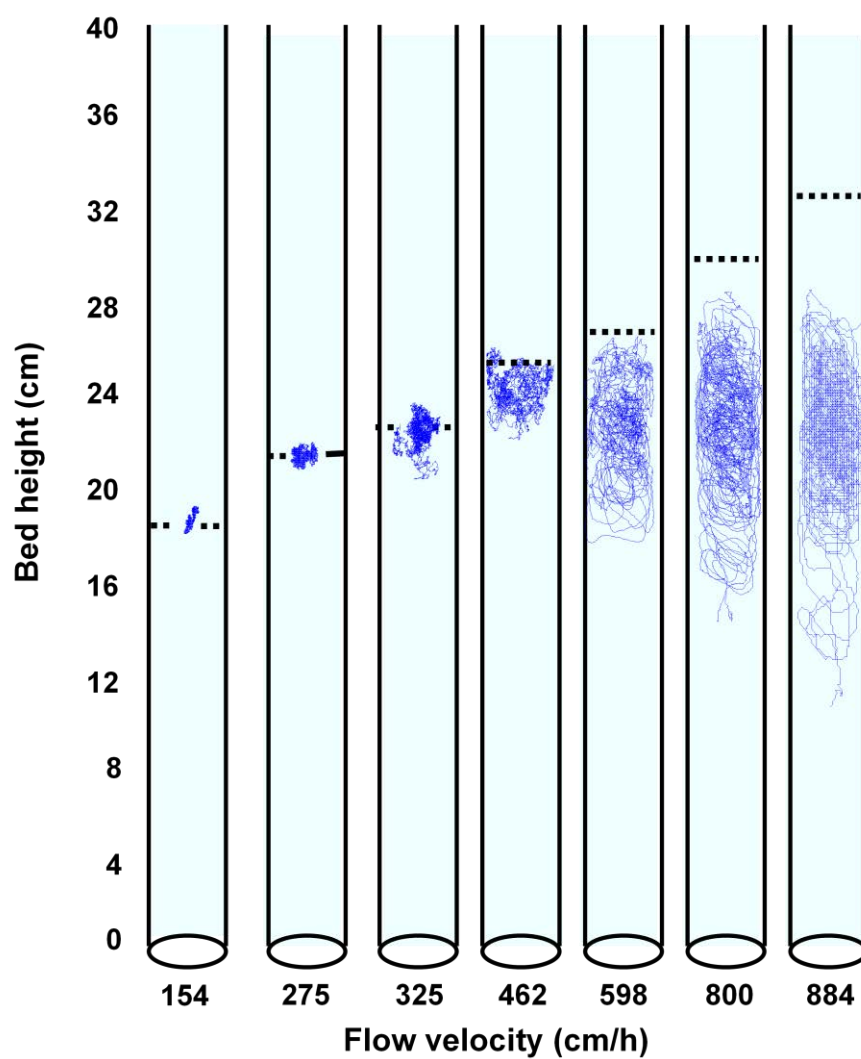
Figure 3.3: Three-dimensional trajectories of a 220 µm ^{61}Cu-labelled Chelex-100 tracer particles within an expanded bed of UFC adsorbents with initial settled bed height H_0 = 15.0 cm in a XK26 column dependent on the superficial liquid flow velocity. Black lines represent column boundaries and expanded bed heights (dotted). Taken from Liu (2009). Copyright by Haiyang Liu.
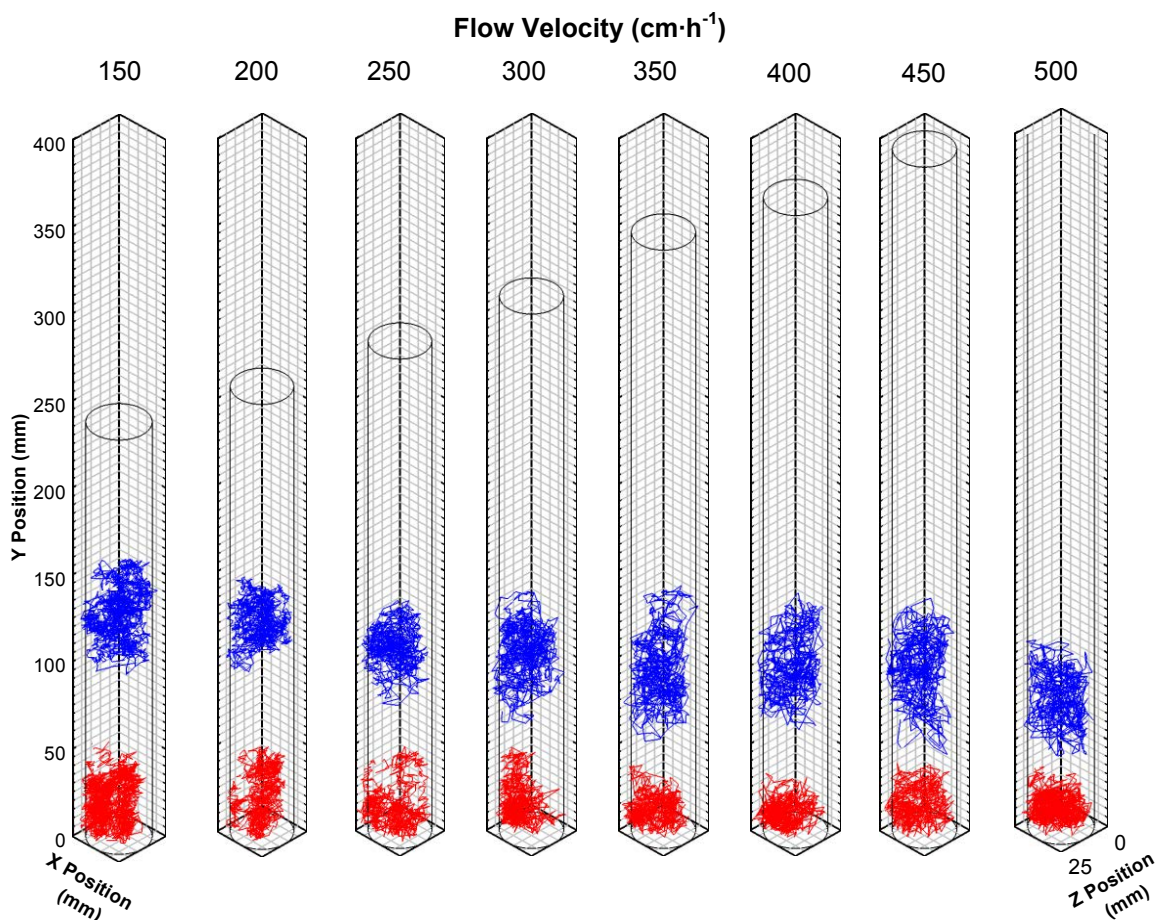
Figure 3.4: Superimposed three-dimensional trajectories of [66]Ga-labelled Q HyperZ tracer particles within an expanded bed of Streamline adsorbents with initial settled bed height H_0 = 15.0 cm in a Streamline25 column dependent on the superficial liquid flow velocity. Locations of a 100 µm and 75 µm tracer particle are displayed in red and blue, respectively. Black lines represent column boundaries and expanded bed heights. Taken from Souquet (2009). Copyright by Jonathan Souquet.
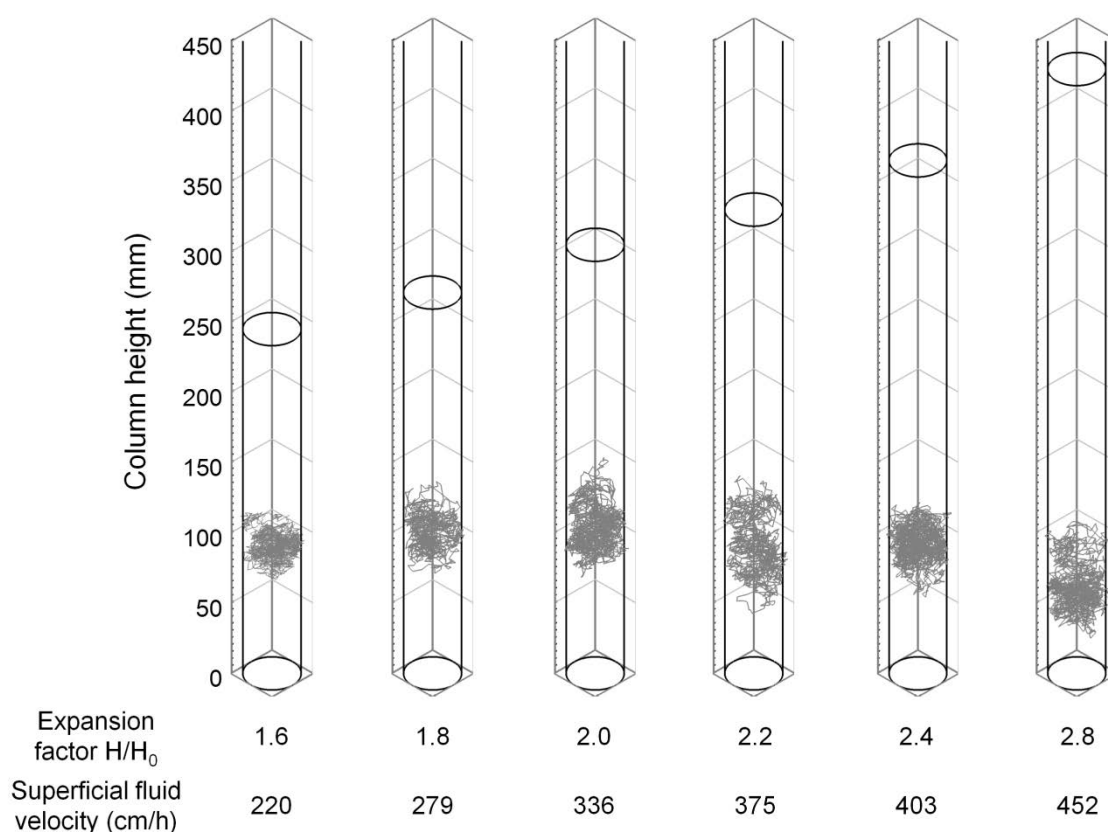
Figure 3.5: Three-dimensional trajectories of a ^{18}F-labelled Q HyperZ tracer particle (90 µm, $h_{T,0}$ = 0.39) within an expanded bed of Q HyperZ adsorbents with initial settled bed height H_0 = 15.4 cm in a 2.5 cm diameter Streamline column dependent on the superficial liquid flow velocity or expansion factor, respectively. Column boundaries and expanded bed height are displayed as black lines.

Comparing Figures 3.3, 3.4, 3.5 and 3.6 with each other and with the three-dimensional trajectories in beds of Rhobust[®] as shown in Chapter 2 (see Section 2.4.3.1 and 2.4.3.2), certain general conclusions can be drawn regarding particle motion in expanded beds and the effect of the liquid velocity.

First, all of the renditions above yet again confirm the observation as described previously for the Rhobust[®] matrix regarding stratification within the beds. The overall axial positioning of the tracers is as expected, i.e. larger/denser particles are located closer to the bottom whereas smaller and lighter beads are positioned further up in the bed. In the bed consisting of UFC adsorbents (Figure 3.3), the 220 µm Chelex-100 tracer particle positioned close to the top of the bed despite ranging in the larger part of the particle size

distribution of the matrix (100 - 300 µm). However, this was anticipated to a certain extent as the density of the Chelex-100 resin bead is smaller than that of the UFC particles (1.2 g/mL cf. 1.5 g/mL).

Second, in all the different experiments using various matrices, columns and tracer particles, generally random motion behaviour within the beds was found. Liu (2009) as well as Souquet (2011) pointed out that no particular flow patterns could be identified across the horizontal planes. However, Liu (2009) observed an axially cyclic motion pattern of particles at the top of the bed (110 µm tracer particle in the bed of Streamline and 220 µm tracer particle in UFC). Velocity profile plots revealed that the particles rose on one side of the column wall and sank on the opposite, in particular at high fluid velocities. Liu (2009) suggested inter-particle interactions, especially in the mixing zone of the column above the fluid distribution, as explanation for this phenomenon. However, results from investigations in this work regarding the influence of the column vertical alignment (see Section 2.4.4) propose a different interpretation. There, a very similar motion pattern, i.e. particles travelling up on one side and subsequently down on the other side of the column, was shown for deliberately vertically misaligned columns particularly at high fluid flow rates. A marginal deviation from perfectly vertical alignment may therefore have caused these comparable findings in Liu's (2009) work. Despite "using multiple spirit levels [...] to ensure strict verticality of the column", it is not proven that verticality could be achieved to a similar degree as with a digital level used in this work. Although not examined further in Chapter 2 as the study focussed on a mid bed tracer particle, the effect may have a greater influence on even smaller and lighter particles in the top of the bed. Hence, at a potentially lesser degree of misalignment than investigated with Rhobust$^{®}$ in Chapter 2 (i.e. <0.5°), this would show in the upper part of the bed first, explaining that the phenomenon was only observed for the smallest, but not the other tracer particles in Liu's study.

Still, for most operating conditions, adsorbent particles move randomly within particular regions of the bed according to their size and density. Considering only data from the last 15 min (Figure 3.4 and 3.6) and 30 min (Figure 3.2 and 3.4) of each run are shown, all tracers appear to travel over relatively large distances, again confirming similar observations found in beds of Rhobust® (see section 2.4.3.1 and 2.4.3.2). This contradicts the suggestion that adsorbent particles only exhibit small, circular movements (Pharmacia 1997; Drossard 2005).

Third, comparison of the overall axial positioning of the tracer particles within each of the presented beds reveals a pattern regarding bed expansion with increasing superficial fluid velocity. Liu (2009) and Souquet (2011) discovered similarities between the behaviour in the three beds of Streamline, UFC and Q HyperZ. They stated that particles close to the bottom of the bed, i.e. the 220 µm tracer particle in the bed of Streamline and the 100 µm tracer in Q HyperZ, retained a relatively constant mean axial height at increasing fluid velocity (approximately 30 and 20 mm, respectively; Figure 3.2 and 3.5). However, particles located in the middle of the bed, both the surrogate 150 µm Chelex-100 tracer in Streamline and the 'native' 75 µm Q HyperZ , gradually sank in the bed with increasing flow rate. Liu (2009) stated a decrease in height of the 150 µm Chelex-100 tracer from ca. 140 mm at 109 cm/h (corresponding to a 1.5-fold expansion) to 100 mm at 301 cm/h (H/H_0 = 2.9) in the bed of Streamline adsorbents, while Souquet (2011) reported a drop from approximately 135 mm at 150 cm/h (H/H_0 = 1.6) to 85 mm at 500 cm/h (H/H_0 = 2.8). These observations were further supported in the present study employing an ^{18}F-labelled Q HyperZ tracer particle during fluidisation with PBS instead of tap water (Figure 3.5). Despite the differences in labelling technique (including coating) and radioisotope used, the findings are in good accordance with Souquet's work. Here, the 90 µm tracer is shown to be axially positioned between the 75 µm and 100 µm [66]Ga-labelled particles as used by Souquet. At lower flow rates, it demonstrates comparable features to the 100 µm [66]Ga-

labelled particles closer to the bottom of the bed as it retains an approximately constant axial position at around 100 mm. At higher fluid velocities however, the tracer shows the same gradual drop as described by Souquet and the mean axial height decreases to ca. 60 mm.

The upper part of the beds could only be investigated in Streamline and UFC resins as neither in Souquet's nor in this work smaller Q HyperZ particles could be activated with sufficient radioactivity for PEPT investigation. In comparison with the bottom and mid bed representative tracers, the 110 µm Chelex-100 tracer in the bed of Streamline and the 220 µm tracer in the bed of UFC adsorbents appeared to be most affected by an increase in fluid velocity. Prominent in both cases are the large increases in the range of motion. The axial tracer movement at the top increased from around 20 mm at fluid velocities up to 325 cm/h to more than 180 mm at 884 cm/h in the UFC bed, while it increased from ca. 45 mm at 108 cm/h to 140mm at 301 cm/h in the bed of Streamline. Furthermore, the mean axial height of both tracers first increased with increasing flow rate up to a certain velocity (462 cm/h for the 220 µm tracer in UFC and 234 cm/h for the 110 µm tracer in Streamline) and then progressively dropped. The maximum height of the tracer particles however increased throughout. These effects (increase in range of motion as well as rise and fall in axial height) are shown to be much more pronounced in the bed of UFC compared to that of the Streamline matrix. Considering that the density of the Chelex-100 tracer particle met that of the Streamline adsorbents but was smaller than the density of the UFC matrix beads, the data acquired by Liu (2009) appears more reliable for the Streamline system.

Comparing these findings to those obtained in beds of Rhobust® as shown previously in Chapter 2 (see section 2.4.3.1 and 2.4.3.2), certain overall similarities but also disparities can be deduced. Analogous to the behaviour of bottom bed representative tracer particles

in Streamline and Q HyperZ above, the largest tracers located in the lower part of the beds of Rhobust[®] retained generally constant axial heights with increasing fluid velocity. However, tracers representing the mid and top part of the column showed a different response to raising flow rates in Rhobust[®] cf. Streamline and Q HyperZ beds. Here, no bed contraction in the middle of the bed could be identified, but very similar to the bottom representative particle, the tracer stayed at its axial position independent of the fluid velocity. The tracer particle at the top demonstrated a gradual rise within the bed at increasing flow rates and did not drop as described above for the Streamline and UFC beds. Furthermore, no comparably large increases in the axial motion range were observed.

Souquet (2011) described particle-particle interactions to cause the pattern of axial tracer position with increasing fluid velocity observed in Streamline and Q HyperZ beds. He suggested that the unexpected phenomenon of bed contraction in lower parts of the bed was likely a result of the increased motion within the upper section. This concept may also explain the different behaviour in the beds consisting of Rhobust[®] adsorbents. As here, the tracers in the upper part of the bed did not exhibit increases in their axial motion ranges as substantially as shown by Liu (2009), the particles further down may not have been as affected and therefore, did not contract. Still, a similar if smaller impact of the particles at the top of the bed may provide an explanation for the constant axial positioning of the lower parts of the bed compared to the expected rise with increasing fluid velocity.

The influence of the column verticality may play a significant role in the development of increased axial movement in the top part of the bed. As mentioned previously, from findings described in Chapter 2, it was concluded that Liu's (2009) observation of a cyclic motion pattern of the top representative tracer at high flow rates may have resulted from a

marginal vertical misalignment of the column. Similarly, an increased axial motion range was found for increasing degrees of misalignment (see section 2.4.4). Again, this may be even more pronounced at the top of the bed (cf. in the middle) and therefore noticeable at lower degrees of misalignment than 0.5° as examined in Chapter 2. If bed contraction was a direct consequence of the increased axial motion range in the upper part of the bed, which in turn resulted from a marginal vertical misalignment of the column, the column's position would offer a possible explanation for the phenomenon. However, a similar behaviour to Souquet's finding was shown in this study regarding Q HyperZ adsorbents (Figure 3.5). In view of the accuracy of the digital level used, it implies that the potentially underlying misalignment must be less than 0.1°. Still, no drops in the axial position of the mid representative tracer particles were detected in the beds of Rhobust[®] with 0.5° and 1.0° degree misaligned columns (see section 2.4.4 and appendix 6.3.).

Considering that differences in columns and fluid distribution systems as well as mobile phases were found to have hardly any influence regarding axial location of the adsorbent particles at various flow rates (see Chapter 2 and above), the differences between the Streamline and Q HyperZ behaviour on the one hand and that of Rhobust[®] may also be a consequence of inherent matrix characteristics. In particular, the differences in particle size distributions may play a considerable role. While Al-Dibouni and Garside (1979) found that at adsorbent size ratios (i.e. the ratio between the maximum and minimum particle diameter) of greater than 2.2 result in classification dominating the bed behaviour, Lihme et al. (2000) suggest an optimal ratio of about 3 to create a stable classified bed. Here, the values of the adsorbent size ratios are 3, 2.63 and 10 for the Streamline (100 - 300 µm), Q Hyper Z (40 - 105 µm) and Rhobust[®] (20 - 200 µm) matrices, respectively. Karau et al. (1997) investigated the influence of the particle size distribution on the adsorption performance in expanded beds. They studied three different particle size fractions and found reduced dispersion for operation using a wider size distribution.

Therefore, the reduced effect of axial motion range increases in the top of the bed in Rhobust® compared to Streamline and Q HyperZ may stem from the wider size distribution and the more than three times higher adsorbent size ratio. Additionally, in contrast to the to others, the Rhobust® matrix exhibits a defined density distribution which may further contribute to a higher particle stability especially at elevated fluid velocities (Pålsson et al. 2000).

Overall however, apart from the abovementioned differences, there still exists a major general trend: despite using various tracer particles and labelling techniques, columns and mobile phases, a non-uniform bed expansion with increasing fluid velocity was found in all beds of Streamline, Q HyperZ and Rhobust®. This poses questions on our understanding of this unit operation.

3.4.2.2.   Relative axial motion ranges

To be able to further compare not only overall positions of the tracer particles in their respective adsorbent beds but also the implication of their movement on solid phase dispersion, the tracer's relative axial motion ranges in beds of Streamline, Q HyperZ and Rhobust® are shown in Figure 3.6.
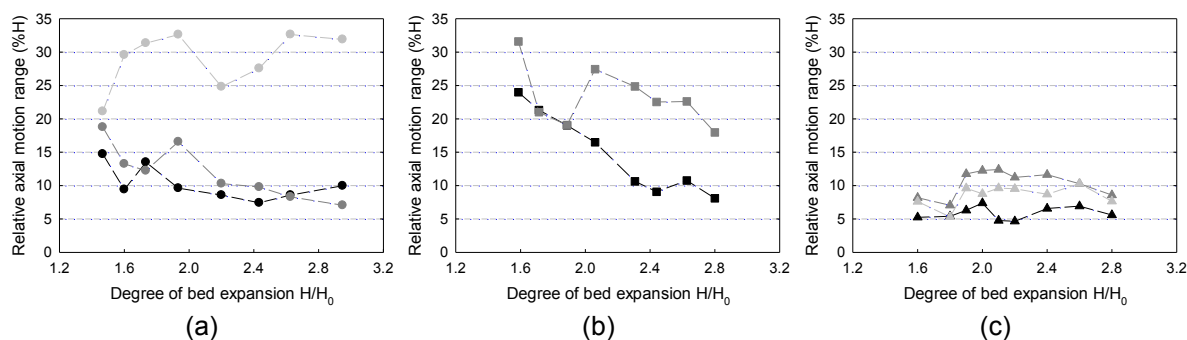
Figure 3.6: Relative axial motion ranges of a tracer particle representing the bottom (black), mid (dark grey) and top (light grey) part of the bed with increasing expansion in beds of (a) Streamline in a XK26 column (Liu 2009), (b) Q HyperZ (Souquet 2011) and (c) Rhobust[®] MabDirect Protein A in a 2.5 cm diameter Streamline column.

In the studies shown here, similarly sized columns with a diameter of 25 and 26 mm were employed. Instead of absolute values, relative axial motion ranges are plotted due to the different settled bed heights used ($H_0 = 15.0$ cm in studies using Streamline and Q HyperZ (Figure 3.6 a and b), $H_0 = 27.5$ cm for Rhobust[®] (Figure 3.6 c)).

As Liu (2009) pointed out for the Streamline adsorbent bed, the bottom and mid representative tracer particles (220 and 150 µm Chelex-100 particles, illustrated in black and dark grey in Figure 3.6 a, respectively) showed similar axial movement ranges. Absolute axial motion ranges were stated between 40 - 45 mm and described as "unaffected by change in flow rate". This corresponds to the decreasing curves in Figure 3.6 a, as the relative values decrease with increasing expanded bed heights. However, the bottom tracer ranges (black circles) are in fact relatively stable between 7.5 - 10% of the expanded bed height from 1.9-fold expansion on. On the contrary, the top tracer (110 µm Chelex-100, light grey in Figure 3.6 a) was found to significantly increase its absolute axial motion span. It moved axially within 25% and up to more than 32% of the expanded bed height for most fluid velocities or bed expansions, illustrating the fact that the trajectory occupied almost a third of the column and highlighting the increased movement at the top of the bed.

Souquet (2011) also described absolute axial motion ranges of tracers in beds of Q HyperZ as independent of the superficial fluid velocity. Both the 100 µm (black squares) as well as 75 µm Q HyperZ tracer particle (dark grey squares) indicate the decreasing relative axial span of movement with increasing degree of bed expansion in Figure 3.6 b. While the mid representative tracer drops from around 32% to 18%, the bottom tracer decreased from 24% to 8% of the expanded bed height with expansions from 1.6- to 2.8-fold.

Overall lower and more constant relative ranges of motion were observed for all three tracers in beds of Rhobust® adsorbents (Figure 3.6 b). Here, the bottom tracer particle (black triangles) shows the lowest span of axial movement with 5 - 8%, while the top and mid ranges are slightly higher with 5 - 10% and 7 - 13% of the expanded bed height, respectively. This suggests a more stable bed with less solid particle mixing was achieved with Rhobust® adsorbents compared to Streamline and Q HyperZ.

3.4.2.3.   *Axial and horizontal tracer velocities*

Mean overall tracer particle velocities for studies of Rhobust® adsorbents were given in Chapter 2 (see section 2.4.3.2). Liu (2009) and Souquet (2011) however analysed axial and horizontal velocities separately. Consequently, for better comparison these are plotted in Figure 3.7 for Rhobust® in the 2.5 cm diameter Streamline column.
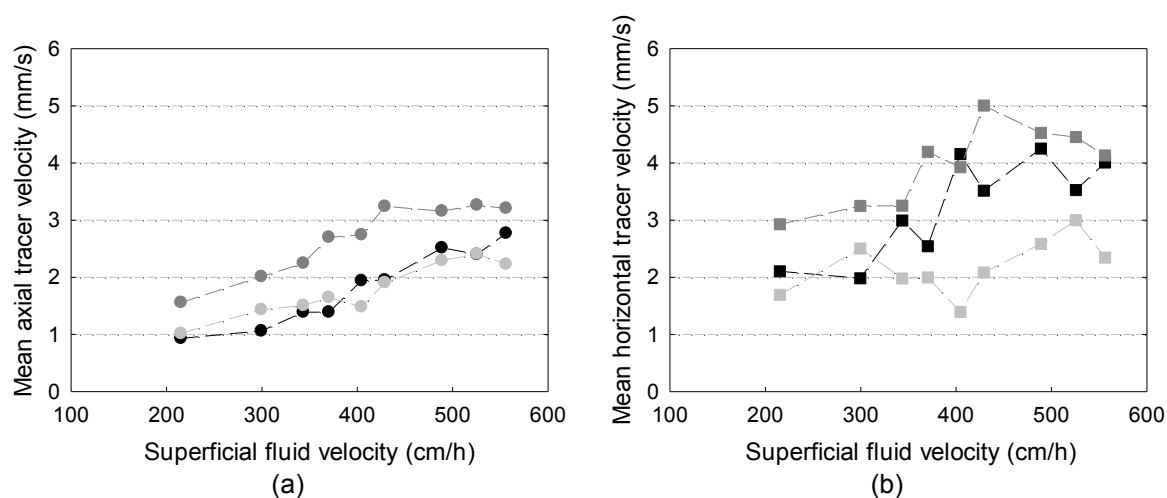
Figure 3.7: Mean axial (a) and horizontal (b) velocities of tracer particles representing the bottom (black, $h_{T,0} = 0.32$), mid (dark grey, $h_{T,0} = 0.60$) and top (light grey, $h_{T,0} = 0.94$) part of the bed with increasing superficial flow velocities during the last 15 minutes of data acquisition in an expanded bed of Rhobust® adsorbents in a 2.5 cm diameter Streamline column with $H_0 = 27.5$ cm.

Generally, higher values for both the axial and horizontal velocities for tracers in an expanded bed of Rhobust® are found here compared to those described in the studies of Liu (2009) and Souquet (2011) examining beds of Streamline and Q HyperZ. The Chelex-100 tracers in Streamline and the 'native' Q HyperZ particles showed axial and horizontal velocities in the range of 0.25 - 1.5 mm/s and 0.5 - 1.2 mm/s, respectively. In contrast, the alumina tracer particle within Rhobust® moved axially at up to 3.2 mm/s and horizontally at up to 5 mm/s. However, it is problematic to directly compare velocity values between the different studies of Liu (2009), Souquet (2011) and the present. First, differences in radioactivity achieved in the labelled tracer particles result in varying accuracies in determining their locations. While activities ranged from 7 - 70 µCi for the Q HyperZ 'native' tracers and from 100 - 200 µCi for the Chelex-100 tracers in beds of Streamline, alumina particles as used in Rhobust® beds showed activities between 300 - 600 µCi. Similarly, very low activities for the ^{18}F-labelled Q HyperZ particle in this work (<6 µCi) resulted in an insufficient amount of data to give accurate velocity values. Second, both Liu (2009) and Souquet (2011) used a different approach to calculate velocities compared to the present work. They employed a moving average trendline, generating a 'best fit'

curve over the PEPT data. However, this may lead to oversmoothing. In contrast, a six point weighted average method (see section 2.3.7) as commonly used in PEPT analyses (Parker et al. 1994; Stewart et al. 2001; Ng et al. 2008) was utilised in this work. For these reasons, the overall higher velocities found here for alumina tracers in beds of Rhobust$^{®}$ may be misrepresentative.

A comparison of tracer particle velocity trends with increasing flow rate may therefore give more decisive conclusions. Souquet (2011) observed a different behaviour for the bottom (100 µm) and for the mid (75 µm) Q HyperZ particle. While the latter showed a similar pattern for both axial and horizontal velocity, i.e. an initial increase with increasing mobile phase flow rate, subsequent levelling off and slight decrease, the former demonstrated a stable horizontal but decreasing axial velocity with increasing superficial fluid velocity. Souquet inferred the decreasing axial velocity of the 100 µm tracer particle to be a further result of the bed contraction phenomenon. Contradictory, this observation was not confirmed by Liu's (2009) findings. No similar decrease in axial velocity of the bottom representative tracer (220 µm Chelex-100) in Streamline could be identified. In contrast, both axial and horizontal velocities were described to increase with increasing fluid flow velocity for all three tracer particles. This in turn is in accordance with the results shown in Figure 3.7 for tracers within a bed of Rhobust$^{®}$ adsorbents. Here, axial velocity curves possess steady but shallow slopes very comparable for all tracers. Horizontal velocity curves are slightly more erratic but still show a clear increasing trend. Interestingly, the mid bed tracer (depicted in dark grey in Figure 3.7) exhibited the highest velocities compared to the top and bottom representative particles both axially and horizontally. Contrary, in Liu's (2009) study, the 110 µm Chelex-100 tracer at the top of the bed of Streamline moved with highest velocities. These observations match with the relative axial motion ranges as shown in Figure 3.6, proving that tracers exhibiting a larger range of motion generally also move at higher velocities and indicate a destabilisation of the

bed. Again, the higher velocity of the top tracer in the Streamline adsorbents compared to the mid and bottom representative is presumed to stem from the previously suggested marginal misalignment of the column.

3.4.2.4.   *Tracer axial positioning and stabilisation in Q HyperZ*

Due to the different experimental procedures as performed by Liu (2009) and Souquet (2011), no data is available with respect to the initial tracer behaviour after start of fluidisation. Liu (2009) used only the last 30 min of data for analysis of Streamline beds after 60 min of fluidisation with tap water, while Souquet (2009) allowed beds of Q HyperZ to equilibrate for 30 min before acquisitioning data for a subsequent 15 min.

Therefore, only data from the additional experiment carried out in this study can be used for comparison of the particles' motion during start up of flow and the time for stabilisation in beds of different adsorbent resins. The axial position of the 'native' ^{18}F-labelled Q HyperZ tracer particle over the entire time period of data acquisitioning (i.e. in this case ca. 30 min due to the low activity) is plotted in Figure 3.8 for all superficial fluid velocities applied.
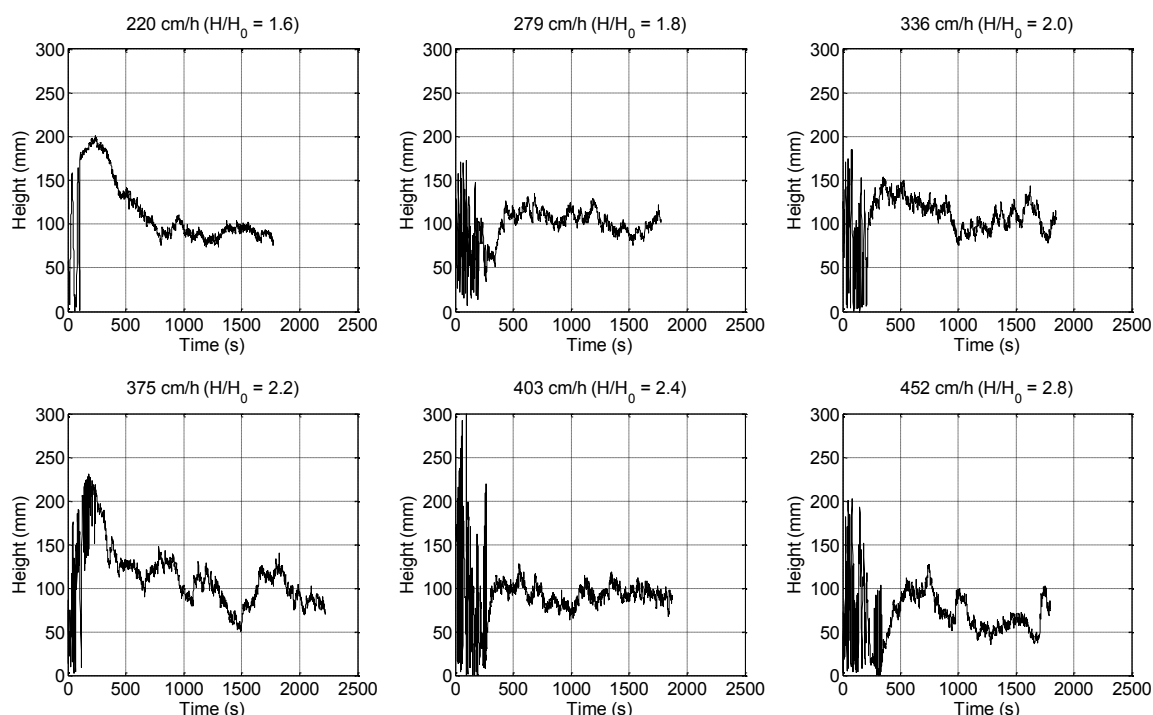
Figure 3.8: Axial position vs. time plots of a ^{18}F-labelled Q HyperZ tracer particle (90 µm, $h_{T,0}$ = 0.39) within an expanded bed of Q HyperZ adsorbents with initial settled bed height H_0 = 15.4 cm in a 2.5 cm diameter Streamline column for various superficial liquid flow velocities or expansion factors, respectively.

Figure 3.8 shows a different behaviour of the Q HyperZ tracer particle compared to that found in beds of Rhobust® in Chapter 2 (see section 2.4.3.3. and Appendix 6.2). The Rhobust® surrogates demonstrated a distinct initial rise and fall, creating a form of overshoot which was explained by a plug-like rise of the resin at start of fluid flow. In contrast, a more erratic motion was detected here for the Q HyperZ particle. Generally, the tracer appeared to be involved in strong mixing within the first 100 - 400 s of fluidisation with PBS, illustrated by the substantial spikes indicating the up- and downward movement. The intensity of this seems to increase with increasing superficial fluid velocity. For 1.6- and 2.2-fold expansion however, an additional overshoot formed, combined with stronger up and down motion at higher flow rate. Contrary to the Rhobust® beads this behaviour suggests that mostly, the Q HyperZ beads do not initially rise

119

together like a plug but are rather swirling within a large part of the bed (between 150 -
300 mm in expanded beds of 246 - 431 mm height).

However, similar to the previous work examining Rhobust®, a mean axial position within a
defined motion range was found after a certain time period. This time can be defined as
≤500 s for most superficial fluid velocities applied apart from the lowest (220 cm/h
corresponding to 1.6-fold expansion), which is very comparable to the stabilisation time
found previously in beds of Rhobust®. Considering only a tracer particle in the lower half
of the bed could be investigated here, the overall time for the bed to stabilise entirely may
be longer as longer times were found for top representative tracer particles in Rhobust®.
Then again, it is questionable whether this would be the same for Q HyperZ in view of the
differences in overall start-up behaviour. Furthermore, the settled bed height in this study
examining Q HyperZ was lower than that of the Rhobust® as described in Chapter 2
(H_0 = 15.4cm cf. 27.5 cm). Shorter stabilisation times of 200 - 300 s were found in a bed
of Rhobust® with more comparable settled bed height of 15.5 cm, although a smaller,
1 cm diameter nozzle inlet column was employed in this study. Hence, it was not clear
whether the shorter stabilisation time could be accounted for by the lower settled bed
height or the lower overall adsorbent volume in the smaller column. Comparison between
overall values for stabilisation times of Q HyperZ and Rhobust® beds is therefore
uncertain.

Still, in addition to Rhobust® resins, a generally significantly shorter time for bed
stabilisation was also found for Q HyperZ adsorbents compared to 30 min (i.e. the
typically suggested equilibration time). These results imply that equilibration times could
be reconsidered universally independent of the adsorbent type employed, indicating a
massive potential for reduction of process time as well as buffer consumption.

3.5. Conclusion

Positron emission particle tracking investigations of solid phase movement in beds of various EBA matrices were analysed and compared. Results obtained in previous studies using 'foreign' Chelex-100 resin beads in beds of Streamline (100 - 300 µm, 1.2 g/mL) and UFC (100 - 300 µm, 1.5 g/mL; Liu 2009) and 'native' Q HyperZ adsorbents (40 - 105 µm, 3.2 g/mL; Souquet 2011) were re-evaluated with respect to new insights gained in this work employing Rhobust® matrix (20 - 200 µm, 2.5 - 3.5 g/mL).

Thus, the extensive study regarding Rhobust® (see Chapter 2) allowed the exposure of an inconclusive motion pattern in Streamline as observed by Liu (2009). Due to a similar behaviour of tracer particles in a deliberately misaligned column, the circular movement of the top representative Streamline surrogate tracer particle was attributed to a possibly marginal deviation from perfectly vertical alignment of the column.

The previously described phenomenon of bed contraction with increasing superficial fluid velocity in lower parts of the bed of Streamline and Q HyperZ adsorbents could be confirmed by further PEPT experiments with a 'native' Q HyperZ particle despite using a different labelling technique and mobile phase compared to Souquet (2011). While increased motion in the top part of the bed and related particle-particle interactions were suggested to cause this observation, the mechanism still remains inconclusive. Generally lower axial motion ranges found in beds of Rhobust®, in particular for the top of the bed, may support this theory as no bed contraction but rather constant axial positions were identified in the lower part of the bed with increasing flow rates. However, still no bed contraction in Rhobust® was observed with demonstrated higher axial motion ranges at deliberate vertical column misalignment. Overall, despite using different tracer particles and labelling techniques, columns and mobile phases, a non-uniform bed expansion with

increasing fluid velocity was found in all beds of Streamline, Q HyperZ and Rhobust®, posing further questions on our understanding of this unit operation.

Lower relative axial motion ranges of respective tracer particles suggest a more stable bed with regard to solid axial dispersion could be achieved with the Rhobust® matrix compared to Streamline and Q HyperZ. However, higher axial and horizontal tracer velocities were found for Rhobust® beds. Still, the validity of comparing velocity values was questioned due to different calculation approaches and varying tracer radioactivities in each study.

Comparison of particle motion at the start of fluid flow was limited to the present study employing Q HyperZ as no data was available from previous works with Streamline and Q HyperZ (Liu 2009, Souquet 2011). In contrast to the distinct overshoot behaviour found for Rhobust® adsorbents, the Q HyperZ tracer particle showed strong mixing during initial fluidisation before locating within its stable axial motion range. Still, a stable expanded bed was achieved within less than 10 minutes, confirming the potential for reduced process time and buffer consumption by adjusting equilibration times.

These findings give a more detailed insight into solid phase behaviour in expanded beds of varying matrices and could be employed to gain a better understanding of EBA as a unit operation using new model systems.

3.6. References

Al-Dibouni, M. and J. Garside (1979). "Particle mixing and classification in liquid fluidised beds." Transactions of the Institution of Chemical Engineers 57: 95-103.

Anspach, F. B., D. Curbelo, et al. (1999). "Expanded-bed chromatography in primary protein purification." Journal of Chromatography A 865(1-2): 129-144.

Arpanaei, A., B. Winther-Jensen, et al. (2010). "Surface modification of chromatography adsorbents by low temperature low pressure plasma." Journal of Chromatography A 1217(44): 6905-6916.

Asgari, S., M. Jahanshahi, et al. (2014). "Cost-effective nanoporous Agar–Agar polymer/Nickel powder composite particle for effective bio-products adsorption by expanded bed chromatography." Journal of Chromatography A 1361: 191-202.

Asghari, F. and M. Jahanshahi (2012). "Fabrication and evaluation of low-cost agarose–zinc nanoporous composite matrix: Influence of adsorbent density and size distribution on the performance of expanded beds." Journal of Chromatography A 1257: 89-97.

Chase, H. A. (1994). "Purification of proteins by adsorption chromatography in expanded beds." Trends in Biotechnology 12(8): 296-303.

Dainiak, M. B., I. Y. Galaev, et al. (2002). "Direct capture of product from fermentation broth using a cell-repelling ion exchanger." Journal of Chromatography A 942(1-2): 123-131.

Drossard, J. (2005). Downstream Processing of Plant-Derived Recombinant Therapeutic Proteins. Molecular Farming, Wiley-VCH Verlag GmbH & Co. KGaA: 217-231.

Fan, X., D. J. Parker, et al. (2006). "Labelling a single particle for positron emission particle tracking using direct activation and ion-exchange techniques." Nuclear Instruments & Methods in Physics Research Section a-Accelerators Spectrometers Detectors and Associated Equipment 562(1): 345-350.

Griffith, C. M., J. Morris, et al. (1997). "Fluidization characteristics of and protein adsorption on fluoride-modified porous zirconium oxide particles." Journal of Chromatography A 776(2): 179-195.

Hjorth, R. (1997). "Expanded-bed adsorption in industrial bioprocessing: Recent developments." Trends in Biotechnology 15(6): 230-235.

Hubbuch, J., J. Thommes, et al. (2005). "Biochemical engineering aspects of expanded bed adsorption." Technology Transfer in Biotechnology: From Lab to Industry to Production 92: 101-123.

Jahanshahi, M., L. Partida-Martinez, et al. (2008). "Preparation and evaluation of polymer-coated adsorbents for the expanded bed recovery of protein products from particulate feedstocks." Journal of Chromatography A 1203(1): 13-20.

Karau, A., C. Benken, et al. (1997). "The influence of particle size distribution and operating conditions on the adsorption performance in fluidized beds." Biotechnology and Bioengineering 55(1): 54-64.

Kelly, W., P. Garcia, et al. (2013). "Experimental characterization of next-generation expanded-bed adsorbents for capture of a recombinant protein expressed in high-

cell-density yeast fermentation." Biotechnology and Applied Biochemistry 60(5): 510-520.

Leadbeater, T. W., D. J. Parker, et al. (2012). "Positron imaging systems for studying particulate, granular and multiphase flows." Particuology 10(2): 146-153.

Lei, Y.-L., D.-Q. Lin, et al. (2005). "Preparation of an anion exchanger based on TiO2-densified cellulose beads for expanded bed adsorption." Reactive and Functional Polymers 62(2): 169-177.

Li, P., P. F. Gomes, et al. (2014). Proteins Separation and Purification by Expanded Bed Adsorption and Simulated Moving Bed Technology. Continuous Processing in Pharmaceutical Manufacturing, Wiley-VCH Verlag GmbH & Co. KGaA: 1-34.

Lihme, A., M. Hansen, et al. (2000). Expanded Bed Adsorption in the Purification of Biomolecules. Downstream Processing of Proteins. M. Desai, Humana Press. 9: 121-139.

Lin, D.-Q., Z.-J. Miao, et al. (2006). "Expansion and hydrodynamic properties of cellulose-stainless steel powder composite matrix for expanded bed adsorption." Journal of Chromatography A 1107(1–2): 265-272.

Liu, H. (2009). "Application of new materials and tools in bioseparations." PhD Thesis, University of Birmingham.

Mattiasson, B. and M. P. Nandakumar (2000). 10 Physicochemical basis of expanded-bed adsorption for protein purification. Separation Science and Technology. A. Satinder, Academic Press. Volume 2: 417-430.

Ng, B. H., C. C. Kwan, et al. (2008). "Granular flow fields in vertical high shear mixer granulators." Aiche Journal 54(2): 415-426.

Pai, A., S. Gondkar, et al. (2000). "Enhanced performance of expanded bed chromatography on rigid superporous adsorbent matrix." Journal of Chromatography A 867(1–2): 113-130.

Pålsson, E., P.-E. Gustavsson, et al. (2000). "Pellicular expanded bed matrix suitable for high flow rates." Journal of Chromatography A 878(1): 17-25.

Parker, D. J., C. J. Broadbent, et al. (1993). "Positron Emission Particle Tracking - a Technique for Studying Flow within Engineering Equipment." Nuclear Instruments & Methods in Physics Research Section a-Accelerators Spectrometers Detectors and Associated Equipment 326(3): 592-607.

Parker, D. J., M. R. Hawkesworth, et al. (1994). "Industrial Positron-Based Imaging - Principles and Applications." Nuclear Instruments & Methods in Physics Research Section a-Accelerators Spectrometers Detectors and Associated Equipment 348(2-3): 583-592.

Pharmacia (1997). Expanded Bed Adsorption: Principles and Methods. Uppsala, Sweden.

Souquet, J. (2011). "Advances in Expanded Bed Adsorption Chromatography." PhD Thesis, University of Birmingham.

Stewart, R. L., J. Bridgwater, et al. (2001). "Granular flow over a flat-bladed stirrer." Chemical Engineering Science 56(14): 4257-4271.

Theodossiou, I., H. D. Elsner, et al. (2002). "Fluidisation and dispersion behaviour of small high density pellicular expanded bed adsorbents." Journal of Chromatography A 964(1-2): 77-89.

Theodossiou, I., M. A. Olander, et al. (2000). "New expanded bed adsorbents for the recovery of DNA." Biotechnology Letters 22(24): 1929-1933.

Thömmes, J. (1997). Fluidized bed adsorption as a primary recovery step in protein purification. New Enzymes for Organic Synthesis, Springer Berlin Heidelberg. 58: 185-230.

Vennapusa, R. R. and M. Fernandez-Lahore (2010). "Effect of chemical additives on biomass deposition onto beaded adsorbents." Journal of Bioscience and Bioengineering 110(5): 564-571.

Viloria-Cols, M. E., R. Hatti-Kaul, et al. (2004). "Agarose-coated anion exchanger prevents cell-adsorbent interactions." Journal of Chromatography A 1043(2): 195-200.

Wright, P. R., F. J. Muzzio, et al. (1999). "Effect of Resin Characteristics on Fluidized Bed Adsorption of Proteins." Biotechnology Progress 15(5): 932-940.

Xia, H.-F., D.-Q. Lin, et al. (2007). "Preparation and characterization of macroporous cellulose–tungsten carbide composite beads for expanded bed applications." Journal of Chromatography A 1175(1): 55-62.

Xia, H. F., D. Q. Lin, et al. (2007). "Evaluation of new high-density ion exchange adsorbents for expanded bed adsorption chromatography." Journal of Chromatography A 1145(1-2): 58-66.

Zhou, X., Q.-H. Shi, et al. (2004). "Dense pellicular agarose–glass beads for expanded bed application:: Fabrication and characterization for effective protein adsorption." Biochemical Engineering Journal 18(2): 81-88.

4. Particle motion in expanded beds during application of crude feedstock

4.1. Abstract

Positron emission particle tracking (PEPT) has previously been demonstrated to be a powerful tool in exploring and analysing particle motion in expanded beds (see Chapters 2 and 3).

In this study, PEPT was employed to study the behaviour within expanded beds of Rhobust® MabDirect Protein A during real operating conditions using porcine serum as feedstock. Again, differently sized alumina particles (density = 3.0 - 3.3 g/mL) were utilised as surrogate tracers to represent the bottom, mid and top part of the bed and their positions were tracked over time. The transient changes within the bed as a result of feedstock application and step changes in the fluid velocity in order to maintain a constant bed height at twofold expansion were investigated.

The results demonstrate the feasibility of maintaining a constant bed expansion by adjusting the superficial fluid velocity while the bed stability is retained. Overall axial motion ranges of the tracer particles were observed as relatively stable and within 12 (bottom) and 14% (mid and top) of the expanded bed height throughout the entire process. No significantly increased particle mixing within the bed during serum application was identified. However, distinct spikes in the form of over- and undershoots from the median axial positions were detected during the transient phases at the start of loading, column washing and elution for the mid and top representative tracer particles. Nevertheless, these rises and falls occurred in a 'controlled' and coherent manner and did not appear to cause a general de-stabilisation of the bed.

Furthermore, a similar behaviour was observed when operating at a higher degree of bed expansion of 2.4-fold. However, an increase of the relative times for over- and undershoots during mobile phase transition was found. While these deviations from the regular axial motion ranges took 13% of the total loading and 20% of the overall washing time at twofold expansion, this increased to 27% and 29%, respectively, at 2.4-fold expansion.

Potential channelling occurring during the process did not appear to have an effect on the motion of the tracer particle. This presents a possible drawback of the PEPT technique, as the tracking of a single particle does not necessarily give information about the entire bed.

4.2. Introduction

In expanded bed adsorption (EBA), it is crucial to minimise liquid and solid axial dispersion to achieve an efficient process with high chromatographic separation performance and resolution (Chase 1994; Hjorth 1997). This is achieved by using specifically designed adsorbent particles with a defined size and density distribution. The application of an upward flow results in a gradient of bead sizes and densities, termed as classification of the bed.

However, during an adsorption process, transient changes within the bed occur inevitably due to the varied physical properties of the mobile phase, affecting the bed's stability (Ghose et al. 2000). In particular, switching from equilibration buffer to crude feedstock at the beginning of the loading phase results in the bed having to respond to the new conditions such as higher viscosity and density. Likewise, this is also the case when ending the feedstock load and switching to the washing step.

Two different operation modes have therefore evolved for EBA processes. Either, the flow rate is kept constant throughout, allowing the bed height to adjust according to the liquid applied and resulting in increased bed expansions (Barnfield Frej et al. 1994; Thömmes et al. 1995). Alternatively, the fluid velocity is adjusted in order to maintain a constant degree of bed expansion (Chase and Draeger 1992).

In a study by Chang and Chase (1996), both approaches were compared for the adsorption of lysozyme to beds of Streamline SP (Pharmacia Biotech, Uppsala, Sweden) with initial settled bed height of 10 cm in a Streamline 50 column. They demonstrated that the latter of the two abovementioned options, i.e. keeping the bed height constant, was more efficient with regard to the dynamic capacity. Furthermore, they examined the influence of mobile phase viscosity on the axial dispersion of the liquid phase conducting residence time distribution (RTD) studies in the presence of various concentrations of glycerol. At constant twofold bed expansion, the plate numbers stayed nearly the same (19, 19 and 18 for 0%, 25% and 32% v/v glycerol solutions) while the overall axial liquid dispersion coefficient decreased. Lin et al. (2015) assessed the effect of mobile phase viscosity on the local axial dispersion via RTDs using in-bed sampling at various heights along the column. A settled bed of 23.1 cm of agarose raw beads was tested in a 2 cm diameter nozzle column under fluidisation with buffer, 14% and 45% glycerol solution at varying expansion factors. In general, RTD profile curves and plate numbers indicated an increased liquid mixing within the bed with increasing mobile phase viscosity. However, they suggested that the EBA system had a certain fluid viscosity tolerance as RTDs of 14% glycerol were similar to those of the buffer. Furthermore, they pointed out that the effect on the local effective axial dispersion coefficient (D_{ax}) was more complicated as it increased with increasing mobile phase viscosity but decreased with the corresponding reduction of flow rate. Still, they found that axial dispersion became stronger especially at the bed bottom at higher glycerol concentration. Tong and Sun (2002) examined the

influence of the liquid viscosity on the particle size distribution also using in-bed sampling. A settled bed of 10 cm of Streamline beads was tested in a 26 mm diameter glass column. Using distilled water, 20% and 40% (v/v) glycerol solutions, they found that variations of the mobile phase viscosity had an insignificant effect on the axial particle size distribution at a constant degree of bed expansion of 2.4-fold.

Studies regarding the bed stability during transition between mobile phases have so far been based on operation at constant fluid velocity. Lin et al. (2003) investigated the hydrodynamic stability of Streamline beds during transient expansion using a yeast suspension as model biomass system. They analysed residence time distributions at different times after starting to load biomass onto the column. It was found that the transient change in bed expansion at constant fluid velocity took place in an "ordered" manner, while the classification was maintained throughout. Yang and Sun (2005) studied the changes of local particle size distribution and bed voidage during changes in mobile phase viscosity using in-bed sampling at three ports along the column. They imitated feed loading with a 10% (w/w) glycerol solution and took samples at various times while switching from fluidisation with deionised water to the glycerol solution and reverse at constant fluid velocity. Transient variations of the local particle size distribution and bed voidage were found to first occur in the bottom of the bed while subsequently progressing to the top in axial direction. However, they observed a non-unidirectional behaviour of the changes in bed voidage. After switching the mobile phase from water to the glycerol solution, the increase in bed voidage in the bottom of the bed was constant. For the middle and top positions though, a notable decrease of the bed voidage was detected before it then increased again. This phenomenon was described by Yang and Sun as a result of a "compression effect" caused by the upward motion of the particles from the lower part of the bed.

To the best knowledge of the author, there have not been similar studies in order to investigate the transient changes at constant bed height. However, some attention was paid to realise monitoring and control of the bed height during EBA operation. Thelen and Ramirez (1997) first developed a distributed-parameter model to predict the dynamic response of the bed height to step changes in the fluidisation velocity. However, this model did not take into account neither the changes in viscosity of the mobile phase nor solute adsorption. In a subsequent study, Thelen et al. (1997) presented a method of using ultrasonic backscattering for measuring the bed height in EBA columns. The system was also shown to identify plugging and air bubbles within the column and was suggested to be used for bed-height regulation via feedback control strategies. Ghose et al. (2000) employed an LED based sensor configuration for measurement of bed height changes. They coupled the information from the sensors to a pump control system via two different algorithms in order to adjust the flow rate according to the observed changes. Three columns with varying diameter (1, 5 and 20 cm) using beds of two different Streamline resins were tested. When switching from buffer to 5 and 10% (w/v) PEG solutions and back, the system was capable of maintaining a twofold bed expansion within approximately ±2.5% of the expanded bed height. However, the LED sensors were not able to identify the top of the bed at breakthrough of crude feedstock, hampering their practical application.

Still, in the abovementioned studies, only the top of the bed and the stability of the bed height were investigated while using PEG solutions to imitate the viscosity changes.

In this work, the transient changes within expanded beds of Rhobust® MabDirect Protein A as a result of feedstock application and step changes in the fluid velocity in order to maintain a constant bed expansion were investigated under real binding conditions. Using

the technique of positron emission particle tracking (PEPT), each a tracer particle representing the bottom, the mid and the top part of the bed were tracked during a full EBA process of equilibration, feedstock load, column washing, elution, cleaning and re-equilibration. First, the influence of fluidising the bed with varying buffers for each of those steps during the process was evaluated in a 'buffer only' run. Subsequently, the effect of feedstock application and protein adsorption on the particle motion was assessed at twofold expansion using porcine serum as raw material. In addition, a run at 2.4-fold expansion was conducted and the results were compared.

4.3. Materials and methods

4.3.1. Materials

The expanded bed adsorbent (Rhobust® MabDirect Protein A) as well as the 2 cm diameter nozzle inlet column used in this study were a gift from Patheon, Groningen, Netherlands. Rhobust® MabDirect Protein A is comprised of cross-linked agarose and incorporated tungsten carbide and shows a size distribution of 20 – 200 µm and a density of 2.8 – 3.2 g/L. Frozen, sterile filtered porcine serum was obtained from Kraeber & Co GmbH (Ellerbek, Germany) and stored at -20 °C until use. For processing, the serum was then thawed at 25 °C in a shaking water bath.

γ-Alumina particles for use as PEPT tracers were purchased from Alfa Aesar (Ward Hill, MA, USA); a lacquer from James Briggs Ltd (Royton, Greater Manchester, UK) was used for coating. The chemicals used for preparation of the buffers employed in this study were sourced as follows: Di-sodium hydrogen phosphate heptahydrate (CAS # 7782-85-6) and sodium acetate trihydrate (CAS # 6131-90-4) were from Merck KGaA (Darmstadt, Germany); potassium phosphate monobasic (CAS # 7778-77-0), sodium chloride (CAS #

7647-14-5) and potassium chloride (CAS # 7447-40-7), from Sigma-Aldrich Company

Limited (St. Louis, MO, USA) and sodium hydroxide (CAS # 1310-73-2) from VWR

International BVBA (Leuven, Belgium).

The Pierce™ BCA Protein Assay Kit was obtained from Thermo Fisher Scientific

(Waltham, MA, USA). Chemicals for SDS-PAGE were purchased as follows: ProtoGel

(30%) from National Diagnostics (Atlanta, GA, USA; a pre-mixed solution of 37.5:1

acrylamide   (CAS #   79-06-1)   to   bisacrylamide   (CAS #   110-26-9));

Tris(hydroxymethyl)aminomethane hydrochloride (CAS # 1185-53-1), Hydrochloric acid

(CAS # 7647-01-0), Sodium dodecyl sulphate (CAS # 151-21-3), Bromphenol Blue

(CAS # 62625-28-9), Glycine (CAS # 56-40-6), β-Mercaptoethanol (CAS# 60-24-2) from

Sigma-Aldrich Company Limited (St. Louis, MO, USA); Ammonium persulphate (CAS #

7727-54-0) from Fisher Scientific (Waltham, MA, USA); Tetramethylethylenediamine

(TEMED; CAS # 110-18-9) from Thermo Scientific Pierce (Waltham, MA, USA) and

SimplyBlue™ SafeStain from Thermo Fisher Scientific (Waltham, MA, USA).

4.3.2.   PEPT tracer fabrication

γ-Alumina particles with a density of 3.0 - 3.3 g/mL, and thus similar to that of the

adsorbent matrix employed in this study, were used as foreign tracers. Sizes covering the

particle size distribution range of the adsorbent (20 - 200 μm) were picked to interrogate

the behaviour of the bottom, mid and top part of the bed. For each representative part, a

few tracer particles of roughly the same size were chosen and labelled together with ^{18}F

using the indirect activation method as described by Leadbeater et al. (2012). Briefly, the

particles were exposed to an aqueous solution of ^{18}F, which was previously prepared by

direct bombardment of purified water using a ^{3}He beam from the Birmingham MC40

Cyclotron (Fan et al. 2006). One millilitre of this solution was then added to the selected

particles. ^{18}F ions were transferred from the aqueous phase onto the particle surface via surface adsorption and the excess water was dried off with the help of an infrared lamp. The tracer particles were subsequently coated with lacquer to prevent the leaching of radioisotopes into the surrounding fluid phase. This was done by dipping the selected particle into a drop of lacquer and subsequent rolling to spread it evenly and as thinly as possible across the whole surface before drying.

The activities of the tracers using this method are mostly dependent on the initial concentration of ^{18}F ions in the aqueous solution used and the exposed surface area of the particle, leading to generally higher activities in bigger particles and lower activities in smaller particles. Furthermore, with decreasing particle size, the influence of the lacquer coating on the tracer particle's density increases. Therefore, it is more challenging to produce sufficiently activated, good tracers from smaller particles than from relatively bigger ones.

4.3.3. Experimental set-up

A 2 cm diameter EBA column with a nozzle and cone inlet was mounted between the two parallel PEPT detector camera heads, which were adjusted to the closest face-to-face separation possible (250 mm) to achieve optimal data acquisition. The column's vertical position was ensured using a digital level (Torpedo DWL-200, Digi-Pas, Avon, CT, USA) to give accuracies of alignment as close as 0.1°. The column was then connected to an ÄKTAprime plus system (GE Healthcare, Uppsala, Sweden), which in turn was connected to the various buffer and feedstock tanks. The ÄKTAprime was used to introduce the respective fluid into the column. A peristaltic outlet pump (Watson Marlow, Falmouth, UK) was employed to pump the exiting liquid from the top of the expanded bed back into the ÄKTA system for absorbance, conductivity and pH measurement. Fraction collection and

switches from and to waste containers were performed manually. A schematic illustration

of the set-up as well as a photographic representation of the actual set-up during

operation are depicted in Figure 4.1 and Figure 4.2.
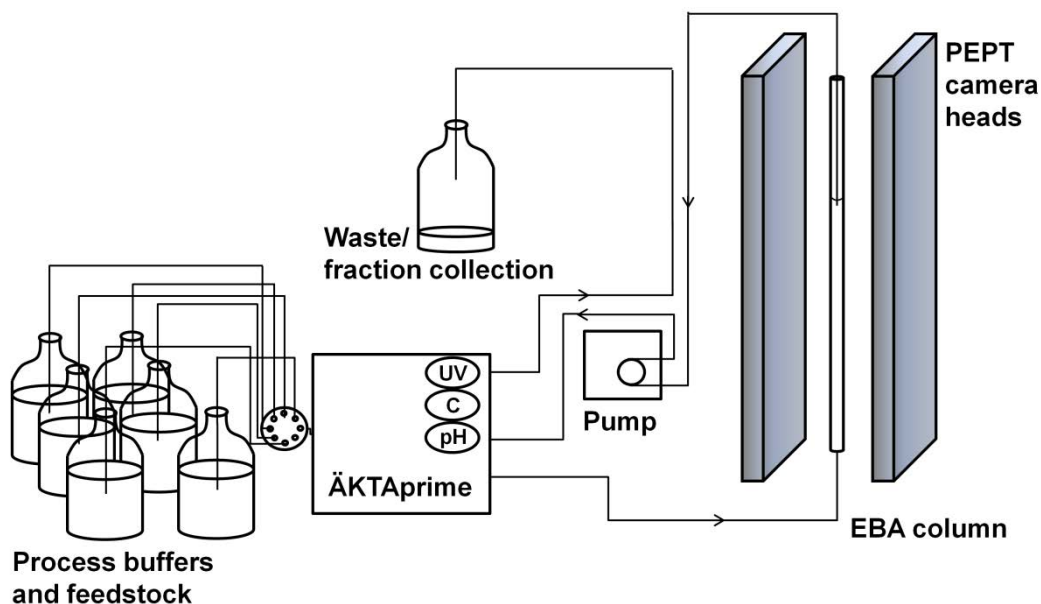
Figure 4.1: Schematic illustration of the set-up during operation of the EBA process while performing particle tracking via PEPT.
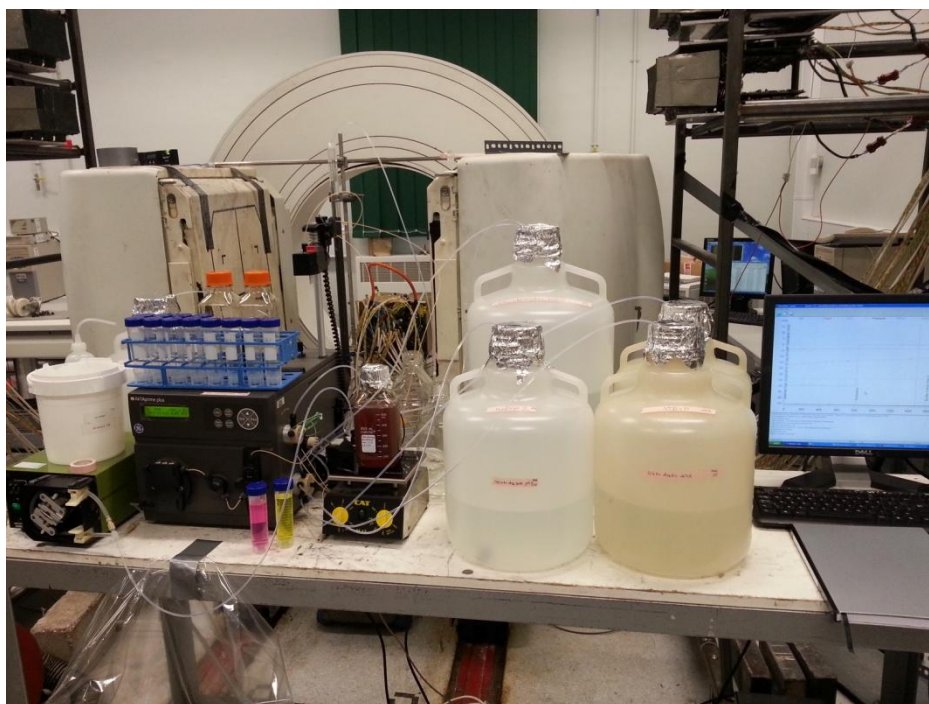
Figure 4.2: Photographic representation of the experimental set up as used for operation of the EBA process under investigation via PEPT.

4.3.4. Experimental procedure

Particle motion in a 2 cm diameter column with a 4 port nozzle and cone inlet and 70 cm length was investigated with PEPT using Rhobust® MabDirect Protein A resin of 25.0 cm settled bed height (SBH or H_0). As stated above (see Section 4.3.2), alumina tracer particles radioactively labelled with ^{18}F were used as surrogates for the Rhobust® MabDirect Protein A adsorbent beads and added to the resin from the top of the column. To facilitate each individual tracer particle's way to its distinct position within the bed, the matrix was initially fluidised with PBS at 2.2-fold expansion for 20 min. The adsorbents were let to settle for 15 min before the run was started.

During each run, bed expansion was kept constant by adjusting the superficial fluid velocity with respect to the mobile phase used in each process step. However, instead of

gradually regulating the flow rate, the flow rate changes were kept to a minimum in order to rapidly regain a steady state.

Porcine serum was selected as feedstock to investigate adsorbent particle movement during processing and purification of immunoglobulin G (IgG). Process conditions were chosen according to Patheon's technical note for application of Rhobust® MabDirect Protein A. The column was equilibrated with PBS with 5 settled bed volumes (SBV). Then 500 mL of serum was loaded, corresponding to approximately 7 SBV. From breakthrough of feedstock as detected by the ÄKTAprime UV signal, 50 mL fractions were continuously collected by manually switching between fraction tubes. Subsequently, the column was washed with PBS for 10 SBV and with 0.1 M acetate (pH 5.5) for 5 SBV to remove residual serum proteins. Elution was performed using 0.1 M acetate (pH 3.0) for 5 SBV to recover the IgG. Column cleaning and regeneration were done via 5 SBV of 0.4 M acetic acid and 30 min of 0.05 M NaOH-1.0 M NaCl buffer followed by re-equilibration with PBS (Table 4.1).

Table 4.1: Process conditions for EBA operation using Rhobust® MabDirect Protein A.

Process step	Buffer	Process volume
Equilibration	PBS (136 mM NaCl, 2.7 mM potassium chloride, 8.9 mM phosphate), pH 7.0	5 SBV
Load	Porcine serum	7 CV (500 mL)
Cell wash-out (Wash I)	PBS, pH 7.0	10 SBV
Wash (Wash II)	100 mM Acetate, pH 5.5	5 SBV
Elution	100 mM Acetate, pH 3.0	5 SBV
Strip	0.4 M Acetic acid	5 SBV
Sanitisation	50 mM NaOH, 1 M NaCl	30 min
Re-Equilibration	PBS, pH 7.0	5 SBV

4.3.5.   Protein analysis

The total protein concentrations in each fraction collected during the runs as well as in the serum applied were determined using a bicinchoninic acid (BCA) protein assay kit. From this, a total protein breakthrough curve was plotted.

Protein composition was analysed with reducing sodium dodecyl sulphate polyacrylamide gel electrophoresis (SDS-PAGE) (Laemmli 1970). The running buffer was prepared by adding 87 µL of β-mercaptoethanol to 1 mL of Laemmli sample buffer. 20 µL of sample (diluted fractions) was mixed with 20 µL of running buffer and heated at 99 °C for 10 min. After cooling down at room temperature for 2 min, the samples were centrifuged for 1 min at 15.600 rcf.

5 µL of each sample was then loaded onto a 15% polyacrylamide gel together with the prestained protein standard. Electrophoresis was run at 120 V until the running buffer almost reached the lower end of the gel. Electrical current was then stopped, the gels removed from the electrophoresis setup and rinsed 3 times with deionised water under gentle shaking for 5 min. Subsequently, the water was discarded and staining of the gels was performed using SimplyBlue™ SafeStain solution and gentle shaking for at least 1 hour. Afterwards, the stain was removed and the gels were washed twice with deionised water for a minimum of 1 hour each. The gels were then scanned at 600 dpi using a Canon CanoScan 9000F scanner.

Scanned images of the gels were then analysed by scanning densitometry using Fiji software (Schindelin et al. 2012).

The detailed composition of the buffers and gels used for SDS-PAGE can be found in Appendix 6.5.

4.3.6. Data analysis

Using PEPT, the position of the labelled tracer particle is determined by means of triangulation from a number of detected pairs of γ-rays. In practice, some of the detected events are corrupt due to scattered or random coincidences. Therefore an iterative algorithm was developed by Parker et al. (1993) to eliminate and reject these corrupt events. It calculates the point which minimises the sum of perpendicular distances between the reconstructed paths of all events within the initial sample. The reconstructions lying furthest away from this point are assumed to be corrupt and removed from the set of events. A new minimum distance point is calculated from the remaining events and the algorithm is iterated until only a predefined fraction of the initial event sample remains.

The resulting data consisting of the tracer coordinates (x, y, z) over time was then used to plot axial trajectories.

4.4. Results and discussion

4.4.1. Effect of buffer changes

To investigate the influence of the changing buffer conditions during EBA operation, the movement of an alumina tracer particle representing the mid of the bed (specified as $h_{T,0}$ = 0.57) was first tracked over time without loading feedstock. The procedure followed the steps and corresponding buffers as defined in Table 4.1 (see Section 2.3.4), while only the feedstock load was omitted. The resulting chromatogram and axial position of the tracer particle over time are shown together in Figure 4.3.

Figure 4.3: Chromatogram and axial position of an ^{18}F-labelled alumina tracer particle specified as $h_{T,0} = 0.57$ against time within an expanded bed of Rhobust® adsorbents with initial settled bed height $H_0 = 25.0$ cm in a 2 cm diameter nozzle inlet column for a 2-fold expansion.

The chromatogram above (Figure 4.3) is shown based on time rather than volume to facilitate comparison to the axial position of the tracer particle (depicted below), as PEPT tracks these locations over time. The switches to the next process step and therefore buffer changes are depicted as vertical dashed grey lines. Due to the system volume ($V_S = 15.16$ mL) contributing to a delay in the signal recording of ca. 45 s at the applied fluid velocity, adding to the time it takes the fluid to pass the twofold expanded bed, the

actual buffer change (i.e. a change in pH and conductivity) only shows ca. 390 s after switching the buffer valve. If the change of fluid composition has an influence on the particle movement, it will show slightly earlier in the position as tracked by PEPT than in the chromatogram since the fluid front reaches the column earlier than the detection afterwards. For the individual adsorbent particles and hence for the tracer, the fluid composition starts changing depending on its position within the expanded bed. In this particular case, for a mid bed tracer particle located at approximately 40% of the twofold expanded bed height, the new buffer corresponding to the current step in the process would reach the tracer just under 200 s after switching the valve. This is, however, only a simplified estimation using a calculated bed voidage of 0.7 for a twofold expanded bed (see Section 1.3.5, Equation 1.5) and does not take into account that the voidage changes along the height of the expanded bed.

Still, the change of the fluid composition as shown by the variation in the conductivity and pH measurement in the chromatogram gives an indication of the time that a change in the tracer particle movement would be expected. Figure 4.3 illustrates that overall, the tracer particle's axial position does not seem to be affected significantly by the different conditions of each step. First, after the start of fluidisation, an overshoot behaviour is found very similar to those observed and explained previously in Chapter 2. The tracer then locates initially at around 230 - 250 mm bed height between t = 350 - 800 s, before then dropping slightly and levelling at around 200 mm bed height. This is not the usual positioning behaviour as shown before, but may be due to a very small air bubble attached to the tracer particle, which then suddenly detached, resulting in the drop at around 800 s. However, the tracer subsequently stayed within the axial motion range between 190 - 220 mm for the remaining equilibration and the immediately following "Wash I", both employing PBS as mobile phase.

In the subsequent second washing step, the tracer particle then appeared to slightly sink in the bed, positioning around 180 - 210 mm and staying there for the following elution and strip. After switching to the sanitisation buffer, a rise of the tracer was noticeable, increasing the particle's position up to 240 mm. To maintain the twofold expansion of the bed, a slight decrease in the superficial fluid velocity from 423 to 412.5 cm/h was necessary. The tracer particle slowly sank back down and positioned between 190 - 220 mm again. The fluid velocity could then be increased during re-equilibration with PBS.

In general, not only the overall axial position, but also the axial movement of the tracer particle as shown by the frequency and nature of the up and down motion as well as the axial motion range appeared to be relatively consistent throughout the whole run. Despite a slight decrease in height during wash II, elution and strip and a brief increased height during sanitisation, the axial motion range maintained between 180 - 240 mm at all times, corresponding to 12% of the expanded bed height. Mostly, the range during one particular step is in fact not more than 30 mm, i.e. 6% of the entire bed. These values, but also the general motion behaviour under these process conditions, should serve as reference when comparing to the following runs employing real feedstock.

4.4.2. Influence of feedstock application

The impact of applying a crude feedstock and running a full process cycle of binding and eluting a target protein on the adsorbent particle movement in expanded beds of Rhobust® MabDirect Protein A was investigated using porcine serum as raw material. The feasibility of using EBA as first capture and recovery step for the isolation of IgG from the serum was analysed. The experimental procedure and the buffers used are described in Section 2.3.4. Three differently sized ^{18}F labelled alumina tracer particles were employed

in three individual batch cycles to represent the bottom, mid and top part of the bed at twofold expansion.

Figure 4.4 illustrates the chromatogram and corresponding axial position of the bottom representative tracer particle ($h_{T,0}$ = 0.28) over the full process time.
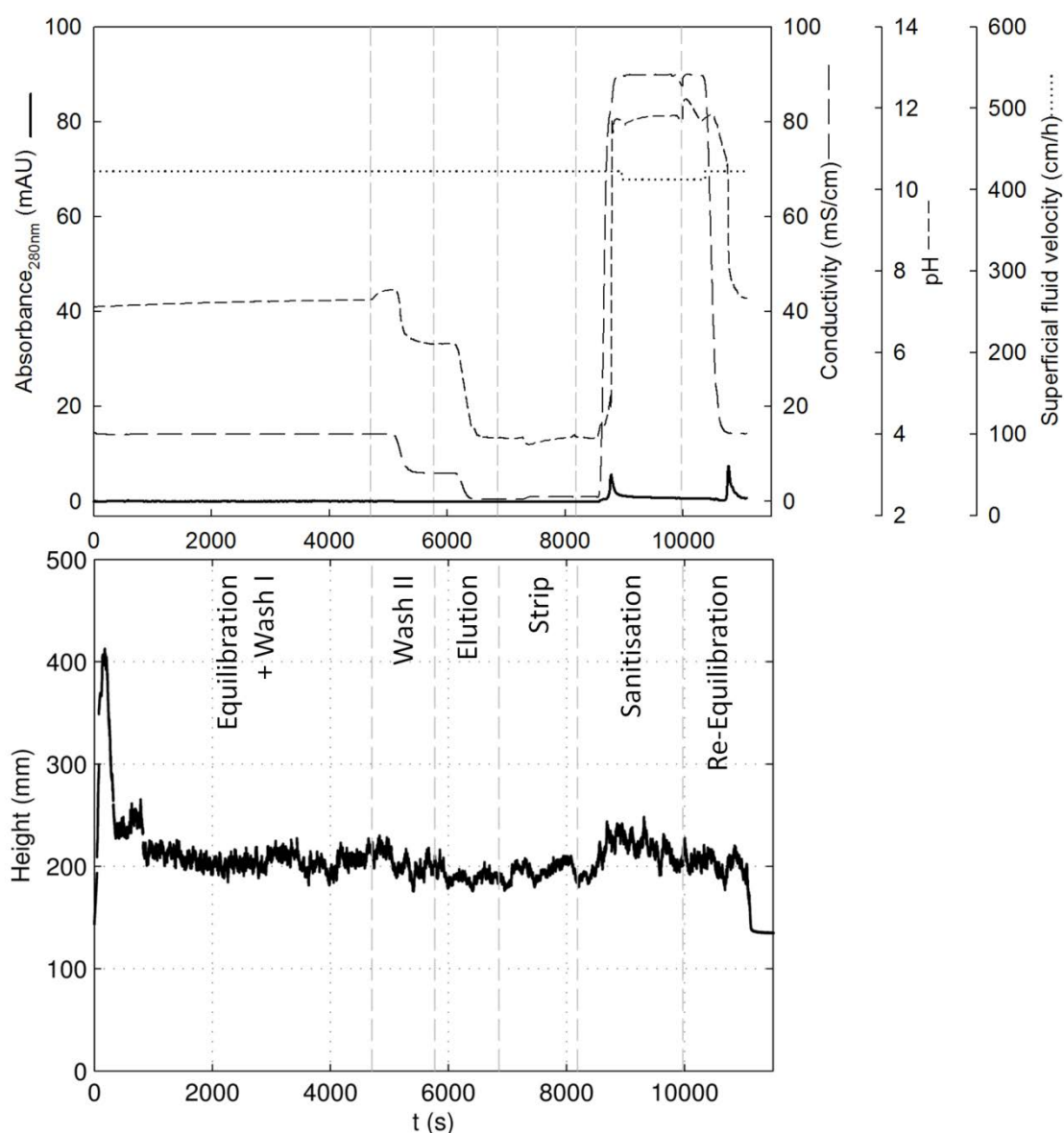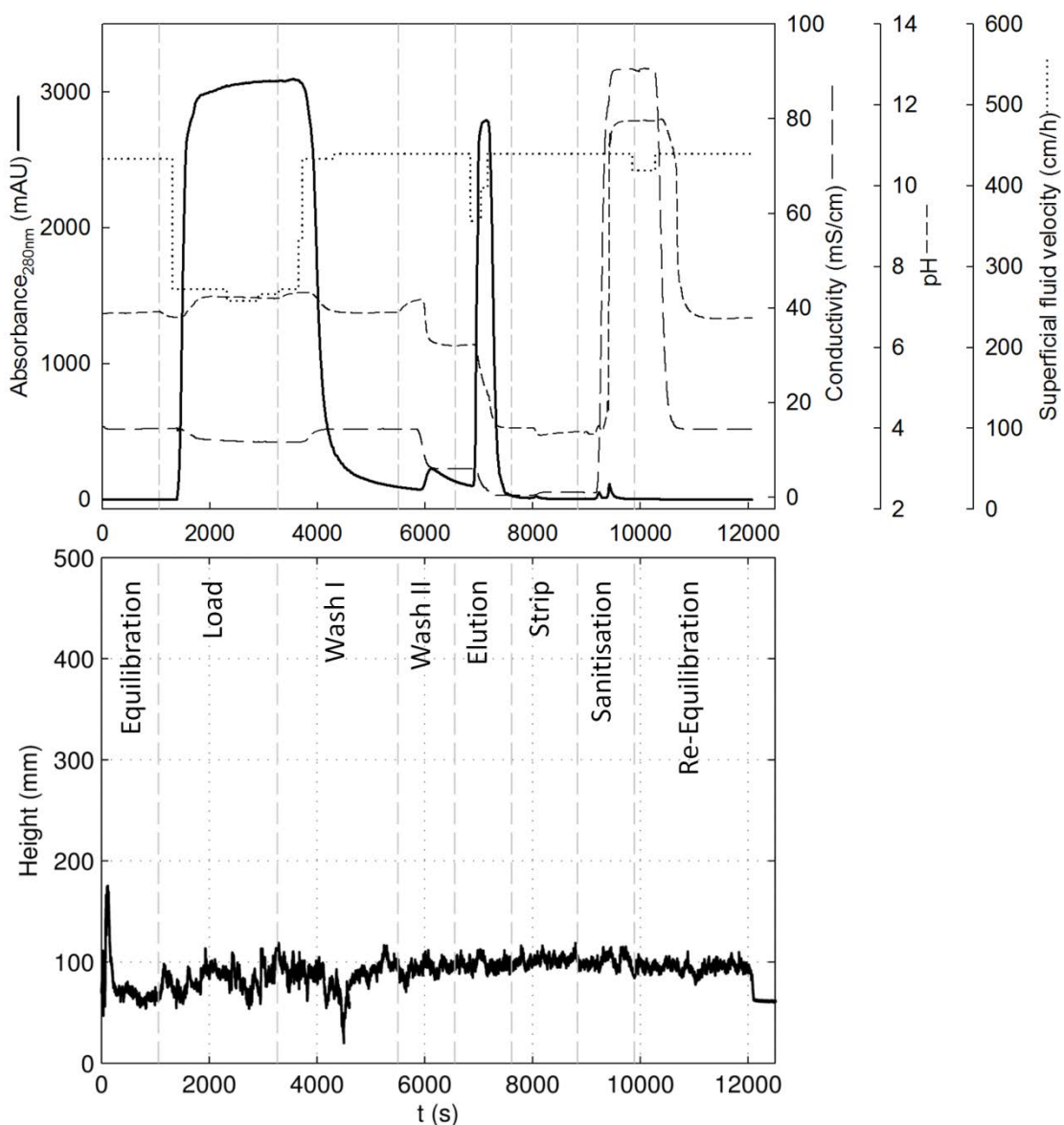

Figure 4.4: Chromatogram and axial position of an ^{18}F-labelled alumina tracer particle specified as $h_{T,0}$ = 0.28 against time within an expanded bed of Rhobust® MabDirect Protein A adsorbents with initial settled bed height H_0 = 25.0 cm in a 2 cm diameter nozzle inlet column at 2-fold expansion.

Again, as elucidated in Section 4.4.1, the chromatogram shown above is based on time for direct comparison with the axial position behaviour of the tracer particle below.

When concentrating on each individual step successively and analysing the tracer particle's movement during that time, first, the equilibration showed a similar tracer particle behaviour as previously demonstrated in Chapter 2. After start of fluidisation, the particle rose in the bed and displayed a form of overshoot, before it dropped down and found its relatively stable, mean axial position. This overshoot was explained as resulting from the previously settled bed first rising up together as a plug, while subsequently particles come loose from the bottom of this plug and sink down. Next, the buffer valve was switched to load the feedstock to the column, as indicated by the first vertical grey dashed line. The serum started to enter the column and the bed began to further expand due to the higher viscosity of the feedstock in comparison to the equilibration buffer (PBS). This is shown in the rise of the tracer particle as picked up by PEPT. While during equilibration, the tracer particle found itself between 55 to 80 mm bed height maximum, it now rapidly rose up to 100 mm. Therefore, the fluid velocity had to be adjusted to maintain the twofold expansion while the serum was increasingly substituting the buffer in the column.

Since the tracer particle here was located in the lower part of the bed at around 20% of the expanded bed height, the shift in fluid composition reached the particle's position relatively soon after switching the buffer valve. The absorbance measurement then only started to rise when the porcine serum had completely passed the column as well as the entire system volume and was detected when returned to the ÄKTAprime. Therefore, the change of the mobile phase showed later in the chromatogram when compared to the axial position as located by PEPT. The time shift was increased by lowering the fluid velocity. Consequently, the chromatogram does not reflect the actual condition in the column for the tracer particle's axial position at that time during transition between steps.

During the subsequent time of loading feedstock, the tracer particle appeared to move randomly up and down over a larger axial motion range than during equilibration (55 - 115 mm column height). This was most likely due to the higher viscosity of the serum, as an increased axial dispersion with increasing liquid viscosity was found in previous studies (Chang and Chase 1996; Lin et al. 2015). The effect of the adsorption of IgG on the adsorbent particle movement was difficult to extract. Although the alumina tracer particle itself did not adsorb IgG, it was expected to show a similar behaviour as the surrounding adsorbent particles. Therefore, if the adsorption has a detrimental influence on the bed stability, this will also affect the tracer particle. However, the axial motion range was still in a relatively confined space of 12% of the expanded bed height and no specific particle motion behaviour could be identified that would indicate an effect of IgG adsorption.

When switching back to PBS to wash the remaining feedstock out of the column (Wash I), the reverse behaviour to the first change was observed. The less viscous PBS entered the column and reached the tracer particle's position, resulting in the particle dropping within the column. The fluid velocity was increased while the buffer successively substituted the serum to control bed expansion. Interestingly however, the fluid velocity had to be further increased when the serum was almost washed out entirely at approximately 4300 s. It was adjusted to 440 cm/h in comparison to 433 cm/h during equilibration, which is only an increase of 1.6% but may be a result of the overloading of the column. Ghose and Chase (2000) described a similar observation as they performed breakthrough curves of lysozyme on 20 cm settled beds of Streamline resin in three small scale columns (0.5, 1 and 5 cm diameter). They found that the bed height tended to drop during the adsorption run. In their case, the fluid velocity had to be drastically increased (almost twice) to maintain a constant expanded bed height. The high binding capacity of the Streamline adsorbent was thought to be the reason for this, as the bound protein

would result in a higher density of the adsorbent particles which then require an increase in mobile phase velocity in order to keep the bed height constant. In this study, the amount of adsorbed protein was estimated to have less influence as the Rhobust[®] resin exhibited a generally higher density compared to the Streamline matrix (2.5 - 3.5 g/mL *cf.* 1.2 g/mL). In this run, a total of 2.96 g of protein was adsorbed as determined from BCA assay analysis of the eluted fractions. Equalling 41.3 mg/mL resin, this corresponded to 1.2 - 1.7% of the matrix density, which is in good accordance with the 1.6% increase in fluid velocity during column washing.

The sudden drop in the tracer's position at around 4500 s (in the mid of Wash I) however was not considered to be a consequence of this overloading, as shortly afterwards the particle rose back up again. The behaviour may therefore be explained by a short-termed aggregation with another particle, which then separated again as the tracer subsequently found itself within the same axial motion range as before.

From the next step (Wash II) onwards, the tracer particle's axial position was observed as very stable. Even during elution, when the fluid velocity was lowered again due to the desorbing IgG, hardly any significant rise or fall could be identified. Neither during sanitisation, although this could have been expected from the previous run using only the process buffers (see Section 4.4.1, Figure 4.3). The particle located between 85 and 115 mm column height, corresponding to 6% of the expanded bed height.

The general feasibility and use of EBA for recovery of IgG has been shown by Lihme et al. (2010). They performed a full core fractionation of human plasma using five consecutive EBA steps, one of which employed mixed-mode ligand beads for IgG fractionation.

Here, despite using porcine serum instead of human plasma and Protein A coupled beads, the application of the serum to study adsorbent particle movement under real binding conditions is shown to be viable by SDS-PAGE of the collected fractions during the run (Figure 4.5).
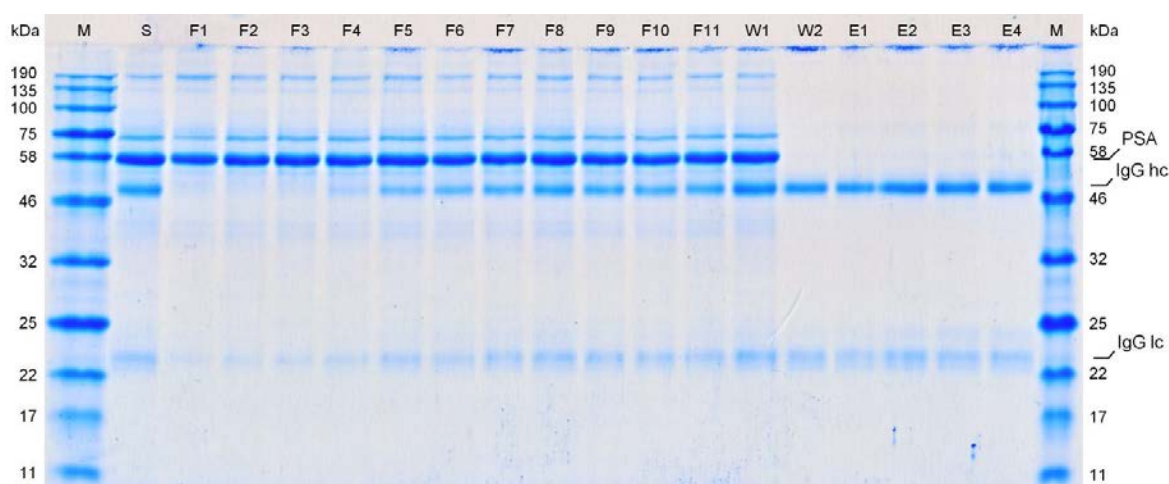
Figure 4.5: Reducing SDS 15% polyacrylamide gel electrophoretogram corresponding to the chromatogram shown in Figure 4.4. Key: molecular weight markers (M); serum feed (S); flowthrough fractions (F1-F11); wash fractions (W1-2); elution fractions (E1-E4).

Figure 4.5 confirms the adsorption of IgG during feedstock application, as the first flowthrough fractions are IgG depleted (lanes F1-F3), before a breakthrough shows from lane F4/F5 onwards. Furthermore, lanes E1-E4 prove IgG desorption during elution, resulting in high purity. The other main serum proteins, i.e. porcine serum albumin (PSA) as well as transferrin (at around 70 kDa) could be completely removed.

In the next run, the effect of the feedstock load on the middle part of the expanded bed was examined using a smaller tracer located at $h_{T,0} = 0.65$ (Figure 4.6).
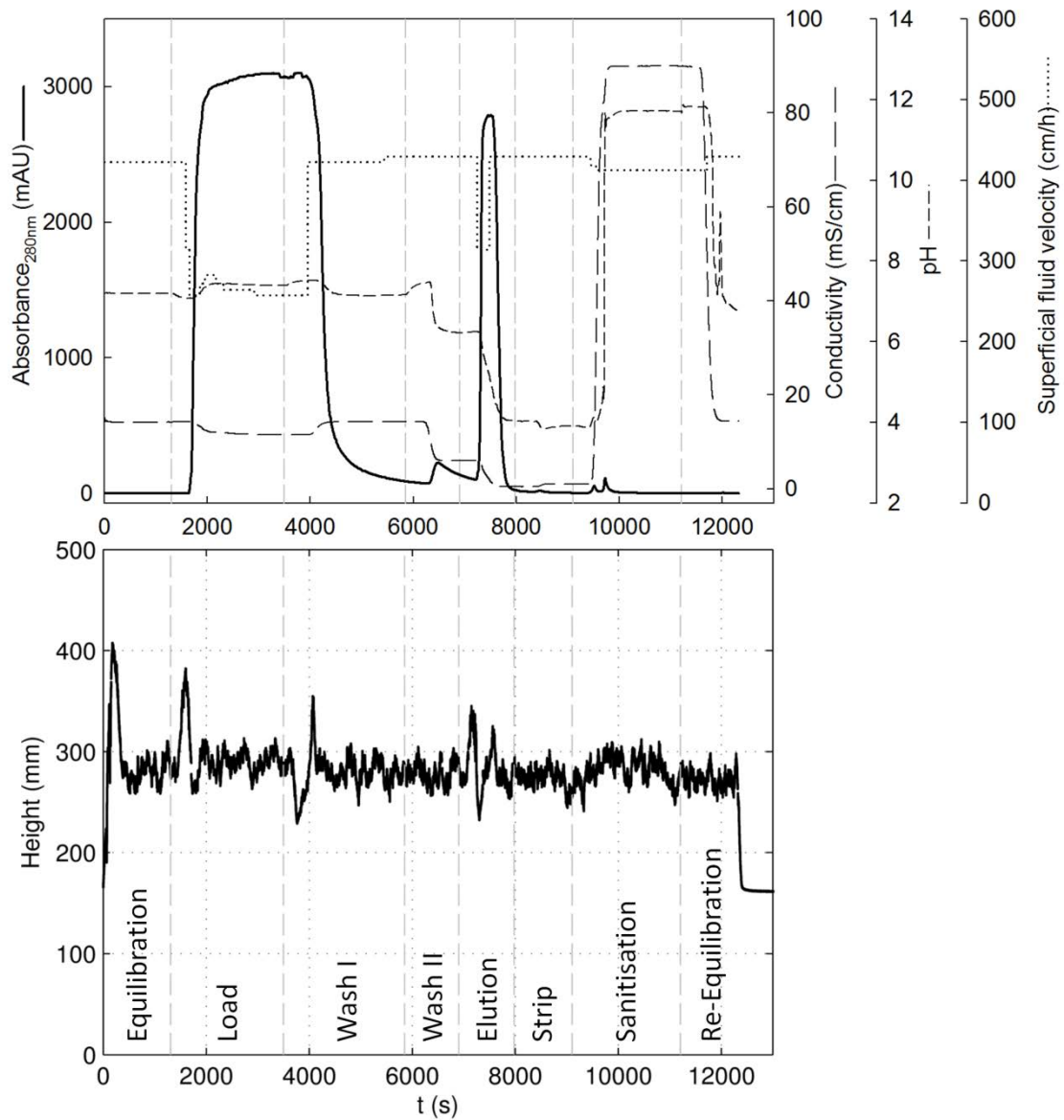
Figure 4.6: Chromatogram and axial position of an ^{18}F-labelled alumina tracer particle specified as $h_{T,0} = 0.65$ against time within an expanded bed of Rhobust® MabDirect Protein A adsorbents with initial settled bed height $H_0 = 25.0$ cm in a 2 cm diameter nozzle inlet column at 2-fold expansion

Similar to the results shown previously for the bottom representative tracer, the chromatogram as well as corresponding axial tracer position are illustrated above on the same time scale (Figure 4.6).

Beginning with the start of fluidisation at t = 0, again, an overshoot behaviour of the tracer particle was observed before it reached a mean axial position of 280 mm around which it irregularly moved up and down. After switching the buffer valve to load the serum, it took

around 150 s for the feedstock front to reach the tracer particle's position, which is when it distinctively started to rise. The fluid velocity was lowered when the top of the bed appeared to increase in height at t = 1580 s, resulting in the tracer particle dropping back downwards. The complete overshoot (rise and fall) took 290 s, corresponding to only 13% of the overall loading time. The absorbance measurement then started to increase as the serum had passed the column and was detected in the ÄKTAprime. During the remaining time of feedstock load, the particle found itself within approximately the same axial motion range as during equilibration (260 - 310 mm column height), relating to 10% of the expanded bed height. Hence, the overall axial motion range of the middle representative tracer particle during serum feed is comparable to that of the bottom representative. However, the transition between the two steps and therefore fluid composition did have a more prominent impact as shown by the much more pronounced rise and fall during the initial loading phase.

Likewise, the reverse behaviour was observed again when the mobile phase changed back to PBS during Wash I. The tracer particle began to sink when the buffer front reached its position in the column, which soon showed in a decreasing bed height. Increasing the fluid velocity then however lead to a brief overshoot of the tracer particle before it then levelled around the previous location while the UV signal showed the wash out of the serum. The overall time for this rise and overshoot behaviour until the tracer particle found back to its regular axial motion range was ca. 470 s, corresponding to 20% of the total washing time (Wash I). Similar to the previous run, the fluid velocity then had to be further increased towards the end of Wash I (t = 5430 s) to maintain a constant expanded bed height. It was adjusted from 423 cm/h as used during equilibration to 429 cm/h, which means an increase of 1.4%. Again, this could be a result of the protein (IgG) now adsorbed to the particles within the column. In this run, yet again very similar to the previous run, 2.95 g of total protein were bound to the resin as determined via BCA

assay analysis of the eluted fractions. This corresponds to 41.2 mg adsorbed protein per mL matrix and hence, meaning an increase in density of the resin particles of 1.2 - 1.6%.

During elution, a close succession of the two events described for the fluid transition phases occurred. This is illustrated by the rapid initial rise of the tracer particle at the beginning of eluting the IgG as a result of the elevated viscosity, subsequent drop due to decrease of fluid velocity as well as re-lowered viscosity and following overshoot when the fluid velocity was increased again.

Afterwards, the tracer particle moved within the previous axial positioning range again during cleaning (strip) and re-equilibration. A slight increase in axial location suggests to have taken place during sanitisation, despite reduced fluid velocity. Still, this is only within 1 cm, i.e. 2 % of the expanded bed height (position during sanitisation 260 - 310 mm cf. 250 - 300 during re-equilibration).

Overall, the particle's axial motion range was stable between 240 - 310 mm (corresponding to 14% of the expanded bed height) during the whole process cycle apart from the initial overshoot, the transitions between PBS and feedstock load and during elution. Even then, the rise and fall movements appeared fairly uncomplicated and in a controlled manner, and no extensive de-stabilisation of the entire bed could be detected.

In this run, too, the general EBA performance with regard to IgG purification from porcine serum was examined by analysing the collected fractions via SDS-PAGE (Figure 4.7).
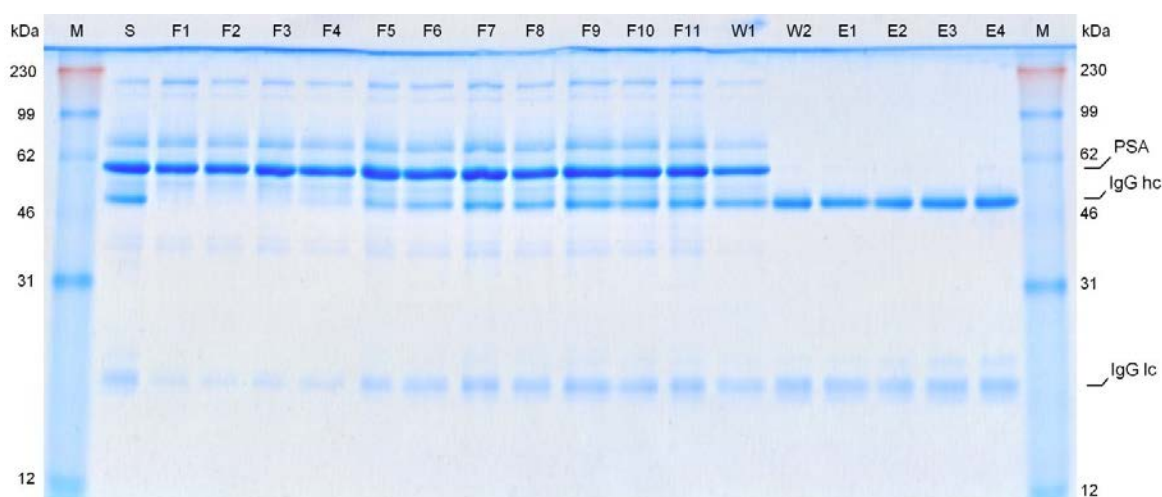
Figure 4.7: Reducing SDS 15% polyacrylamide gel electrophoretogram corresponding to the chromatogram shown in Figure 4.6. Key: molecular weight markers (M); serum feed (S); flowthrough fractions (F1-F11); wash fractions (W1-2); elution fractions (E1-E4).

Very similar to the electrophoretogram of the previous run (with the bottom representative tracer), Figure 4.7 depicts the IgG adsorption (lanes F1-F3/F4), breakthrough (lanes F4/F5) and desorption as highly purified target molecule in the elution fractions (lanes E1-E4). This confirms yet again that the axial positions of the tracer particle as detected by PEPT were produced under real binding conditions.

In the last of this series of experimental runs, an even smaller alumina tracer particle was employed to study the effect of applying feedstock on the top part of the expanded bed. The corresponding chromatogram and axial position of the tracer particle during the run are illustrated in Figure 4.8.
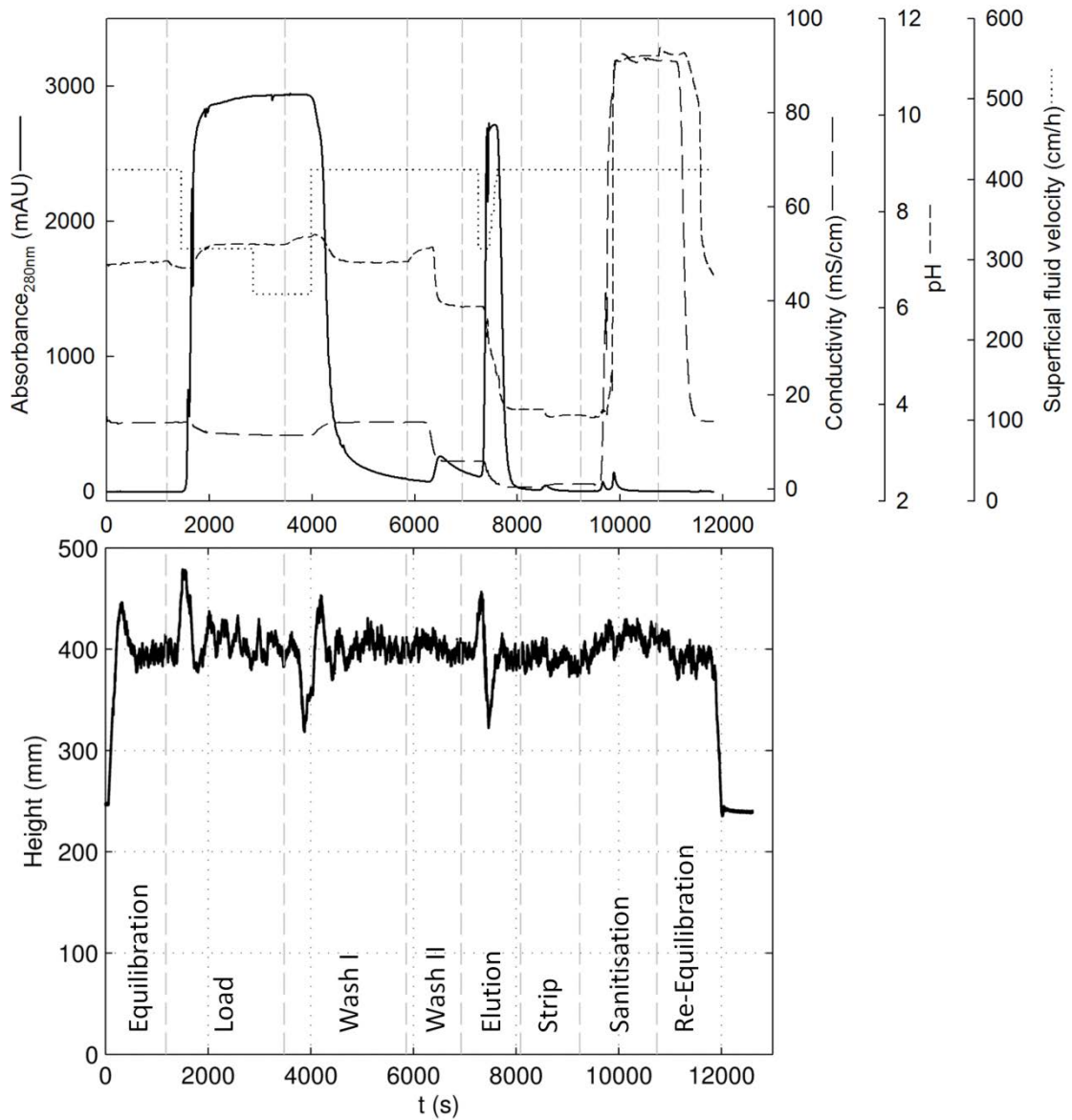
Figure 4.8: Chromatogram and axial position of an ^{18}F-labelled alumina tracer particle specified as $h_{T,0}$ = 0.95 against time within an expanded bed of Rhobust® MabDirect Protein A adsorbents with initial settled bed height H_0 = 25.0 cm in a 2 cm diameter nozzle inlet column at 2-fold expansion.

Overall, the axial locations of the top representative tracer particle as detected by PEPT and shown above in Figure 4.8 closely resemble the mid tracer's axial trajectory (Figure 4.6).

First, the established behaviour during equilibration was found as the tracer shows overshoot and subsequent levelling at a mean height. The buffer valve was then switched to start loading the serum. Here, after approximately 185 s, the feedstock front appears to

have reached the tracer particle's position, as it notably began to rise. As discussed before, this took obviously longer for the top representative tracer particle in this run compared to the one in the middle due to its higher overall position in the bed. The fluid velocity was reduced from 413 cm/h to 314 cm/h at t = 1450 s to maintain the twofold expansion and the tracer particle sinks back to its previous position within the bed. For this tracer, the overshoot took 340 s, corresponding to just under 15% of the total loading time. During the remaining loading phase, the axial motion range is slightly increased (380 - 440 mm) in comparison to the equilibration (375 - 415 mm), but is still contained within 12 % of the expanded bed height. Interestingly, however, the fluid velocity had to be further reduced to 258 cm/h halfway through the serum loading phase. This is different to the previous runs as in those, the fluid velocity was lowered once and then kept essentially constant, while here it was done in two steps. However, this did not seem to have an influence on the tracer particle's axial position.

Subsequently, very similar to what was described above for the tracer particle located further towards the middle of the bed, a drop and overshoot behaviour was found during transition from serum load back to PBS when switching to the next step (Wash I). This was explained as a result of the buffer front reaching the tracer particle's position, leading to its drop; followed by a brief overshoot due to the increased fluid velocity. Here, this motion pattern took approximately 540 s, which corresponded to just under 23% of the total washing time during Wash I. Subsequently, the tracer motion was judged as mostly stable, apart from a rise, drop and (small) overshoot during elution, as well as a minor increase in axial height during sanitisation. In general, the axial motion range lay between 370 - 410 mm (390 - 430 mm during sanitisation), corresponding to 8 % of the expanded bed height.

Interestingly, here, unlike previous runs, there was no need to adjust the flow rate during Wash I. Generally, a slightly decreased fluid velocity was used during this run in comparison to the other two runs, which might have resulted from minor temperature changes. It may be possible that a further flow rate adjustment was only needed at marginally higher fluid velocities. However, the total protein adsorbed in this run was 3.26 g and hence slightly higher than previously.

The collected fractions from the EBA process were analysed via SDS-PAGE (Figure 4.9).
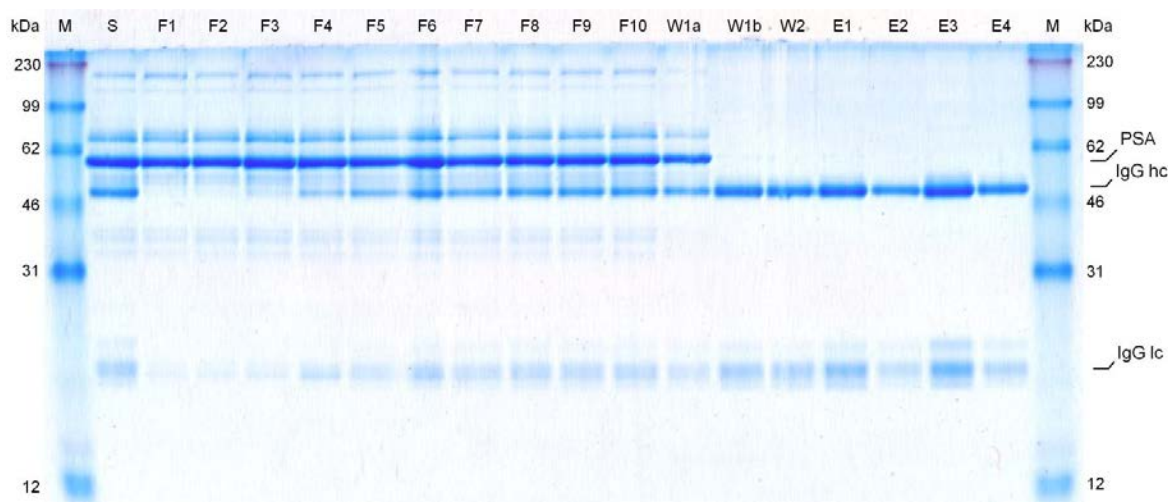
Figure 4.9: Reducing SDS 15% polyacrylamide gel electrophoretogram corresponding to the chromatogram shown in Figure 4.8. Key: molecular weight markers (M); serum feed (S); flowthrough fractions (F1-F11); wash fractions (W1-2); elution fractions (E1-E4).

Again, the electrophoretogram of this run as shown above (Figure 4.9) is very much comparable to the ones from the previous two runs. IgG was adsorbed from the serum as illustrated by lanes F1-F3, before breaking through (lanes F4-F10) and being eluted at high purity (lanes E1-E4).

Scanning densitometry of the electrophoretograms of each of the three runs as well as results from measurements of the total protein content of the collected flowthrough fractions (via BCA assay) were used to determine breakthrough curves as illustrated in Figure 4.10.
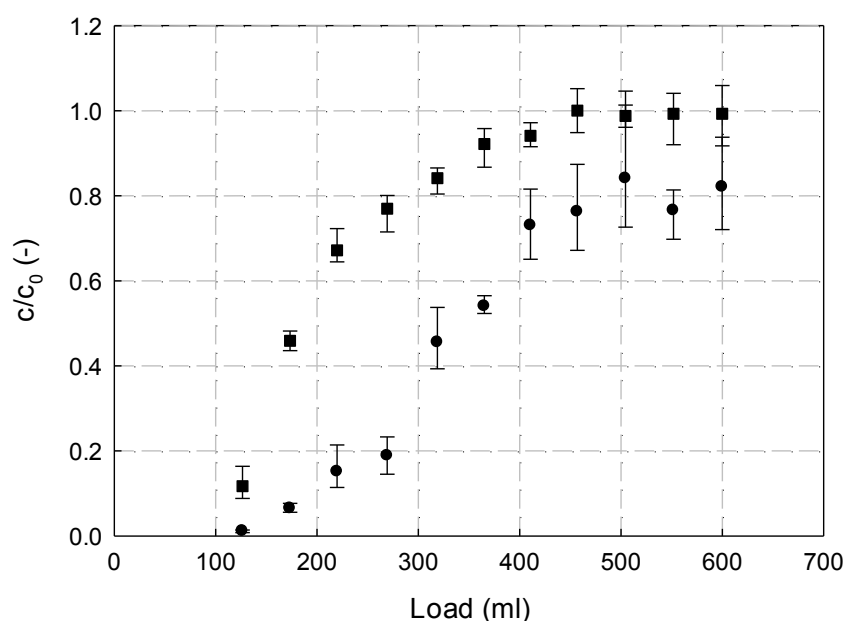
Figure 4.10: Total protein (squares) and IgG (circles) breakthrough depending on the volume of porcine serum loaded onto an expanded bed of Rhobust® MabDirect Protein A adsorbents with initial settled bed height H_0 = 25.0 cm in a 2 cm diameter nozzle inlet column at 2-fold expansion.

First, Figure 4.10 shows the protein breakthrough plotted against the effluent volume as recorded from switching the buffer valve to loading the serum. The system volume including the bed voidage space was found to be 98.5 mL, which is when the UV signal showed the detection of serum after the step change. From then onwards, 50 mL fractions were collected and analysed as stated above. Mean values from all three runs (employing a bottom, mid and top representative tracer particle) are graphed with the error bars illustrating maximum and minimum, respectively.

IgG appeared to break through relatively early, which may be due to the comparatively high fluid velocities employed. Breakthrough increased more substantially during the fifth

fraction (around 300 mL), which confirmed the visual observation of the electrophoretograms.

Most importantly however, the full binding capacity appeared to have been reached. The total protein values from the BCA assay were found to be more accurate than the IgG values from the scanning densitometry. This confirmed that the investigation of the adsorbent particle motion was conducted in a 'worst case' of binding a maximum amount of protein. If there was any influence of the adsorbed IgG on the particle motion, it should show under these conditions.

Analyses of the eluted fractions of each run revealed amounts of adsorbed protein of 2.95 - 3.26 g, corresponding to binding capacities of 41.2 - 45.5 mg protein per mL resin.

To be able to better compare the three runs each using a bottom, mid and top representative tracer, the axial positions as located by PEPT are plotted together in Figure 4.11.
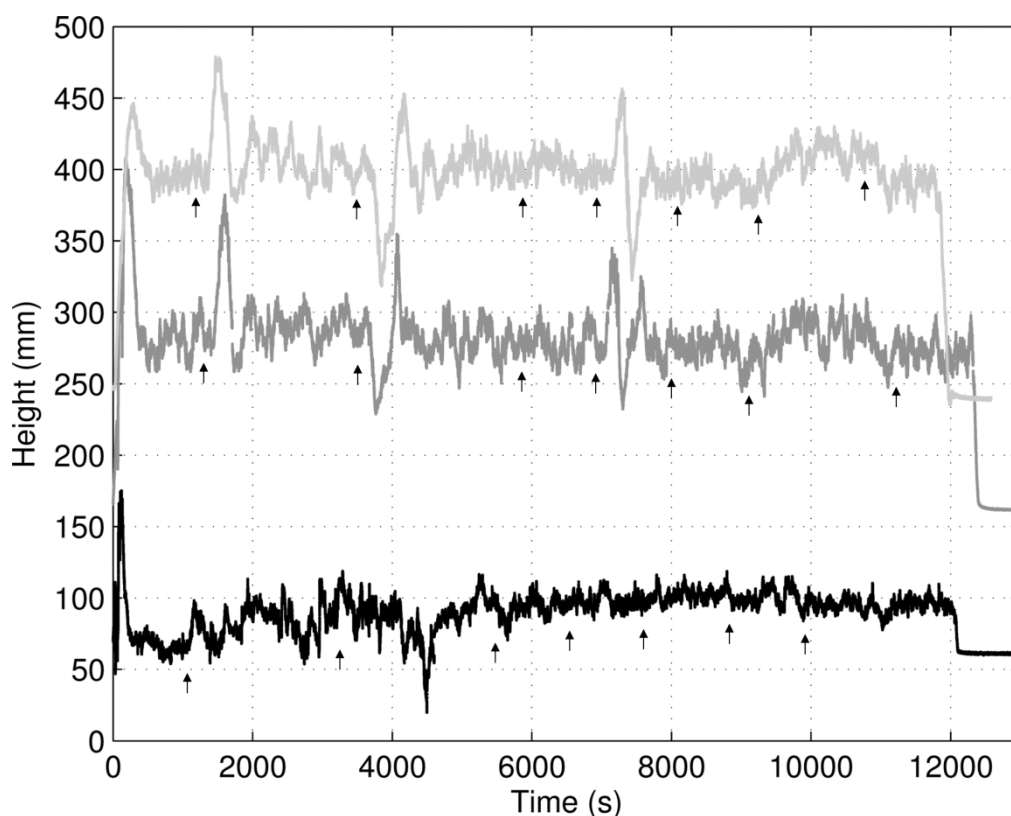
Figure 4.11: Superimposed axial trajectories of ^{18}F-labelled alumina tracer particles specified as $h_{T,0} = 0.28$ (black), 0.65 (dark grey) and 0.95 (light grey) against time within an expanded bed of Rhobust[®] MabDirect Protein A adsorbents with initial settled bed height $H_0 = 25.0$ cm in a 2 cm diameter nozzle inlet column for a 2-fold expansion. Black arrows indicate process condition/step changes.

Figure 4.11 illustrates the axial motion of a bottom (black), mid (dark grey) and top (light grey) representative alumina tracer particle during an entire EBA process run employing porcine serum as feedstock. The vertical black arrows indicate the step changes as the buffer valve was switched, corresponding to the vertical, grey dashed lines in previous figures (Figure 4.4, 4.5 and 4.7). These were not performed at the same time for each run, as different flow rates were used at different stages during each run. Nevertheless, the superimposed trajectories allow a direct comparison even if not on the same timescale.

First, when comparing the entire runs and the axial positions during these runs, a different behaviour of the bottom representative tracer particle can be observed as opposed to the two tracers located further above. These two, as mentioned before, show very similar

overall axial motion patterns. In particular the step changes caused very analogous responses, which is illustrated by the rise and sink at the beginning of the load phase, the drop and overshoot when changing back to PBS during the first washing step and the succession of these events during elution. Furthermore, both tracers demonstrated a slight increase in axial position during sanitisation (the penultimate step), while the axial motion ranges during the other phases of the process appeared reasonably stable.

In contrast, the bottom tracer most notably did not show the abovementioned distinct responses to the step changes or at least not to the same extent. There was still a discernible rise and drop at the start of elution as well as a potential drop when the feedstock was washed out again, but these were within the normal axial motion range. The apparent, sudden drop of the tracer particle during Wash I (at approximately 4500 s) did not seem related to this and was explained by a potential short-termed aggregation with another particle. Interestingly, the brief increase in viscosity and resulting need for a lower fluid velocity during elution did not appear to have an influence on the location and movement of particles in the lower part of the bed.

Apart from the behaviour during phase transition, all three tracer particles exhibited a relatively stable positioning within their respective axial motion ranges. This is in accordance with findings by Tong and Sun (2002), who stated that the particle size distribution within the expanded bed was not influenced by the mobile phase viscosity. Comparing the axial motion ranges during the loading phase (i.e. at higher viscosity) to the equilibration, they increased for the bottom and top tracer while it remained constant at 10% expanded bed height for the mid representative tracer. Although relatively, this increase was higher for the bottom part of the bed (from 5 to 12% of the expanded bed height), overall it was comparable to that of the top part (from 8 to 12%). If the axial motion range is seen as an indication for the axial dispersion, this observation was not

quite in accordance to results found by Lin et al. (2015). A general increase of axial dispersion with increasing mobile phase viscosity could be confirmed, but in their study, it was shown to have a more pronounced effect in the bottom part of the bed.

However, the present findings are in good accordance with those of a previous study conducted by Souquet (2011). There, similarly stable axial motion ranges and overall axial positions of 'native' Q HyperZ tracer particles during processing of bovine serum albumin (BSA) were observed. Using BSA in two different buffers to study both the native globular and denatured protein state, the effect of adsorption dynamics on adsorbent particle movement both in mid and bottom parts of expanded beds were shown to be minimal. Furthermore, despite high dynamic binding capacities of up to 80 mg/mL and loading the beds with feedstock past 100% breakthrough, axial positions of the Q HyperZ particles did not drop during load while increasing amounts of BSA adsorbed. Although this was neither detected in the present study, it was mentioned that potential drops of the tracer particles may have been covered by the adjustment of the flow rate. Souquet (2011) however worked at constant superficial fluid velocities rather than constant bed height, which was suitable as the viscosities of the mobile phases during the run were likely similar. In contrast, when loading sonicated calf thymus DNA onto Q HyperZ beds, striking increases in the range and frequency of axial motion of the tracer particles were found (Souquet 2011). In the most severe case, both the mid and bottom tracer particle travelled almost along the entire bed height. Unexpectedly, despite an overall bed contraction, DNA induced particle aggregation did not impair adsorbent mobility but rather resulted in its intensification. Particle crosslinking and subsequent shear-induced break up were given as explanation for the significant axial up and down movement of the tracers.

Considering the results of the present work employing Rhobust® MabDirect Protein A, the stable axial positions indicate that no aggregation or interaction between components of the porcine serum and the adsorbent particles occurred.

4.4.3.   Effect of the degree of bed expansion

To examine the influence of the degree of bed expansion on the adsorbent particle movement under real process conditions, a mid representative tracer particle characterised as $h_{T,0} = 0.65$ was tracked with PEPT within a 2.4-fold expanded bed of Rhobust® MabDirect Protein A during a run using porcine serum as raw material. The experimental procedure and the buffers used are the same as in previous runs (Section 4.4.2) and are described in Section 2.3.4. Here, however, an increased superficial fluid velocity was employed to achieve a 2.4-fold expansion. The resulting chromatogram and corresponding axial position are depicted in Figure 4.12.
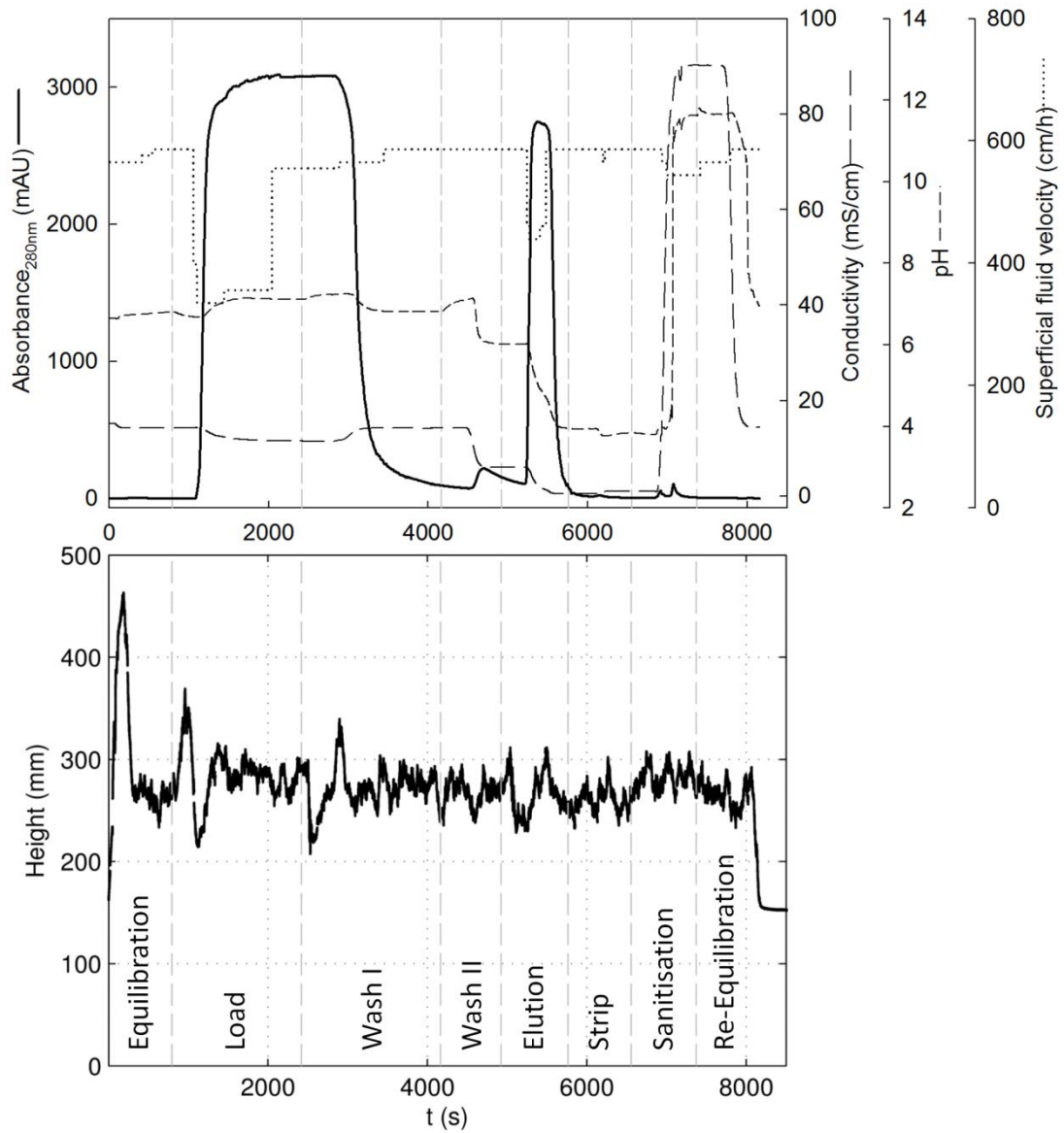
Figure 4.12: Chromatogram and axial position of an ^{18}F-labelled alumina tracer particle specified as $h_{T,0} = 0.65$ against time within an expanded bed of Rhobust® adsorbents with initial settled bed height $H_0 = 25.0$ cm in a 2 cm diameter nozzle inlet column for a 2.4-fold expansion.

Despite the increased bed height of 600 mm, the axial position of the tracer particle is illustrated in the same scale as the previous runs at twofold expansion for better comparison.

First, in accordance with previous findings as described in Chapter 2, the higher superficial fluid velocity applied to achieve the higher degree of bed expansion of 2.4 resulted in a higher overshoot at the start of fluidisation. Afterwards, the tracer particle

positioned at an axial height between 240 - 285 mm during equilibration. Considering a tracer with the same specification as the one during the process with 2.0-fold expansion was used to represent the middle part of the bed ($h_{T,0}$ = 0.65), the axial position was further in agreement with results from Chapter 2. As a mid representative tracer particle, it did not locate higher in the bed at higher superficial fluid velocity (cf. 260 - 310 mm at 2.0-fold expansion).

After switching the buffer valve to load the serum, the feedstock front appeared to reach the tracer particle within a relatively short time of approximately 70 s which is when the rise in the tracer particle is detected by PEPT. This is unexpected, especially in comparison to the run using twofold expansion, where the front took more than twice that time (150 s) to reach a similarly positioned tracer. This may be an indication of channelling that was happening especially in the lower half of the expanded bed at this higher fluid velocity. The following overshoot was in a similar height range as during the twofold expansion run and reached a maximum axial position of 370 mm. Then, the fluid velocity was decreased and the tracer particle dropped. In contrast to the run using twofold expansion, it was found to be more problematic to maintain a constant bed height at 2.4-fold expansion. This showed in the further drop of the tracer even below the previous position (215 mm), a kind of undershoot, which did not occur in previous runs. It then rose back up to around 300 - 315 mm. Overall, it took ca. 440 s for the tracer particle to find back to its normal axial motion range, corresponding to 27% of the total loading time. This is about twice as long as compared to the twofold expansion (13%).

Interestingly, during further serum load the fluid velocity had to be increased. First, at around 1450 s, the superficial fluid velocity was raised from 335 to 356 cm/h and then even further to 555 cm/h at 2040 s, which is close to the 586 cm/h applied during equilibration. Still, despite this increase in fluid velocity, the tracer particle appeared to

even slightly sink within the bed. This may have been resulting from the IgG overloading as mentioned before, but no increase in flow rate during Wash I cf. equilibration was necessary. Therefore, it may in fact be further indication of the abovementioned channelling.

The switch to the first wash step then resulted in a similar behaviour again as seen previously; a drop, rise and overshot during replacement of the serum by PBS. This took approximately 500 s, corresponding to 29% of the washing time (cf. 20% at twofold expansion)

Overall, for the remaining time of the process, the tracer particle stayed within an axial motion range between 235 - 315 mm. Notably, the tracer response during elution was not as distinct as in the run using twofold expansion. The overall axial motion range here was slightly larger than in the twofold expanded bed (80 mm cf. 60 mm), but in the same scale when considered relative to the expanded bed height (13.3% cf. 14%).

The collected fractions from this EBA run were also analysed via SDS-PAGE (Figure 4.13).
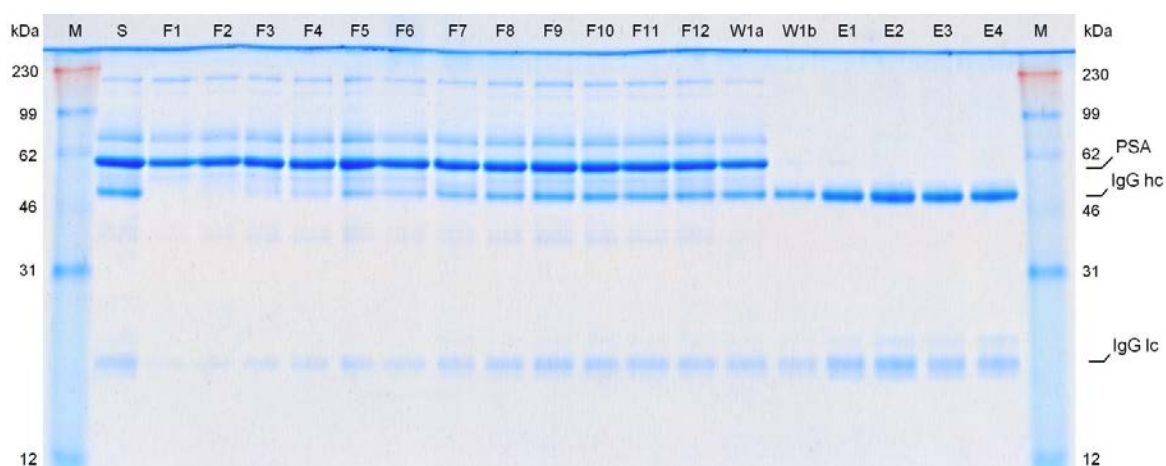
Figure 4.13: Reducing SDS 15% polyacrylamide gel electrophoretogram corresponding to the chromatogram shown in Figure 4.12. Key: molecular weight markers (M); serum feed (S); flowthrough fractions (F1-F12); wash fractions (W1a-b); elution fractions (E1-E4).

Again, the electrophoretogram of this run as shown above (Figure 4.9) is very much comparable to the ones from the previous runs at twofold expansion. Interestingly, no distinctive earlier breakthrough of the IgG can be observed. An earlier breakthrough would have been expected at severe channelling. However, the channelling may have only occurred in the lower half of the bed, while the IgG was still adsorbed in the upper half, leading to IgG depletion in the first fractions collected.

The determination of the total protein content of the eluted fractions gave a total amount of adsorbed protein of 2.67 g which is slightly lower than that of the runs at twofold expansion. This may be due to hindered mass transfer at higher superficial fluid velocity, or, again, due to channelling problems.

4.5.   Conclusion

The adsorbent particle movement in expanded beds of Rhobust® MabDirect Protein A was investigated under real process conditions using the technique of positron emission particle tracking. Tracer particles representing the bottom, mid and top parts of the

expanded bed were tracked at a constant degree of bed expansion of twofold for the entire process using porcine serum as feedstock. The influence of changing process conditions and adjustments in the superficial fluid velocity in order to maintain a constant bed height was studied.

Overall axial positions of the tracer particles were observed as relatively stable. The tracer particles generally maintained a constant axial position within the expanded bed throughout the entire process. However, distinct rises and falls were detected for tracers representing the mid and top part of the bed during transient phases at the beginning of the serum load and subsequent washing, as well as during elution. The change of the viscosity of the mobile phase therefore had a more pronounced effect on the smaller, lighter particles in the upper part of the expanded bed. Still, it was pointed out that these deviations from the normal axial motion range occurred relatively controlled and within a defined timeframe. After 13 and 15% of the loading time the mid and top tracer, respectively, found back to their axial positions, while it took 20 and 23% of the washing time.

Excluding these over- and undershoots from their mean position, axial motion ranges were found to be 60 mm (for the bottom tracer specified as $h_{T,0} = 0.28$) and 70 mm (mid and top, $h_{T,0} = 0.65$ and $h_{T,0} = 0.95$) throughout the entire process, corresponding to 12 and 14% of the expanded bed height, respectively. This proved as not significantly higher than during a process omitting the loading step, i.e. without adsorption (60 mm axial motion range).

A higher degree of bed expansion of 2.4 lead to an increase of the relative times for over- and undershoots during mobile phase transition. Here, a mid tracer particle regained its normal axial position after 27% of the overall loading time and 29% of the column washing (cf. 13 and 20% at twofold expansion).

4.6.   References

Barnfield Frej, A.-K., R. Hjorth, et al. (1994). "Pilot scale recovery of recombinant annexin V from unclarified escherichia coli homogenate using expanded bed adsorption." Biotechnology and Bioengineering **44**(8): 922-929.

Chang, Y. K. and H. A. Chase (1996). "Development of operating conditions for protein purification using expanded bed techniques: The effect of the degree of bed expansion on adsorption performance." Biotechnology and Bioengineering **49**(5): 512-526.

Chase, H. A. (1994). "Purification of proteins by adsorption chromatography in expanded beds." Trends in Biotechnology **12**(8): 296-303.

Chase, H. A. and N. M. Draeger (1992). "Affinity Purification of Proteins Using Expanded Beds." Journal of Chromatography **597**(1-2): 129-145.

Fan, X., D. J. Parker, et al. (2006). "Labelling a single particle for positron emission particle tracking using direct activation and ion-exchange techniques." Nuclear Instruments & Methods in Physics Research Section a-Accelerators Spectrometers Detectors and Associated Equipment **562**(1): 345-350.

Ghose, S. and H. Chase (2000). "Expanded bed chromatography of proteins in small diameter columns. I. Scale down and validation." Bioseparation **9**(1): 21-28.

Ghose, S., H. A. Chase, et al. (2000). "Bed height monitoring and control for expanded bed chromatography." Bioprocess Engineering **23**(6): 701-708.

Hjorth, R. (1997). "Expanded-bed adsorption in industrial bioprocessing: Recent developments." Trends in Biotechnology **15**(6): 230-235.

Laemmli, U. K. (1970). "Cleavage of Structural Proteins during the Assembly of the Head of Bacteriophage T4." Nature **227**(5259): 680-685.

Leadbeater, T. W., D. J. Parker, et al. (2012). "Positron imaging systems for studying particulate, granular and multiphase flows." Particuology **10**(2): 146-153.

Lihme, A., M. B. Hansen, et al. (2010). "A novel core fractionation process of human plasma by expanded bed adsorption chromatography." Analytical Biochemistry **399**(1): 102-109.

Lin, D.-Q., M.-R. Kula, et al. (2003). "Stability of expanded beds during the application of crude feedstock." Biotechnology and Bioengineering **81**(1): 21-26.

Lin, D.-Q., W. Shi, et al. (2015). "Evaluation and characterization of axial distribution in expanded bed: II. Liquid mixing and local effective axial dispersion." Journal of Chromatography A **1393**: 65-72.

Parker, D. J., C. J. Broadbent, et al. (1993). "Positron Emission Particle Tracking - a Technique for Studying Flow within Engineering Equipment." Nuclear Instruments & Methods in Physics Research Section a-Accelerators Spectrometers Detectors and Associated Equipment **326**(3): 592-607.

Schindelin, J., I. Arganda-Carreras, et al. (2012). "Fiji: an open-source platform for biological-image analysis." Nat Meth **9**(7): 676-682.

Souquet, J. (2011). "Advances in Expanded Bed Adsorption Chromatography." PhD Thesis, University of Birmingham.

Thelen, T. V. and W. Fred Ramirez (1997). "Bed-height dynamics of expanded beds." Chemical Engineering Science **52**(19): 3333-3344.

Thelen, T. V., A. P. Mairal, et al. (1997). "Application of Ultrasonic Backscattering for Level Measurement and Process Monitoring of Expanded-Bed Adsorption Columns." Biotechnology Progress **13**(5): 681-687.

Thömmes, J., M. Halfar, et al. (1995). "Purification of monoclonal antibodies from whole hybridoma fermentation broth by fluidized bed adsorption." Biotechnology and Bioengineering **45**(3): 205-211.

Tong, X.-D. and Y. Sun (2002). "Particle size and density distributions of two dense matrices in an expanded bed system." Journal of Chromatography A **977**(2): 173-183.

Yang, Z. and Y. Sun (2005). "Variations of particle size and bed voidage distributions in expanded bed during transient operation processes." Journal of Chromatography A **1077**(2): 143-150.

5. Conclusions and future work

Expanded bed adsorption (EBA) is a powerful technology in downstream processing of bioproducts due to its ability to perform chromatographic separations with crude feedstocks. Allowing the combination of several steps – i.e. clarification, concentration and capture – into one single unit operation, EBA has the potential for increased overall yields, lower costs and reduced process times. However, despite initial hype after its introduction in the mid 1990s and some impressive demonstrations of its capabilities, industry's faith in EBA has largely been lost. The lack of robustness was identified as main issue since given that variations during loading in particular severely compromised the control of EBA processes, and problem components in many feedstocks caused fouling of the fluid distribution system and/or biomass induced particle-particle cross-linking and ensuing collapse of the expanded bed. At the root of all these issues lies a poor understanding of the complex hydrodynamic behaviour prevailing within expanded beds.

To address this fundamental deficiency, the powerful, non-invasive tomography technique 'Positron Emission Particle Tracking' (PEPT) was employed intensively in this work to assess solid phase behaviour in expanded beds. Following on from previous studies in Birmingham using PEPT for examination of EBA, further in-depth investigations presented here focussed on Rhobust® adsorbents (Patheon, The Netherlands). Initially, the hydrodynamic behaviour of tracer particles representing the bottom, mid and top parts of the expanded bed were analysed in 'clean' systems using three different 'buffer fluidised' columns (Chapter 2). A non-uniform bed expansion was observed, in which only the top part of the bed accounted for the increased expansion at increasing flow rates, while the axial positions of particles in lower parts were constant. These findings suggested complex interactions between adsorbent particles to be a key factor contributing to the

discrepancies to commonly held views. For the first time, solid axial dispersion coefficients were calculated from the acquired data and used to evaluate solid phase motion. Overall higher values than proposed in literature indicated that solid mixing may have been underestimated to date. Furthermore, bed stabilisation kinetics were determined by analysing the tracer particles' axial positioning over time after starting fluidisation. In contrast to judging a bed stable merely by visual inspection at the column wall, accurate times could be deduced from PEPT data, revealing the potential for reducing process times and buffer consumption by shortening equilibration times. Purposeful vertical misalignment of the column revealed axial and horizontal circular patterns of tracer particle motion and systematic increases in the degree of misalignment resulted in enhanced destabilisation inferred by increases in both liquid and solid axial dispersion.

These new insights allowed for re-evaluation of results obtained in previous PEPT studies of EBA employing different commercial adsorbents (Chapter 3). In this way for instance, a potential marginal vertical misalignment of the column was suggested as real cause for a circular motion pattern which at the time was attributed to interparticle interactions. Motion behaviour in beds of various matrices were analysed and compared. Overall, despite using different tracer particles and labelling techniques, columns and mobile phases, a non-uniform bed expansion with increasing fluid velocity was found in all beds, posing further questions on our understanding of this unit operation.

Finally, adsorbent particle motion was investigated under real process conditions during isolation of IgG from porcine serum (Chapter 4). Overall axial positions and motion ranges of the tracer particles were observed to be relatively stable. No significantly increased solid mixing during feedstock load was identified and slight effects of changing process conditions and adjustments in the superficial fluid velocity on particles' axial position

suggest a robust process can be achieved by maintaining a constant bed height. Automatic bed height control with a more incremental flow rate adjustment could result in an even more stable process at production scale. However, considering a relatively pure serum was used in this study, feedstocks based on CHO cells as commonly employed in production of monoclonal antibodies may exhibit higher viscosities and therefore have a more pronounced effect on bed stability.

Overall, this in-depth work complements the generated PEPT dataset, giving further insight into hydrodynamic behaviour within expanded beds. Ultimately, a comprehensive knowledge of solid phase dispersion in EBA will help in developing complex models for any given expanded bed adsorbent matrix while taking into account particle-particle interactions. More PEPT investigations will however be needed to achieve a full understanding of the interdependencies between process parameters. New techniques will be required that allow radioactive labelling of native adsorbent beads as tracer particles. Furthermore, the scale down models as used in this work should be compared with large scale production EBA columns. Influences such as those from vertical misalignment of the column are expected to be less marked with increasing column diameters.

6. Appendix

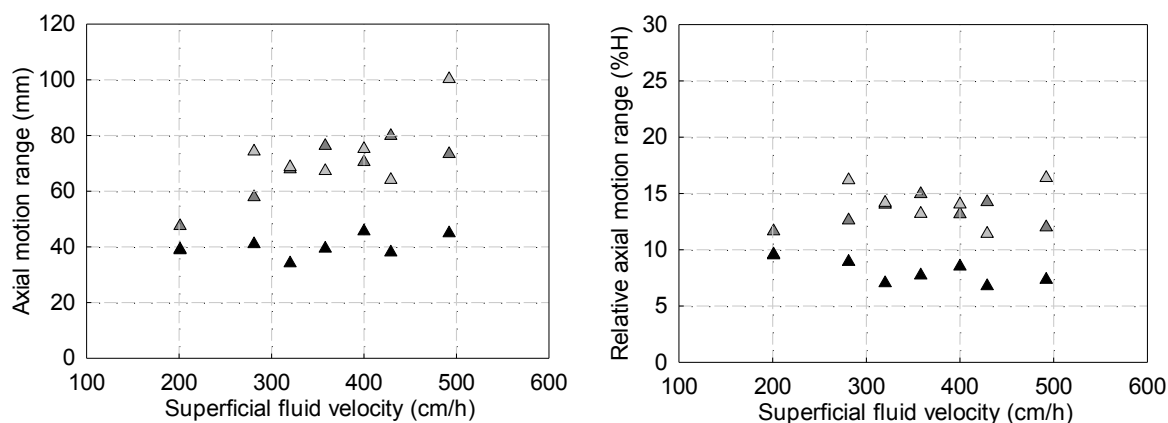## 6.1.   Axial motion ranges of tracers in beds of Rhobust® particles

Figure 6.1: Absolute and relative axial motion ranges of ^{18}F-labelled alumina tracer particles representing the bottom (black), mid (dark grey) and top (light grey) of an expanded bed of Rhobust® MabDirect Protein A adsorbents with initial settled bed height H_0 = 25.5 cm in a 2.0 cm diameter nozzle inlet column with increasing superficial fluid velocity.
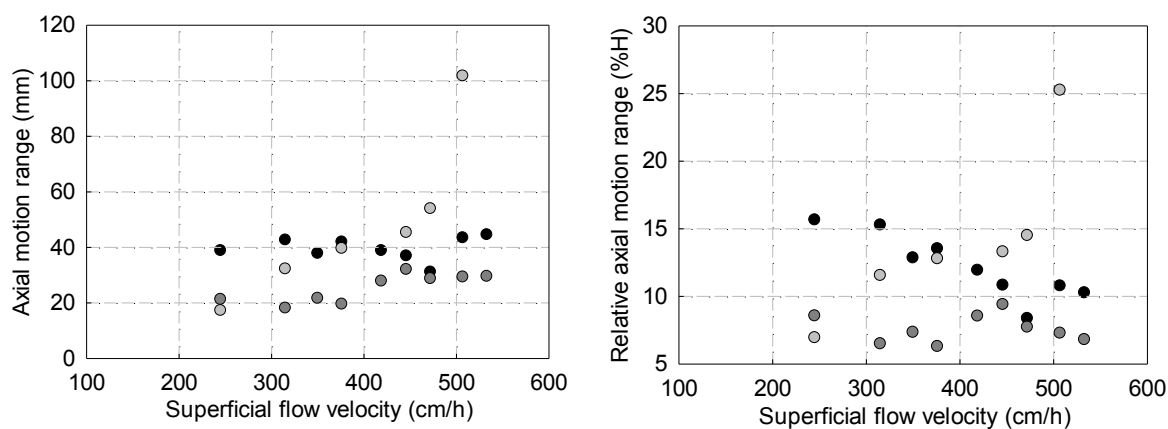

Figure 6.2: Absolute and relative axial motion ranges of ^{18}F-labelled alumina tracer particles specified as $h_{T,0}$ = 0.52 (black), 0.82 (dark grey) and 0.90 (light grey) within an expanded bed of Rhobust® MabDirect Protein A adsorbents with initial settled bed height H_0 = 15.5 cm in a 1 cm diameter nozzle inlet column with increasing superficial fluid velocity.
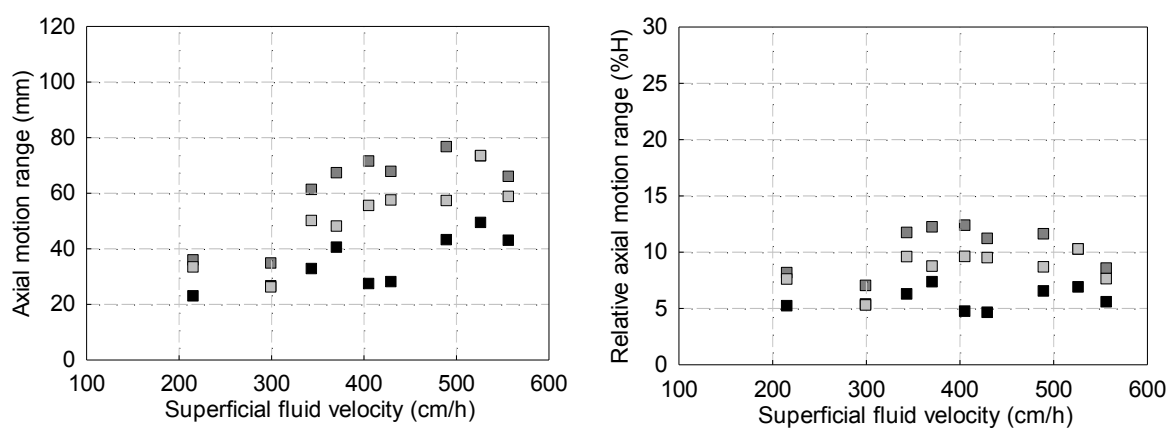
Figure 6.3: Absolute and relative axial motion ranges of ^{18}F-labelled alumina tracer particles specified as $h_{T,0}$ = 0.32 (black), 0.60 (dark grey) and 0.94 (light grey) within an expanded bed of Rhobust[®] MabDirect Protein A adsorbents with initial settled bed height H_0 = 27.5 cm in a 2.5 cm diameter Streamline column with increasing superficial fluid velocity.

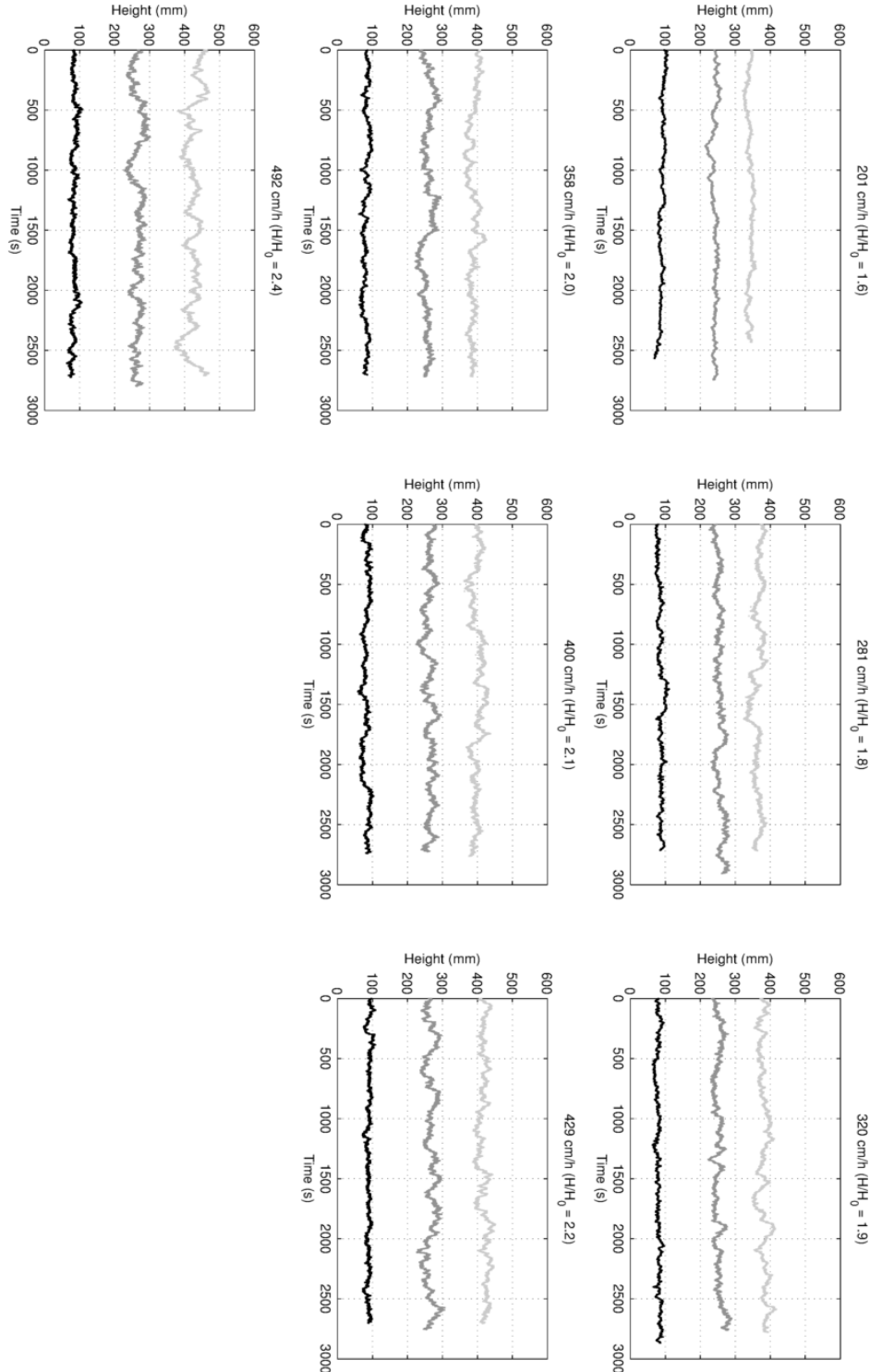## 6.2. Full axial trajectories of alumina tracers in beds of Rhobust®

particles

Figure 6.4: Superimposed axial positions of ^{18}F-labelled alumina tracer particles representing the bottom (black), mid (dark grey) and top (light grey) of an expanded bed of Rhobust® MabDirect Protein A adsorbents against time with initial settled bed height H_0 = 25.5 cm in a 2.0 cm diameter nozzle inlet column for all superficial fluid velocities applied.
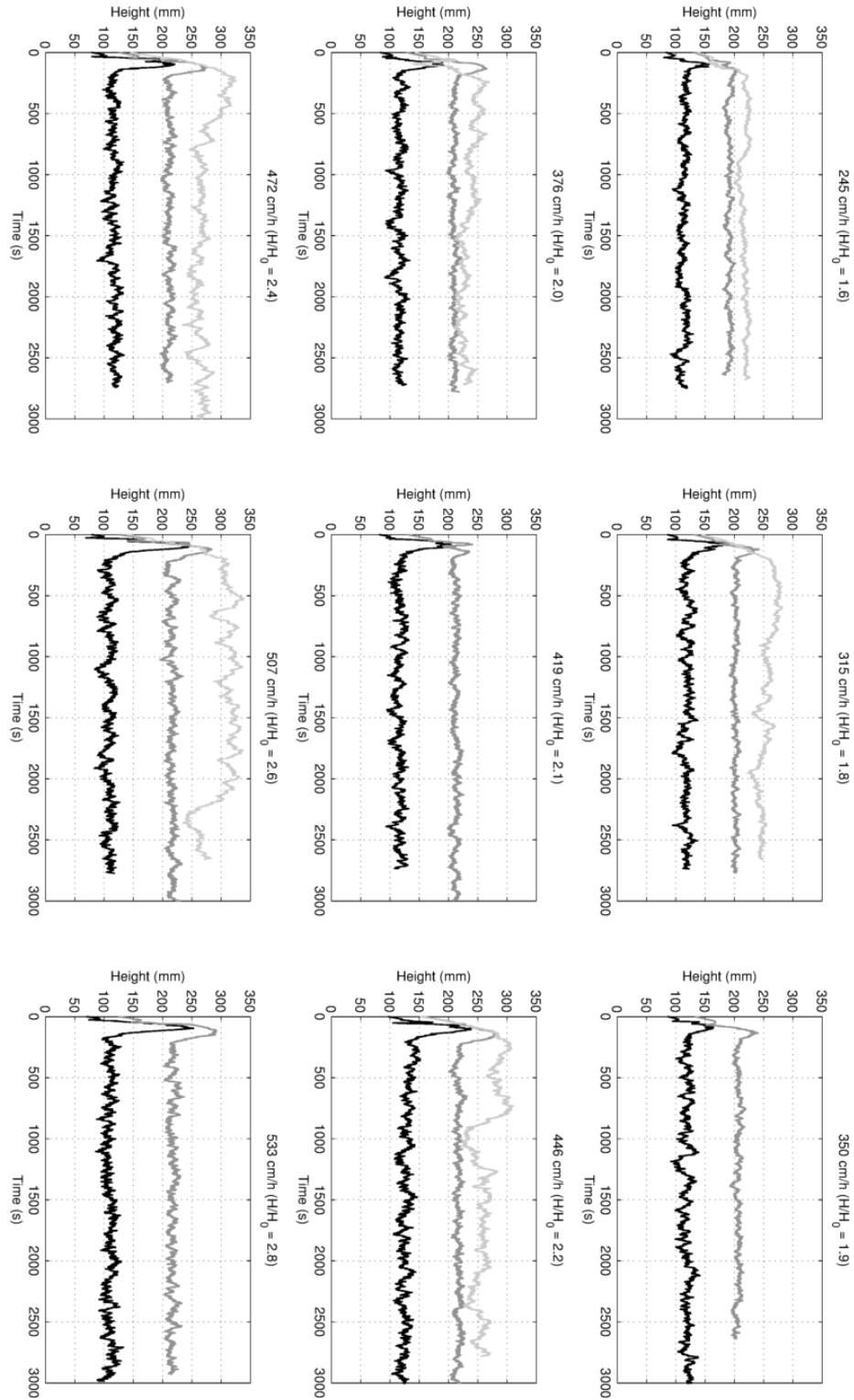
Figure 6.5: Superimposed axial positions of ^{18}F-labelled alumina tracer particles specified as $h_{T,0}$ = 0.52 (black), 0.82 (dark grey) and 0.90 (light grey) against time within an expanded bed of Rhobust® MabDirect Protein A adsorbents with initial settled bed height H_0 = 15.5 cm in a 1 cm diameter nozzle inlet column for all superficial fluid velocities applied.
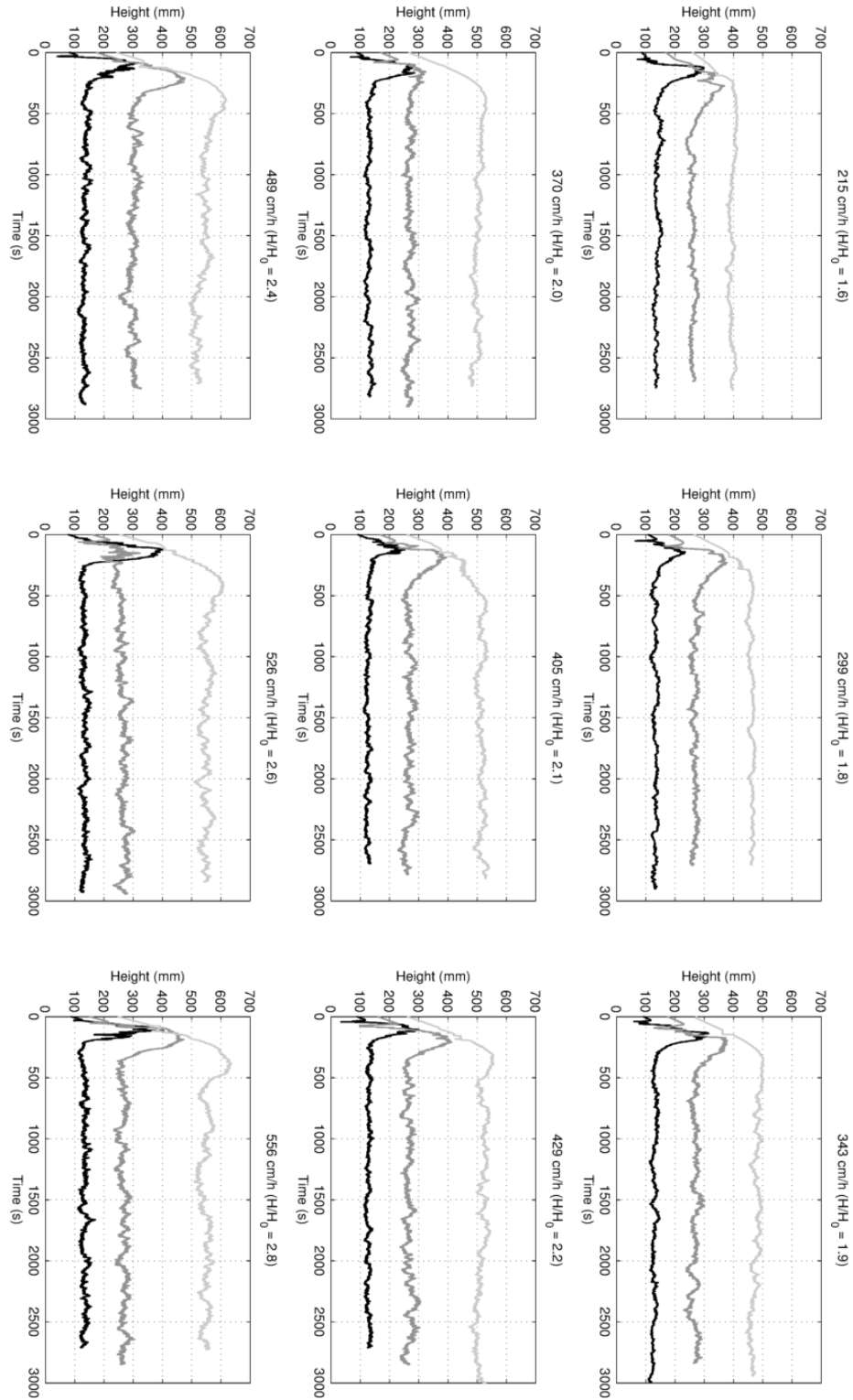
Figure 6.6: Superimposed axial positions of ^{18}F-labelled alumina tracer particles specified as $h_{T,0}$ = 0.32 (black), 0.60 (dark grey) and 0.94 (light grey) against time within an expanded bed of Rhobust$^{®}$ MabDirect Protein A adsorbents with initial settled bed height H_0 = 27.5 cm in a 2.5 cm diameter Streamline column for all superficial fluid velocities applied.

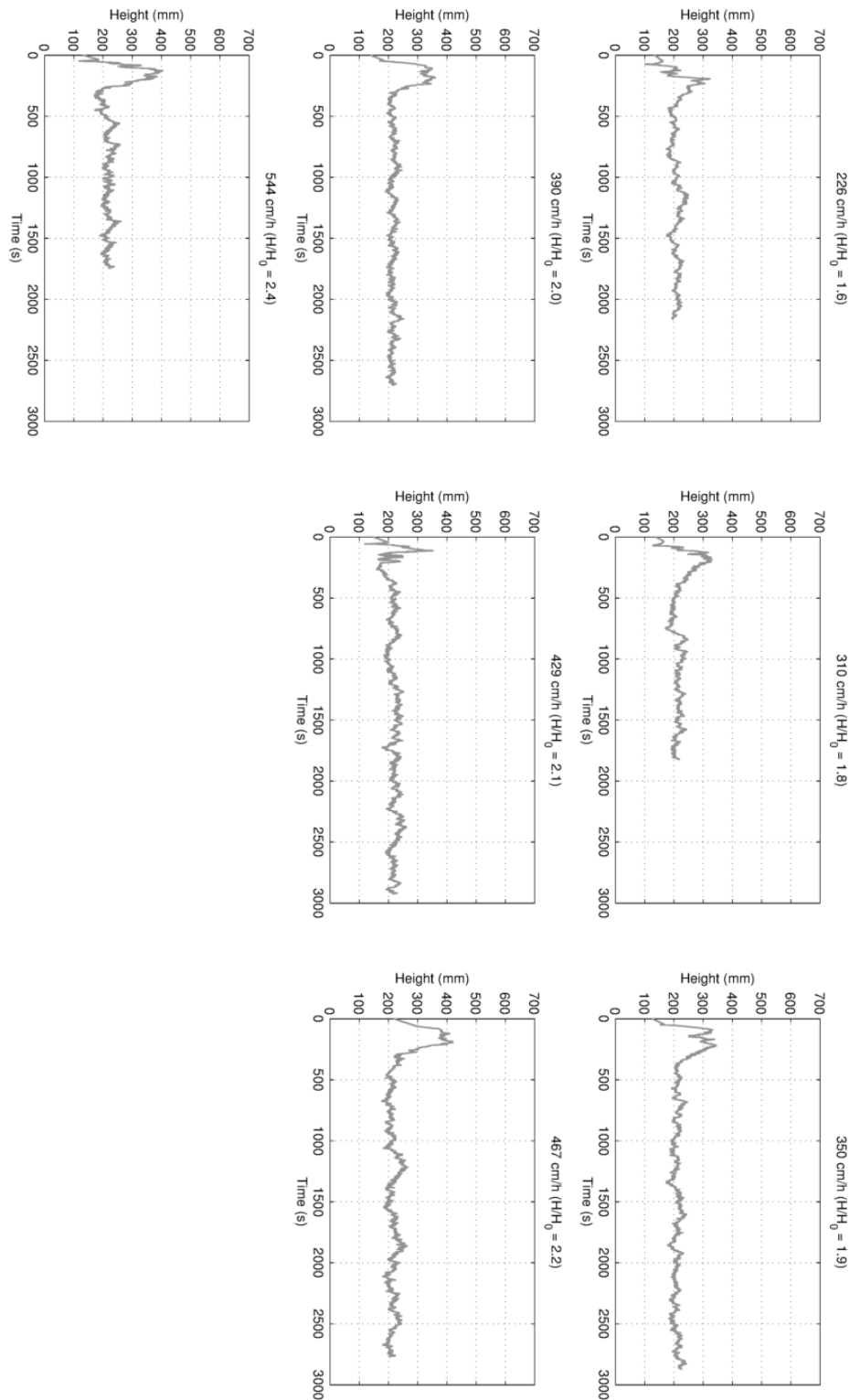## 6.3.   Further documentation of the effect of column misalignment

Figure 6.7: Axial positions of a ^{18}F-labelled alumina tracer particles specified as $h_{T,0}$ = 0.52 in an expanded bed of Rhobust® MabDirect Protein A adsorbents against time with initial settled bed height H_0 = 26.5 cm in a 2.0 cm diameter nozzle inlet column 0.5° misaligned to the vertical for all superficial fluid velocities applied.
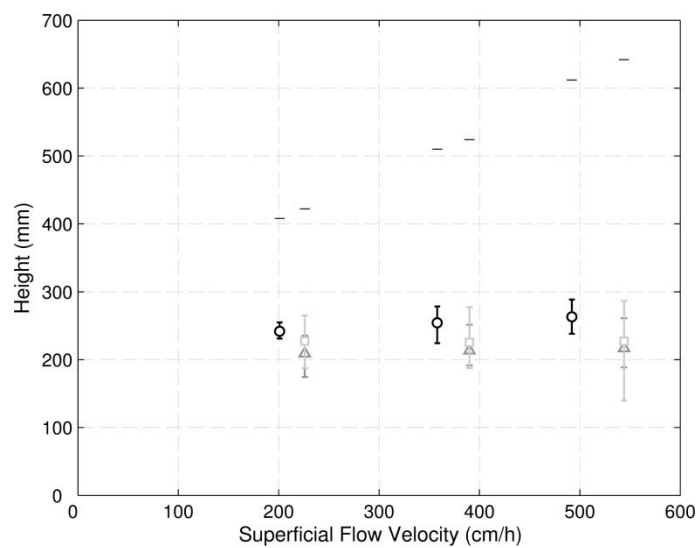
175

Figure 6.8: Superimposed mean (symbol), maximum and minimum (error bars) axial positions of 'mid' tracer particles in expanded beds of Rhobust® MabDirect Protein A adsorbents in a 2 cm diameter nozzle inlet column misaligned by 0° (○), 0.5° (□) and 1.0° (△) off vertical, operated at different expansions (1.6, 2.0 and 2.4). Expanded bed heights are marked with black dashes.

6.4.   Full comparison of PEPT studies of EBA conducted to date

Table 6.1: Conditions and settings for the different PEPT studies of EBA compared in Chapter 3.

Study	Liu (2009)		Souquet (2011)	Present work			
Resin (Manufacturer)	Streamline (GE Healthcare)	UFC (Upfront Chromatography)	Q HyperZ (Pall)	Rhobust MabDirect Protein A (Patheon)			Q HyperZ (Pall)
Resin properties (size and density distribution)	100 - 300 µm 1.2 g/mL	100 - 300 µm 1.5 g/mL	40 - 105 µm 3.2 g/mL	20 - 200 µm 2.8 - 3.2 g/mL			40 - 105 µm 3.2 g/mL
Column (Manufacturer)	XK26 (GE Healthcare)		Streamline 25 (GE Healthcare)	1 cm 'NC' (Patheon)	2 cm 'NC' (Patheon)	Streamline 25 (GE Healthcare)	Streamline 25 (GE Healthcare)
Column diameter	26 mm		25 mm	10 mm	20 mm	25 mm	25 mm
Fluid distribution	10 µm perforated mesh, 5 cm layer of ballotini beads (3-5 mm diameter)		Perforated plate and mesh	4 port nozzle and cone	4 port nozzle and cone	Perforated plate and mesh	Perforated plate and mesh
H_0	15 cm	15 cm	15 cm	15.5 cm	25.5 cm	27.5 cm	15.4 cm
Tracer particles	Chelex-100	Chelex-100	Q HyperZ	γ-alumina	γ-alumina	γ-alumina	Q HyperZ
Tracer sizes	110 µm, 150 µm, 220 µm	220 µm	75 µm, 100 µm	Specified by their relative position in the settled bed rather than size			90 µm
Radionuclide	^{61}Cu, ^{66}Ga	^{61}Cu	^{66}Ga	^{18}F	^{18}F	^{18}F	^{18}F
Mobile phase	Tap water (warmed to 21-22° C)		Tap water	PBS	PBS	PBS	PBS

6.5. SDS-PAGE protocol

6.5.1. Buffer preparation

- <u>Stock Running Gel Buffer</u> *(0.75M Tris/HCl pH 8.3):* Dissolve 18.172g of Tris(hydroxymethyl)methylamine in 100 mL deionised water. Adjust to pH 8.3 with HCl. Make up to 200 mL with deionised water. Filter through a Whatman filter.

- <u>Stock Stacking Gel Buffer</u> *(1.25M Tris/HCl pH 6.8):* Dissolve 75.73 g of Tris in 300 mL deionised water. Adjust to pH 6.8 with HCl. Make up to 500 mL with deionised water. Filter through a Whatman filter.

- <u>20% Sodium Dodecyl Sulphate (SDS):</u> Dissolve 20 g SDS in 80 mL deionised water while heating gently and stirring. Make up to 100 mL with deionised water.

- <u>Ammonium Persulphate (APS):</u> Dissolve 80 mg in 1 mL deionised water. Store at -20°C in 1 mL aliquots.

- <u>Sample Buffer:</u> Mix 2 g SDS, 20 mL glycerol and 5 mg bromophenol blue (sulphone form). Dissolve in 92 mL of 10x diluted stock stacking gel buffer.

- <u>Electrode Buffer Stock Solution:</u> Dissolve 150 g glycine in 600 mL deionised water. Dissolve 30 g Tris. Make to 1L with deionised water.

- <u>Electrode Buffer Working Solution:</u> Add 5 mL 20% SDS to 100 mL electrode buffer stock solution. Make up to 1 L with deionised water.

6.5.2. Casting gels

The composition of the gels is listed in Table 6.2.

Table 6.2: Composition of gels for SDS-PAGE.

Resolving Gel (15%)		Stacking Gel (6%)	
Stock Running Gel Buffer	20 mL	Stock Stacking Gel Buffer	3 mL
Acrylamide solution	20 mL	Deioinised water	21 mL
20% SDS	200 µL	Acrylamide solution	6 mL
APS	400 µL	20% SDS	150 µL
TEMED	20 µL	APS	300 µL
		TEMED	15 µL